DYNAMIC INTERACTIONS IN AN ARTIFICIAL PHOTOTROPHIC

BIOFILM FOR BIOTECHNOLOGICAL APPLICATIONS

Inaugural - Dissertation

zur

Erlangung des Doktorgrades

der Mathematisch-Naturwissenschaftlichen Fakultät

der Universität zu Köln

vorgelegt von

Tong Li

aus *Urumqi, China*

Köln

2016

Berichterstatter/in: **Prof. Dr.   Michael Melkonian**

                                              Prof. Dr.   Ulf-Ingo Flügge

Tag der letzten mündlichen Prüfung:

                                              29.1.2016

Acknowledgements

I would like first to thank my parents, who supported me in every aspect of my study. Thank you for being proud of me and for your trust in me! Thanks to my girlfriend for her support, for her understanding! Thanks to professor Michael Melkonian, for giving me the chance to do my Ph.D. study, for giving me great advices during the last 4 years and for being a great supervisor. Thanks to Dr. Björn Podola, who always gives me good advice and supported me with the production of all my publications. Thanks to Bastian Piltz for giving me advice for the manuscripts and for all his help in finishing this thesis. Thanks to Dr. Dirk de Beer and his workgroup for their advice and support in the microsensor measurements. And thanks to all the members of AG Melkonian for being the perfect colleges!

Table of Contents

1. Introduction

1.1. Microalgae and their biotechnological potential

"Algae" are defined as a polyphyletic group of oxygenic phototrophs that encompasses both prokaryotes and eukaryotes. The endosymbiotic theory hypothesizes that eukaryotic algae have originated from the endocytobiosis of cyanobacteria inside eukaryotic heterotrophic cells. Through several secondary endocytobiosis events, a variety of algal species have since evolved (Douglas 1998; Moreira and Philippe 2001; Whatley 1993). Algae can be divided into 10 monophyletic groups. Until now, there are 40,000 known algal species. However, it is estimated that the actual number is more than 10 million, and among these microalgae are the most numerous (Norton et al. 1996). This biodiversity of microalgae is the foundation of their biotechnological potentials. E.g., through various metabolic pathways, microalga can produce a wide range of substances, some of which can be synthesized chemically at high costs, whereas others cannot be synthesized at all (Cardozo et al. 2007; Shimizu 1996).
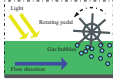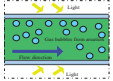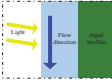
The utilization of microalga by human is not a novel concept: *Arthrospira platensis* (*Spirulina platensis*) has been used since centuries as food by people living in the tropical regions (Ciferri 1983). However, the controlled mass cultivation of microalgae was only introduced in the middle of the last century, and so far, of the known forty thousand microalgal species, only a fraction is used for biotechnological applications (Becker 1994; Moore 2001). Nevertheless, microalgae or substances derived from microalgae can be found today in a variety of different products, e.g. as human food and food supplements, as feed for aquaculture, as raw material for high value chemical compound production, or as additive in cosmetic and pharmaceutical products (Borowitzka et al. 1991; Muller-Feuga 2000). Also, microalga have been successfully applied in wastewater treatment processes (Abdel-Raouf et al. 2012; Davis et al. 2003; de la Noüe et al. 1992).

1.2. Microalgal cultivation system for biotechnological applications

The design of cultivation system is a major factor in the biotechnological application of microalga. Compared to heterotrophic biological systems for biotechnological applications (e.g. biomass and/or metabolites production, waste water treatment relying on bacteria or fungi), another factor has to be taken into consideration when designing bioreactors for microalgae: microalgal cells require light for photosynthesis. Hence, such bioreactors were named "photobioreactors". Photobioreactors can be divided into two major categories: suspension-based and biofilm-based systems (Gross et al. 2015; Olivieri et al. 2014).

In application, suspension system can be subdivided into open and closed system. In an open system, the suspension is directly exposed to the environment; typically, the suspension is kept in a pond-like structure (e.g. race way pond) and to achieve better light utilization and mass transfer efficiency, energy has to be put into the system to ensure proper light distribution and mass transfer (Olivieri et al. 2014). In a closed system, the suspension is isolated from the environment, thus minimizing the risk of contamination. However, high construction costs are typically associated with this type of photobioreactors, in order to achieve a sufficiently large illuminated surface area for optimal growth (Olivieri et al. 2014). Currently, commercial production of microalgal biomass relies heavily on suspension cultivation systems: E.g. open ponds for large scale microalgal biomass production and closed tubular (or of other forms) photobioreactors for more valuable products (Olivieri et al. 2014). Also, open 'high rate algal ponds' have been successfully applied to treat wastewater (Park et al. 2011). However, the cell densities in such suspended systems are typically low (e.g. 0.5 g L^{-1} and 2 – 6 g L^{-1} dry weight in open ponds and in photobioreactors, respectively; Davis et al. 2011), which results in low productivity (or efficiency in wastewater treatment) per volume and high cost of harvesting (i.e. separation of cells from culture medium).

Table I: Typical system design, major advantage and disadvantages of suspension-based and biofilm-based photobioreactors.

Type of photobio-reactor	Suspension-based		Biofilm-based
	Open	Closed	
Typical system setup	Suspension culture kept in a container open to the environment, stirring and aeration provided by mechanical mixing.	Suspension culture kept in an enclosed transparent container, stirring achieved by pumping the suspension through the system and/or aeration with gas bubbles.	Most of the algal cells are immobilized inside the biofilm, only the culture medium flows in the system. Mass transfer achieved mostly through diffusion.
Prominent advantages	Simple construction (i.e. low construction cost).	Minimized risk of contamination. Controlled culture environment.	High biomass concentration (easy harvesting). Low operational cost (i.e. less energy required for pumping).
Major drawbacks	Easily contaminated. High harvesting cost (i.e. dewatering).	High construction cost. High operational cost. High harvesting cost (i.e. dewatering).	Easily contaminated. Biofilm detachment.

*a: Refer to the citations in section

A more recent development in photobioreactor design are the biofilm-based photobioreactors: typically, the algal cells are immobilized onto a substrate to form a biofilm, and the culture medium flows above the biofilm. Compared to suspension-based systems, such a system offers a much higher biomass density (10% – 20% of the harvested biofilm is dry biomass, similar to post-centrifuge biomass from suspension cultures), and thus can reduce the harvesting cost (e.g. biomass dewatering) considerably. In addition, light transfer and mass transfer (especially for gases like CO_2) are more efficient in biofilm-based photobioreactors (Gross et al. 2015). As a result, various biofilm-based photobioreactors have been developed, and both bench-scale and pilot-scale experiments have already been carried out for biofilm-based systems both for biomass production and for wastewater treatment (Abdel-Raouf et al. 2012; Berner et al. 2015; de la Noüe et al. 1992; Olivieri et al. 2014).

Compared to suspension-based systems, biofilm-based photobioreactors offers several advantages. However, in a 'traditional' biofilm-based photobioreactor setup as described above, the biofilm remains completely or partially (spatially and/or temporally) submerged in culture suspension. Thus, such biofilms are subjected to shear forces due to the movement of the liquid phase above, which may cause detachment of the biofilm. Also, the liquid phase above the biofilm can lead to a fast spreading of contaminants, once a contaminating organism enters the system (Berner et al. 2015). The typical system design, advantage and disadvantages of suspension-based and biofilm-based photobioreactors as mentioned above are summarized in Tab. 1 (summarized from references cited previously).

1.3. Porous substrate biofilm photobioreactor (PSBR)

To overcome the problems in the existing photobioreactors, a novel biofilm-based photobioreactor was developed. The new system, developed first by Podola and Melkonian (Twin-Layer system; Podola and Melkonian 2003), and now known best as Porous Substrate Biofilm Photobioreactors (PSBRs), as defined by Murphy et al. (Murphy and Berberoglu 2014), eliminates the problems encountered in "traditional" biofilm-based systems by separating the bulk culture medium from the microalgal biomass. To achieve this, as inspired by membrane based bioreactors, in a PSBR, algal cells are immobilized on one side of a micro-porous membrane (contrary to a solid substrate in a "traditional" biofilm-based photobioreactor), and the culture medium is supplied from the other side of the micro-porous membrane by means of a medium-saturated macro-porous material or by simply applying the medium between two inoculated micro-porous membranes (Shi et al. 2007).
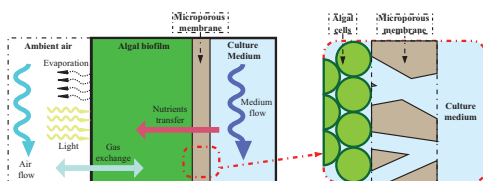
Figure 1: Schematic representation of a Twin-Layer porous substrate biofilm photobioreactor as described by Shi et al. (2007).

The schematic setup of a typical PSBR is illustrated in Fig. 1. The separation of algal cells and culture medium does not only eliminate the problem of biofilm detachment due to shear force, but also maximizes the gas transfer efficiency by directly exposing the surface of the biofilm to the ambient gas phase. In a PSBR, the nutrients are supplied to the biomass by diffusion through the micro-porous membrane (with pore size small enough to prevent algal cells from penetrating). The elimination of a flowing liquid phase around the algal cells also minimizes the spread of contamination, and the removal of a liquid phase (which could contain suspended solids such as detached algal cells) above the algal biofilm maximizes the light transfer efficiency. Furthermore, this absence of liquid phase above the biofilm further increases the dry biomass concentration in the algal biofilm (up to 40%, *Symbiodinium sp.* cultivated on Twin-Layer PSBR, unpublished data). To illustrate this, a photograph of a PSBR biofilm is shown in Fig. 2.
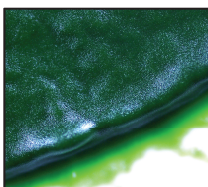

Figure 2: 100x magnified *Halochlorella rubescens* PSBR biofilm cultivated on polycarbonate filter disk.

Previous studies have shown that PSBRs can have very high footprint productivities (productivity per ground area) compared to other cultivation systems under comparable conditions, as presented in Tab. II (Berner et al. 2015; Liu et al. 2013; Olivieri et al. 2014; Schultze et al. 2015). Also, studies carried out at both bench- and pilot-scales have proven the potential application of such PSBR in wastewater treatments (Li et al. 2015a; Shi et al. 2007; Shi et al. 2014). The data presented in these studies demonstrated clearly the potential of a viable large-scale PSBR for biomass production and/or for other applications (e.g. wastewater treatment). However, to transform a bench-scale system into a commercially viable system, several important advancements have to be made. Among these, an automated control system for growth optimization and/or an optimal growth strategy (e.g. light, CO_2 and nutrient supply, harvesting circle etc.) have to be developed. To achieve this, a comprehensive understanding of the dynamic processes inside such PSBR is essential.

Table III: [a]Efficiency in pollutant removal by porous substrate biofilm photobioreactor (PSBR) based systems.

Algal strain	Target pollutant	Operational mode	Removal efficiency	Source
Halochlorella rubescens isolated from wastewater	Nitrate Phosphate Ammonia	Batch	[b]>85% per day [b]>70% per day [b]>70% per day	Shi et al., 2014
Stichococcus bacillaris isolated from Zn contaminated stream	Zn	Batch Continuous	95% in 2 days 35%	Li et al., 2015

*a: Efficiency calculated as one minus concentration of targeted pollutant after treatment divided by that in the original untreated sample. b: In their study, different batches of wastewater samples were used.

Table II: [d]Examples of biomass productivity by different photobioreactors.

Type of photobioreactor	Algal strain	Light intensity (µmol photons m^{-2} s^{-1}) and [b]L/D	Growth medium	CO_2 supple-ment (v/v)	[a]Productivity (g m^{-2} d^{-1})	Source
Porous substrate biofilm photobioreact or (PSBR)	Twin-Layer PSBR					
		Halochlorella rubescens	1000, 14:10	Synthetic medium	/	51	Schultze et al., 2015

Type of photobioreactor	Algal strain	Light intensity (µmol photons m^{-2} s^{-1}) and [b]L/D	Growth medium	CO_2 supple-ment (v/v)	[a]Productivity (g m^{-2} d^{-1})	Source
Porous substrate biofilm photobioreact or (PSBR)	Twin-Layer PSBR	Halochlorella rubescens	1000, 14:10	Synthetic medium	/	51	Schultze et al., 2015
	Attached cultivation PSBR	Scenedesmus obliquus	100, continuous	Synthetic medium	1%	80	Liu et al., 2013
	Evaporation driven PSBR	Anabaena variabilis	110, continuous	Synthetic medium	/	[c]32	Murphy et al., 2014
Submerged biofilm photobioreact or	Biofilm flow cell	Wastewater consortium	230, continuous	Synthetic wastewater	/	[c]25	Boelee et al., 2011
	Algal turf scrubber	Natural consortium	40-140, 16:8	Synthetic	/	42	Mulbry et al., 2008
Closed suspension	Tubular	Spirulina sp.	80, continuous	Synthetic medium	/	[c]8.4	Converti et al., 2006
	Flat-plate photobioreactor	Chlorella sp.	Natural sunlight	Synthetic medium	/	25	Carkozzi et al., 2000
Open suspension	Open pond	Scenedesmus sp.	Natural sunlight	Synthetic medium	/	[c]9	Ketheesan and Nirmalakhandan, 2012
	Raceway pond	Nannochloropsis salina	Natural sunlight	Synthetic medium	/	3.5	Crowe et al., 2012

*a: Productivity per footprint area (i.e. ground area); b: Light dark circle; c: Calculated from original data by the author; d: For further data on productivity of different photobioreactors, refer to citations in section 1.3.

1.4. Investigating dynamic processes inside PSBR biofilms

Unlike for bacterial biofilms or submerged phototrophic biofilms, due to its novelty, the processes inside PSBR biofilms have not yet been studied extensively. There are, until now, only few studies investigating processes inside PSBR biofilms: Murphy and Bergeroglu (2014) developed a model for a PSBR biofilm. However, the model focused more on the gradients (e.g. nutrients, dissolved inorganic carbon and growth etc.) along the medium flow direction rather than the gradients perpendicular to the medium flow (i.e. along the biofilm depth gradient) in an evaporation driven (instead of gravity) PSBR. Furthermore, an over-simplified model (i.e. effect of scattering was not considered in their model) was used to predict light distribution (discussed in the 3rd manuscript, Li et al. 2015b, presented in this thesis in detail), even though previous studies suggested otherwise (Berberoglu and Pilon 2007; Berberoglu et al. 2007; Jøsrgensen 1969; Richardson et al. 1983). In addition, no extensive experimental measurements were carried out to verify their proposed model. In another study, Wang et al. (2015) used a rather primitive method to investigate the effect of light on biomass productivity in PSBR biofilms with different thickness. They speculated that the respiration in the 'non-illuminated' zones in the biofilm caused the decrease of total biomass productivity in prolonged cultivation of PSBR biofilms. However, in their study, instead of a grown biofilm, cells were filtered onto micro-porous membranes to simulate PSBR biofilms grown to different thicknesses. Thus, the effects of adaptation of the biomass due to immobilization (e.g. cellular pigment content), as suggested by previous observations from other researchers (Jøsrgensen 1969; Richardson et al. 1983) and from observations made by the author (Fig. 3), were excluded in their study.

Schultz et al. (2015) observed an increased biomass productivity in PSBR biofilm with increasing surface light intensity up to a photosynthetically active radiation (PAR) intensity of about 1000 µmol photon m^{-2} s^{-1}. This light intensity was well above the saturation PAR intensity expected in suspension cultures. This phenomenon has also been observed in other studies (Liu et al. 2013), and this is suspected to be caused by the following hypothesis: Higher light intensity on the biofilm surface led to deeper light penetration into the PSBR biofilm, thus increasing the total biomass productivity, even though the growth of the surface cells were inhibited by the strong PAR. However, until now, no experimental studies have been conducted to verify this hypothesis.
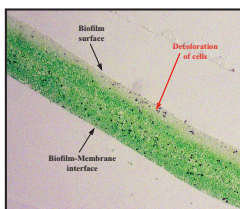
Figure 3: Photo from a 200x magnified sectioned *Halochlorella rubescens* PSBR biofilm cultivated on polycarbonate filter disk (embedded in Epon and sectioned to 10 μm thick section along the direction of the depth gradient). The decoloration observed in the photo indicate the cells closer to the biofilm surface contain less pigments.

In their study, Wang et al. (2015) have also observed a higher light dilution rate (light availability per cell in total biofilm/suspension volume) in a PSBR biofilm compared to a suspension with the same amount of biomass density per unit area. This can be translated to a more effective light transfer in the PSBR biofilm compared to that in suspensions. It has been observed in previous investigations, that in a very dense suspension culture, the forward-scattering of light can significantly increase the efficiency of light transfer (i.e. light dilution rate). Models have already been developed to describe this phenomenon, both in suspension and in phototrophic biofilms (Berberoglu et al. 2007; Murphy and Berberoglu 2014). However, until now, no experimental study has been carried out to verify the light distribution in PSBR biofilms as predicted by the model.

Moreover, as in a PSBR the nutrients are supplied from the opposite direction as light (and, inorganic carbon, if it is not supplied through bubbling the medium with CO_2, or by adding bicarbonates into the medium, Fig. 2). It could thus be imagined, that the nutrients might not be sufficiently supplied to the 'illuminated' zone in a PSBR biofilm. Also, submerged phototrophic biofilms are known to accumulated exceptionally high dissolved oxygen (DO) concentrations (Pringault and Garcia-Pichel 2000). This phenomenon, as summarized by Raven et al. (2008), can have negative effects on photosynthetic productivity. In a PSBR biofilm, due to its direct exposure to the ambient gas phase, a better gas exchange is expected, thus, a lower [DO] compared to submerged systems should be present. The pH is another important factor, since it affects photosynthetic productivity by changing the speciation of dissolved inorganic carbons (DICs) and/or due to other mechanisms (Danilov and Ekelund 2001; Heber et al. 1976). However, pH gradients in a PSBR biofilm along the biofilm depth gradient have not been investigated yet. Since most of the culture media used for microalgal cultivation are buffered, it is expected, if fresh medium is sufficiently supplied, that the pH gradient along the depth gradient of the PSBR biofilm would be rather stable (Murphy and Berberoglu 2014). All the above-mentioned hypotheses and/or speculations have not been verified by experimental studies or otherwise (e.g. using a well verified model) until now.

1.5. Framework of this study

The goal of this study is to create a solid basis (e.g. experimental methods and analytical approaches) in order to achieve a more comprehensive understanding of the dynamic processes (including: light transfer, mass transfer, growth dynamics and chemical equilibriums) in PSBR biofilms in future studies, and, the verification of previously established hypothesis. To realize this, experimental studies and a modeling study were carried out. The developed model was then applied to find explanations for the observations made in the experimental studies (e.g. by comparing results from simulated biofilms and the results from real experimental observations under identical culture conditions). To eliminate uncertainties originating from the behavior of different strains cultivated under the same conditions, a single algal strain that has been studied intensively in previous studies (green alga *Halochlorella rubescens*, CCAC 0126; Culture Collection of Algae at the University of Cologne; www.ccac.uni-koeln.de) was used throughout the present study.

To determine the distribution of different parameters (light intensity, DO, pH, and photosynthetic productivity) in the *H. rubescens* Twin-Layer PSBR (TL-PSBR) biofilm experimentally, microsensor measurements (in collaboration with Max-Planck Institute for Marine Microbiology; Bremen, Germany) were carried out. In this study, microsensors were used for the first time to measure parameters in a non-submerged phototrophic biofilm. In

consequence, several changes were made in the microsensor experimental setup for TL-PSBR biofilm measurement compared to microsensor setup used for measurements on submerged biofilms. Also, a new mathematical method was developed in order to evaluate the data (for photosynthetic productivity measurement) acquired from the microsensor measurements more accurately. The first manuscript presented in this thesis (Li et al. 2015c): *A method to determine photosynthetic activity from oxygen microsensor data in biofilms subjected to evaporation*, was dedicated to these topics.

After the establishment of the experimental methods, a systematic microsensor measurement was carried out: PAR, DO, pH and photosynthetic productivity distributions were measured in *H. rubescens* PSBR biofilms cultivated at different surface PAR intensity and/or exposed to different CO_2 concentrations in the gas phase. The measurement data from this part of the study is presented in the second manuscript included in this thesis (Li et al. 2015b): *Microscale profiling of photosynthesis-related parameters in a highly productive biofilm photobioreactor*.

Finally, a model was developed for the *H. rubescens* TL-PSBR biofilm. To make the model more realistic, experiments were carried out in the framework of this study to determine the parameters required by the model. The model is described in the last manuscript presented in this thesis (Li et al., 2015d, manuscript under review): *Investigating dynamic processes in a porous substrate biofilm photobioreactor – A modeling approach*. Also, in this manuscript, the experimental results both from this study and from a previous study (Schultze et al. 2015) were compared with that from the model simulation.

2. Publications included in this thesis

1St manuscript: *A method to determine photosynthetic activity from oxygen microsensor data in biofilms subjected to evaporation* (Published in 'Journal of Microbiological Methods', 2015, 117:100-107).

2nd manuscript: *Microscale profiling of photosynthesis-related variables in a highly productive biofilm photobioreactor* (Accepted in Oct. 2015 by 'Biotechnology and Bioengineering').

3rd manuscript: *Investigating dynamic processes in a porous substrate biofilm photobioreactor – A modeling approach* (Submitted to the journal 'Algal research', under review).

2.1. A method to determine photosynthetic activity from oxygen microsensor data in biofilms subjected to

   evaporation

Published in 'Journal of Microbiological Methods', 2015, 117:100-107.

DOI: 10.1016/j.mimet.2015.07.022

Presented here in the original published version, reformatted for the presentation in this thesis (with section

numbers removed and corresponding changes).

A method to determine photosynthetic activity from oxygen microsensor data in biofilms subjected to evaporation

Tong Li[a]#, Björn Podola[a], Dirk de Beer[b] & Michael Melkonian[a]

University of Cologne, Botanical Institute, Biocenter Cologne, Germany[a]; Max-Planck-Institute for Marine Microbiology, Bremen, Germany[b]

Running Head: Microsensor photosynthesis measurement in biofilms

#Address correspondence to Tong Li, lit2@uni-koeln.de.

Dirk de Beer and Michael Melkonian contributed equally to this work.

Abstract

Phototrophic biofilms are widely distributed in nature and their ecological importance is well recognized. More recently, there has been a growing interest in using artificial phototrophic biofilms in innovative photobioreactors for production of microalgal biomass in biotechnological applications. To study physiological processes within these biofilms, microsensors have been applied in several studies. Here, the 'light-dark shift method' relies on measurement of photosynthetic activity in terms of light-induced oxygen production. However, when applied to non-submerged biofilms that can be found in numerous locations in nature, as well as in some types of photobioreactors, limitations of this approach are obvious due to rapid removal of gaseous species at the biofilm surface. Here, we introduce a mathematical correction to recover the distribution of the actual photosynthetic activity along the depth gradient in the biofilm, based on a numerical solution of the inversed diffusion equation of oxygen. This method considers changes in mass transport during the measurement period as can found on biofilms possessing a thin flow/mass transfer boundary layer (e. g. non-submerged biofilms). Using both simulated and real microsensor data, the proposed method was shown to be much more accurate than the classical method, which leads to underestimations of rates near the biofilm surface. All test profiles could be recovered with a high fit. According to our simulated microsensor measurements, a depth resolution of ≤ 20 μm is recommended near the surface. We conclude that our method strongly improves the quality of data acquired from light-dark measurements of photosynthetic activity in biofilms.

Keywords

Introduction

Phototrophic biofilms are attached microbial communities driven by photosynthesis, and their importance in nature has long been recognized (Roeselers et al., 2008; Seckbach and Oren, 2010). In recent years, phototrophic biofilms have been applied to biotechnology and environmental biotechnology of microalgae, as well. Here, most applications rely on submerged biofilms, where the light exposed biofilm surface is covered by a layer of water (Berner et al., 2014; Roeselers et al., 2008). Some more recent developments make use of the advantages of biofilms exposed to ambient air (Berner et al., 2014; Schultze et al., 2015; Shi et al., 2007), referred to as Porous Substrate Bioreactors (PSBRs) (Murphy et al., 2014). In view of the technical development of photobioreactors, detailed micro-scale (microsensor) analyses of parameters along the axis (gradient) perpendicular to the biofilm surface have been proposed (Roeselers et al., 2008; Schultze et al., 2015). Such studies might also be of interest to analyze non-submerged (aerial) phototrophic biofilms in the natural environment (Berner et al., 2014).

A number of approaches have been developed to investigate structures and processes inside phototrophic biofilms at the micro-scale level, such as confocal microscopy, microsensor studies, fluorometry, and mathematical modelling (Bachar et al., 2008; Beutler et al., 2009; Kühl and Polerecky, 2008; Ramanan et al., 2013; Revsbech et al., 1981; Wolf et al., 2007). Among these methods, the microsensor-based "light-dark shift method" is a well-established technique to estimate gross photosynthetic activity in phototrophic biofilms since its introduction in the 1980s (Revsbech and Jorgensen, 1983). The method determines the rate of decrease in the dissolved oxygen concentration by an oxygen microsensor, which is induced by applying a short period of darkness to a steady state phototrophic biofilm (Revsbech and Jorgensen, 1983). However, since the diffusion rate of oxygen changes during this dark period, the gross productivity estimated using the acquired data directly might be inaccurate. This limitation was soon recognized and solutions were suggested in serval previous studies, which established a solid basis for evaluating data acquired by light-dark shift method. However, these solutions require either a hypothetical distribution of photosynthetic activity or rely solely on the regression of measured data (Glud et al., 1992; Lassen et al., 1998; Revsbech and Jorgensen, 1983; Revsbech et al., 1986). For non-submerged biofilms, besides the limitation referred to above, other processes have to be taken into account: the dynamics of oxygen in a non-submerged biofilm can be described by Eq.1, assuming that the biofilm is homogenous in planes parallel to its surface (Bergman et al., 2011).

$$\frac{\partial c}{\partial t} = P_g - R_l + D_e \frac{\partial^2 c}{\partial x^2} + u \frac{\partial c}{\partial x} - R_s \qquad \text{(Eq.1)},$$

The terms on the right hand side represent gross photosynthesis P_g, respiration during light R_l, diffusion and advection caused by evaporation on the surface, and the removal of dissolved gaseous species due to air flow above the surface R_s. D_e is the effective diffusion coefficient, C is the concentration of dissolved oxygen, u is the convective flow rate inside the biofilm,

$$u = q_e /(A_e \cdot \theta) \qquad \text{(Eq.2)},$$

and can be calculated with the rate of liquid volume lost q_e, the exposed surface area of the biofilm A_e and the areal porosity of the biofilm θ (Eq.2). t is time and x is the depth. Without light, no oxygen evolution can be expected (Pessarakli, 2005). Thus after darkening oxygen decreases with a rate:

$$\frac{\partial c}{\partial t} = 0 - R_l + D_e \frac{\partial^2 c}{\partial x^2} + u \frac{\partial c}{\partial x} + R_s \qquad \text{(Eq.3)}.$$

Values measured by the light-dark shift method are the rate of change for the term on the left hand side of Eq.3 during the measurement period. Immediately after the removal of light (at 0 s of the measurement), $\partial C/\partial t$ does represent accurately the gross photosynthetic productivity. However, its value changes gradually with time, as the removal of light leads to change of the values on the right hand side (Glud et al., 1992; Revsbech, 1986; Revsbech and Jorgensen, 1983). In consequence, an accurate representation of the photosynthetic rate is provided only if all terms on the right hand side of Eq.3 remain constant with time (as the measurement time has to be > 0 s), which cannot be assumed: Previous work (Glud et al., 1992) concluded that the respiration rate can be considered stable during the measurement period, but the change in rate of diffusion can have a significant effect on the measured results (Glud et al., 1992; Revsbech and Jorgensen, 1983; Revsbech et al., 1986).

When applying the light-dark shift method for measuring photosynthetic activity to a non-submerged biofilm, two additional factors attributed to the absence of a thick liquid phase on the biofilm surface have to be considered (Bergman et al., 2011; Schlichting and Gersten, 2000):

1) For a non-submerged system directly exchanging dissolved gases with the gas phase above the biofilm surface, the flow/mass transfer boundary layer (compared to submerged biofilms) can be considered as non-existent in case of a considerable air flow. With the gas phase above the biofilm being in effect a sink for the oxygen produced inside the biofilm, during the light-dark cycle, the rate of change of oxygen concentration at the biofilm surface will always be 0 (or almost 0), and the change rate near the surface an underestimation of the photosynthetic activity. This effect also occurs in submerged system at the interface between the boundary layer and the bulk liquid, however, the effect in the biofilm itself is dampened due to the relatively thicker flow/mass transfer boundary layer.

2) The evaporation of water at the biofilm surface exposed to air induces a convective flow through the biofilm in the direction perpendicular to the biofilm surface, which in effect adds a mass flow towards the surface.

These two processes have a strong effect throughout a non-submerged biofilm, and, therefore, need to be considered for the interpretation of acquired experimental data to obtain a profile representing a valid photosynthetic activity.

In summary, direct results from the light-dark shift measurement do not accurately represent the actual photosynthetic activity in biofilms, especially for measurements performed in non-submerged biofilm systems. Thus, in the present contribution we propose a mathematical treatment to achieve an adequate recovery of the distribution of actual photosynthetic activity from measured microsensor data.

Materials and Methods

Suspension and biofilm cultivation of microalgae

In this work, a Twin-Layer algal biofilm, which is an immobilized biofilm system that separates the bulk medium and biomass by means of a micro-porous membrane (Nowack et al., 2005), was used as a model for a non-submerged biofilm. Stock cultures of the green algae *Halochlorella rubescens* (strain CCAC 0126; Culture Collection of Algae at the University of Cologne; www.ccac.uni-koeln.de) in suspension was kept at 16 °C at a light intensity of about 20 µmol photon m^{-2} s^{-1} photosynthetically active radiation (PAR). To obtain sufficient material for biofilm inoculation, stock cultures were transferred into 2 L Erlenmeyer flask filled with 1.3 L of Bold's basal medium (BBM) (Bischoff and Bold, 1963), and were cultivated at a light intensity of about 50 µmol m^{-2} s^{-1} PAR at 23 °C with 0.5 L min^{-1} compressed air with 1% (v/v) supplementary CO_2. Biomass was harvested after 3 weeks of growth, and was inoculated onto polycarbonate filters (PC40, 0.4 µm pore size, 25 mm diameter, Whatman, Dassel, Germany) with a circular inoculation area of 2.55 cm^2 as described by Naumann et al. (2013). Inoculated filters were then transferred into a bench-scale Twin-Layer system for cultivation according to Schultze et al. (2015). Tubes were aerated with a flow rate of 0.75 L min^{-1} with compressed air. Sodium discharge lamps (SON-T AGRO 400W, Philips, Hamburg, Germany) were used as light source with a 14-10 hour light-dark cycle at an intensity of 1,000 µmol m^{-2} s^{-1} PAR. Temperature in the tubes was 25±2 °C. 1 L BBM culture medium was used at a medium flow rate of 3 mL min^{-1} per tube and the culture medium was replaced every 2 days.

Microsensor measurements

A schematic representation of the experimental setup for microsensor measurements based on previous works by Gieseke and de Beer (2004) is given in Figure 1: the biofilm immobilized on a polycarbonate membrane was placed inside the biofilm measurement cell under a controlled atmosphere of compressed air at a flow rate of 1 L min^{-1} (Figure 1A). The non-inoculated area of the polycarbonate filter and glass fiber were covered with a black plastic foil to exclude light and gas exchange in this area. 50 mL of BBM culture medium were circulated though the measurement cell with a flow rate of 3 mL min^{-1} by means of a peristaltic pump and were exchanged every 1 hour during the measurement. The evaporation rate was monitored by recording the change of the volume in the medium container. Biofilm temperature during the experimental period was 23 ± 0.5 °C. Light was supplied at an intensity of 1,000 µmol m^{-2} s^{-1} (on biofilm surface) from the front side by a halogen lamp (KL-1500, Schott, Mainz, Germany) equipped with a 3-fold splitter to ensure even distribution. The movement of the sensor was enabled by the computer-controlled micromanipulator (Pollux Drive, PI miCos, Eschbach, Germany). Data were recorded with a depth resolution of 20 µm until 500 µm depth (at which the switch from light to dark has no significant effect on the oxygen concentration measured). Microsensor measurements were carried out on biofilms cultivated for 30 days. Microsensor signals were amplified and converted into digital data (DAQpad 6015 and 6009, National Instruments, Munich, Germany) prior to their further processing on a computer (Figure 1B). Software used for system control and data acquisition were custom made (can be acquired upon request from Dr. Lubos Polerecky, Utrecht University, Netherlands, l.polerecky@uu.nl). A picoampere meter and Clark-type oxygen microelectrodes with tip diameters ≤ 10 µm, and a 95 % response time < 0.5 s were used for the light-dark shift measurement

(Revsbech, 1989). Linear calibration of oxygen microsensor was carried out as described by Revsbech (1983) using BBM saturated with nitrogen gas or compressed air. A shutter connected to a timer was used to control light-dark cycling: the total dark period was 3 s, and a linear regression slope of oxygen concentration change between 0.7 and 2.1 s of the dark period was determined as the measured value. For each measurement depth, three light-dark cycles were performed after steady state was reached (this could be as long as 10 min), and these 3 values acquired were considered as triplicates. The PAR light intensity profile was acquired using a fiber optic light microsensor with a spherical tip (80 µm diameter) and a portable spectrometer (USB 4000, Ocean optics, Dunedin, USA) (Kühl et al., 1994a, 1994b). At each measurement depth, the average value of a 3 s measurement period was taken as the PAR intensity.
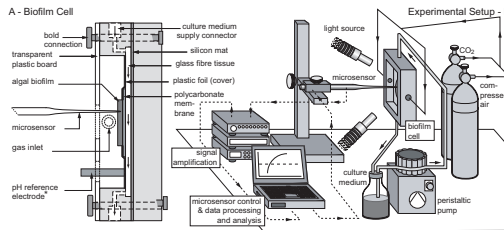

Figure 1: Experimental setup for microsensor studies in non-submerged microalgal biofilms. **A**: Schematic drawing of the vertical cross section of the measurement in artificial biofilms. Solid arrows in the glass fiber tissue indicate flow direction of the culture medium. **B**: Schematic drawing of the complete experimental setup, dotted lines with arrow indicate signal flow, whereas solid arrows represent medium and gas flows in the system. *The pH reference electrode and CO_2 input were installed but not used for measurements shown in the present paper.

Electron transfer rate (ETR) measurement

For measuring the photosynthetic performance at different depths in the algal biofilm by PAM (pulse amplitude modulated) chlorophyll fluorescence analysis, the biofilm was sectioned stepwise in parallel to its surface plane with a resolution of 50 µm by means of a custom-made hand microtome (Figure 2). The biofilm immobilized on a polycarbonate membrane was placed onto a height-adjustable stage on a thin layer of culture medium, whereas the stage allows levelling the biofilm sample into the sectioning plane by means of a micrometer screw. The sectioning plane was defined by a solid brass support over which a rigid microtome blade was passed manually to remove the overlying algal biofilm (Figure 2).
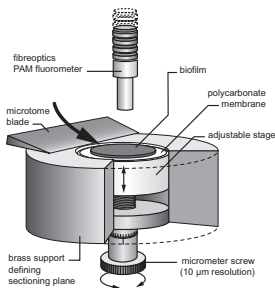
Figure 2: Schematic drawing of the experimental setup used for pulse amplitude modulated fluorometry and biofilm sectioning. The sample holder allows moving the biofilm in vertical direction by means of a micrometer screw (indicated by the thin solid arrows). The biomass above the sectioning plane was removed with a solid microtome blade prior to the fluorescence measurement in the respective layer. The cutting direction is indicated by the thick arrow.

Measurements of chlorophyll fluorescence were carried out from surface to a depth of 500 μm without removing the biofilm from the stage. Using a PAM-2000 Chlorophyll Fluorometer (WALZ, Effeltrich, Germany), PAM chlorophyll a fluorescence of photosynthetically active cells of the exposed biofilm surface was measured by application of the saturation pulse method: The fiber-optic cable of the chlorophyll fluorometer was centered in a 20 mm distance perpendicular to the biofilm surface (Figure 2). A weak beam of modulated (20 kHz) red light (0.03 μmol m^{-2} s^{-1} PAR with a maximum intensity at 650 nm and a maximum cutoff wavelength at 670 nm) was used to excite chlorophyll fluorescence (F_0 or F), which was then detected by a photodiode with a minimum cutoff wavelength of 700 nm. Maximal fluorescence F_m or F'_m was induced by applying a saturation pulse of white light of about 2,000 mol m^{-2} s^{-1} and a duration of 600 ms. Fluorescence data were recorded during rapid light curves with an ascending light intensity applied to each section: directly after each sectioning procedure, the biofilm was dark-adapted for 10 min and F_0 and F_m were recorded at the end of the dark period to determine the maximal quantum efficiency F_v/F_m. Subsequently, a rapid light curve was recorded using actinic white light applied stepwise at 11 consecutive intensities (7, 12, 18, 38, 66, 122, 209, 373, 642, 1099, and 1762 mol m^{-2} s^{-1} PAR) for 60 s (Herlory et al., 2007), followed by the determination of F and F'_m to calculate effective quantum yield of electron transport $\Delta F/F'_m$ according to Genty et al. (Genty et al., 1989) for each of the light intensities. During the measurement, the samples were kept water-saturated by regularly adding a few drops of medium to the edges of the membrane filter (resulting in a total volume of 50 - 100 μL culture medium for the whole experimental period). ETR measurements were carried out on biofilms cultivated for 97 days.

The electron transfer rate (ETR) can be used to estimate the primary productivity of photosynthetic biofilms and is related to (gross) rates of oxygen production. The ETR was calculated as (Hofstraat et al., 1994; Ralph et al., 1999):

$$ETR = 0.5 \times I_{PAR} \times \Delta F/F'_m \times Abs \qquad (Eq.4)$$

I_{PAR} is the PAR intensity and Abs represents the PAR absorptivity of the sample material. Abs was determined by an IMAGING-PAM Chlorophyll Fluorometer (equipped with Maxi-Head; WALZ, Effeltrich, Germany) for all measured depths. Measurements were performed in triplicates (three independent biofilm samples). From rapid light curve data for every section, light intensity was plotted against the ETR and was mathematically fitted using the Photosynthesis-Irradiance (P-I) model of Platt et al. (Platt et al., 1980) by means of GraphPad Prism v5.02 statistical software (GraphPad Software Inc., La Jolla, USA). Based on microsensor measurements of the light intensity profiles, available light intensities for all of the measured depths can be determined by using the "Point to point" function in GraphPad Prism. These data were used to derive the potential ETR for the sectioned depths to obtain an overall ETR depth profile.

Mathematical treatment

The following mathematical treatment was proposed for correcting data acquired from the light-dark shift method: Take the derivative of time on both sides of Eq.3, and assume the time t and spatial variables x are not dependent (as during the measurement period, the thickness of the biofilm hardly changes):

$$\partial(\frac{\partial c}{\partial t})/\partial t = 0/\partial t - \partial R_l/\partial t + D_e \frac{\partial^2(\frac{\partial c}{\partial t})}{\partial x^2} + u\frac{\partial(\frac{\partial c}{\partial t})}{\partial x} - \partial R_s/\partial t \qquad (Eq.5).$$

The term $\partial R_s/\partial t$ represents the rate change of the removal of dissolved gaseous species at the submerged biofilm surface due to the flow of bulk liquid, or, in the case of an aerial biofilm (or PSBR biofilm), due to air above the biofilm:

$$\partial R_s/\partial t = (D_e \frac{(C - C_s)}{x^2} + u \frac{(C - C_s)}{x})/\partial t$$

$$= (\frac{D_e}{x^2} + \frac{u}{x}) \cdot \partial C/\partial t \qquad \text{(Eq.6)}.$$

C_s represents the oxygen concentration on the very surface of the aerial biofilm, or at the interface between the boundary layer and the bulk liquid in the case of a submerged biofilm, which is in equilibrium with the phase above and is considered to be a constant. Considering that the rate of respiration remains stable during the measurement period (Glud et al., 1992), and take $\partial C/\partial t = P(x, t)$, as $\partial C/\partial t$ is a function of depth x and time t. Substitute Eq.6 into $\partial R_s/\partial t$ and $\partial C/\partial t$ to $P(x, t)$, Eq.5 becomes:

$$\frac{\partial P(x,t)}{\partial t} = 0 - 0 + D_e \frac{\partial^2 (P(x,t))}{\partial x^2} + u \frac{\partial (P(x,t))}{\partial x} - (\frac{D_e}{x^2} + \frac{u}{x}) \cdot P(x,t) \qquad \text{(Eq.7)}$$

Eq.7 is a nonhomogeneous diffusion equation with a source term (here a negative source, or a sink) and can be solved by using any of the methods summarized by Crank or Polyanin (Crank, 1975; Polyanin, 2002). Using initial condition $P(x, t = 0) = P(x, 0)$ and boundary condition $\partial P(x = 0, t)/\partial t = 0$. The exact solution of Eq.7 at $t = \tau$ can be expressed as:

$$P(x,\tau) = \int_0^\delta P(y,0) \cdot \left[e^{\left(\frac{-(y-x+u\cdot\tau)}{4\cdot D_e\cdot\tau}\right)} - e^{\left(\frac{-(y+u\cdot\tau)}{4\cdot D_e\cdot\tau}\right)} \cdot erfc(\frac{x}{\sqrt{4 \cdot D_e \cdot \tau}}) \right] \cdot dy$$

$$\text{(Eq.8)},$$

δ is the total depth of the biofilm, or, alternatively, the depth until which the shift from light to dark has an effect on the dissolved oxygen concentration. $P(x, \tau)$ is the measured value from the light-dark shift method with measurement time τ at measurement depth x, and $P(y, 0)$ is the actual photosynthetic activity at position y (the integrating variable), which is the desired term. For measurements taken at all depths, the measured value $P(x, \tau)$ at a depth x depends on the $P(y, 0)$ across the complete photosynthetic active region of the biofilm (surface to depth δ). The effect of diffusion and advection inside the biofilm is reflected by the first term in the square brackets (inner term). The effect of surface flow removal is reflected by the second term in the same brackets (surface term, and $erfc$ represents the complement error function). In this form, the terms representing the inner and surface effects are separated.

Eq.8 is a Fredholm integral equation of the first kind (Kress, 2014), and can be solved by using numerical methods (Baker et al., 1964; Neumaier, 1998). The numerical approach used in this paper is: Discrete the system perpendicular to the biofilm surface using a simple 1D upwind scheme by setting the dissolved oxygen concentration in a discretion element equal to the value at its knot closer to the biofilm surface (Courant et al., 1952); then calculate the approximated solution of Eq.8 using Tikhonov regularization (Tikhonov et al., 1995) with a non-negative constrain applying the active-set algorithm purposed by Gill et al. (1981). Discrete δ by n, and let $P(x_j, \tau) = g_j$, $P(y_i, 0) = h_i$; $(i, j = 1, 2, …, n)$ and write Eq.8 in the discrete operator notion:

$$g_j = \sum_i^n k_{i,j} \cdot h_i \qquad \text{(Eq.9)},$$

$k_{i,j}$ is the operator term which contains both the term that reflects the effect of diffusion and advection of dissolved oxygen inside the biofilm (inner term) and the term that reflects the effect of dissolved oxygen removal due to surface flow (surface term). In matrix notion, let G be a vector containing g_j, H a vector containing h_i, and K a matrix containing the operator terms $k_{i,j}$:

$$G = K \cdot H \qquad \text{(Eq. 10).}$$

Since a profile with only positive values is expected, and the diffusion is expected to be the dominant process affecting the measured value, generalized Tikhonov regularization with a second derivative operator is used (Hansen, 1994; Varah, 1983). Apply the regularization and non-negative constrain to Eq.10, and let L be the second derivative operator, an approximation of H can be acquired numerically by solving the minimization problem:

$$\min_{H \geq 0} \{\|G - K \cdot H\|^2 + \lambda^2 \cdot \|L \cdot H\|^2\} \qquad \text{(Eq. 11).}$$

The problem represented by Eq.11 can easily be solved by using solvers designed for this kind of problems as explained by Stewart (1973). The regularization parameter λ can be found by using several methods (Calvetti et al., 2000; Hansen, 1994; Hansen and O'Leary, 1993), in this paper, the L-curve method purposed by Hansen & O'Leary (1993) was used to find the best λ.

The solution of H for problems represented by Eq.11 is straightforward. However, as the operator K contains terms that represent both the effect of diffusion and advection inside the biofilm and removal due to surface flow, a direct solution might be inaccurate near to the surface if the noise level in the input data is high. Since the term representing surface flow removal tends to smoothen the profiles near to the surface (Hansen, 1992), a peak in the true profile near the surface can be smoothened out in the solution. This, however, can be resolved by mathematical manipulation of the operator K. Rewrite Eq.10 as:

$$(G_{in} + G_{surf}) = (K_{in} + K_{surf}) \cdot H \qquad \text{(Eq.12),}$$

The subscripts *in* and *surf* represent the effect from the inner term and the surface term in Eq.8 respectively, operators K_{in}, K_{surf} can be calculated using Eq.8, as well as g_{in} and G_{surf}, if an H is given. The problem in Eq.11 thus became:

$$\min_{F \geq 0} \left\{ \left\|(G_{in} + G_{surf}) - (K_{in} + K_{surf}) \cdot H\right\|^2 + \lambda^2 \cdot \|L \cdot H\|^2 \right\}$$

or,

$$\min_{F \geq 0} \left\{ \left\|(G_{in} - K_{in} \cdot H) + (G_{surf} - K_{surf} \cdot H)\right\|^2 + \lambda^2 \cdot \|L \cdot H\|^2 \right\}$$

$$\text{(Eq.13).}$$

Observing the surface term in Eq.8, notice the maximum value of the surface term is controlled by the position of the actual activity y, but a complement error function dependent solely on the position of the measurement taken (x) controls the final value. Furthermore, for a given G, under the same measurement conditions, G_{surf} always has the same set of values. Thus, for a given G, the minimization of the term $\left\|G_{surf} - K_{surf} \cdot H\right\|^2$ will always yield the same solution. The problem in Eq. 13 can be simplified to:

$$\min_{f \geq 0}\{\|G_{in} - K_{in} \cdot H\|^2 + \lambda^2 \cdot \|L \cdot H\|^2\} \qquad \text{(Eq. 14)}.$$

Eq.14 does not contain the surface term, but the solution of the problem still leads to H, which is the desired original profile.

The complete procedure of the calculation is given below:

1) Discrete the system and calculated L as the discrete second derivative operator.

2) Calculate operator K_{in}, K_{surf} and K using Eq.7. No knowledge other than diffusion coefficient D_e, flow rate u (calculated from Eq.2) inside the biofilm and measurement time τ is required. A λ was calculated using L and the operator K.

3) A preliminary H (here denoted as H_0) was calculated by solving Eq.11 using the measured data as G, the operator L, K and the λ calculated from the previous step.

4) G_{in} and G_{surf} were calculated by using H_0, K_{in}, K_{surf} and Eq.12. And a new λ was calculated using operator L and K_{in}.

5) Solve Eq.14 for H using the calculated G_{in}, K_{in}, L and the λ calculated from the previous step.

H_0 does not necessarily give a faithful representation of the true profile, but gives the same measured distribution G, and thus G_{in} and G_{surf} (as G_{surf} has a fixed value for the same measurement condition) when used in Eq.10 and Eq.12 respectively. In total, 5 inputs are needed: measured data points from the light dark shift method, effective diffusion coefficient in the biofilm, evaporation rate, porosity of the biofilm and measurement time.

The treatment procedure was coded in MATLAB (version 2013a, MathWorks, Ismaning, Germany), and the inbuilt *quadprog* was used for solving the minimization problems. *L-curve* function from the regularization tools (Hansen, 1994) was used to find the λ value. The mean values of triplicates acquired from the microsensor measurement were randomly added or subtracted with a random value in range of the calculated standard deviation (SD) at the same position. These values were used as input for the calculation. The calculation procedure was repeated 3 times, and the mean value of the 3 results was taken as the final result (a SD can also be calculated). Data interpolation, if needed, was done by simply connecting two measured data points with a straight line (linear interpolation, using MATLAB inbuilt function *interp1*).

Test problems setup

To test the proposed treatment, first, simulated measurement data points were generated using known actual profiles, in total, 5 different test profiles adopted from previously reported possible photosynthetic activity distribution in phototrophic biofilms were used (Glud et al., 1992; Lassen et al., 1998; Revsbech and Jorgensen, 1983; Revsbech et al., 1986). These known profiles, together with assumed diffusion coefficient, evaporation rate, porosity and measurement time (which were similar or identical to the values encountered in actual biofilm measurements) were put into Eq.8 to generate simulated measurement data points. The acquired profiles (simulated measurement data points), were then sampled every 5, 10, 20, 40 or 80 μm to simulate the different depth resolutions used. Then a random error $\leq 20\%$ of the maximum value in the simulated data was added to simulate

noise in the measurement. The simulated profiles together with other parameters were then used for recovering the original distribution.

The test was also carried out using data acquired from light-dark shift measurements on a *H. rubescens* Twin-Layer biofilm: The porosity of the biofilm was estimated from the volume of cells (biovolume) in the biofilm divided by the total biofilm volume. The biovolume was calculated as described by Hillebrand et al. (1999) from suspended biofilm samples with a 100 μm resolution to a depth of 500 μm using the sectioning technique described above (n = 3 filters). The determination of porosity showed no significant differences in depth sections of 100 μm each (one-way ANOVA test using GraphPad Prism v5.02, as described above), and the mean value of 0.76 was taken as volumetric porosity for the calculation. Using this value, the diffusion coefficient was estimated using the relationship suggested by Weissberg (1963), and effective diffusion coefficients were calculated to be 0.68 of that in pure water. Evaporation rate during the measurement was 0.68 mL min^{-1}, which corresponded to an advective flow rate of 5.4 μm s^{-1} inside the biofilm. 2.0×10^{-9} m^2 s^{-1} was taken as diffusion coefficient of dissolve oxygen in water (Bergman, 2011) for all calculations. The recovered photosynthetic profile was than compared with the measured ETR profile. The n values used for discretion for both simulated and real profiles were 10, 25, 50, 100, 200 and 500.

Results

To assess the performance of the proposed mathematical method, a comparison between the input test distribution used for generating the simulated measurement data points and the recovered distribution using the proposed method with different simulated depth resolutions was performed (Figure. 3). Only recovered distributions using n = 50 were shown, since further increase in n did not lead to significant improvement in the results and a decrease in n, in some cases, tends to produce physically impossible results (in combination with a low depth resolution). The maximum computation time (n = 500) using a DuoCore 2.8 GHz CPU (Intel, Santa Clara, USA) was less than 1s. The following test profiles were used (Figure. 3A-E): A test distribution following the shape of measured light distribution in the biofilm (3A); a biofilm that has lower activity at the surface as proposed by Glud et al. (1992) (3B); distributions following the shape proposed by Revsbech et al. (1983) and Revsbech & Jorgensen (1986) (3C+D); a profile with a double peak as described by Lassen et al. (1998) (3E). All profiles tested were recovered with relatively high fidelity by the proposed method. However, a more accurate representation of the actual profiles was acquired with higher depth resolutions in the simulated measurement. For all test profiles, resolution of 20 μm produced profiles that are not different from the original distributions, whereas, at 40 μm and 80 μm resolution, this was observed only for some profiles (Figure. 3A-D and 3B, respectively). A further increase in resolution to < 20 μm produced better results in only one of the test profiles (Figure. 3E). Even though all sharp edges in the original distribution in the biofilm were smoothened, the discontinuities on the surface were successfully recovered in all cases.
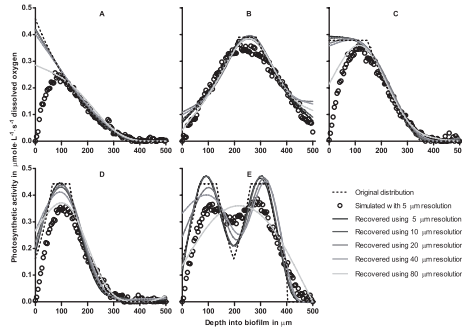
Figure 3: Comparison between the simulated, actual, and recovered distribution of photosynthetic activity (oxygen production in terms of µmol O_2 L^{-1} s^{-1}) for five different test profiles (panel **A** to **E**): Black dashed lines show the original/actual distributions, whereas the simulated profiles are given in empty circles (with 5 µm resolution); solid lines represent the recovered distributions using the proposed method, and the simulated measurement depth resolutions used for recovery decreases with increasing brightness.

Results for the test conducted using real measurement data from the *H. rubescens* biofilm are presented in Figure 4. The data points from direct measurement showed reduced activity at the biofilm surface. In comparison, the recovery profile follows the trend of light profile recorded in the biofilm, displaying a monotonical decrease of photosynthetic activity with increasing depth. At a depth of about 450 µm, the recovered photosynthetic activity dropped to 0 µmol O_2 L^{-1} s^{-1} in congruence with the measured PAR light intensity (Figure 4A). Furthermore, the recovered distribution of photosynthetic activity from microsensor measurements and the photosynthetic electron transfer rates (ETRs) measured by means of chlorophyll fluorescence showed an almost identical distribution of photosynthetic activity (Figure. 4B) in the *H. rubescens* biofilm. This indicates that the corrected profile is a better representation of the actual photosynthetic activity distribution.
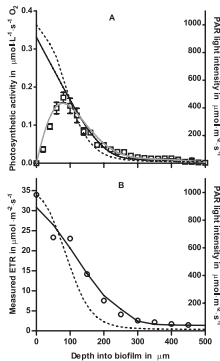
Figure 4: Comparison between measured photosynthetic activity (oxygen production in µmol O_2 L^{-1} s^{-1} and ETR in µmol electrons m^{-2} s^{-1}), and the calculated distribution of photosynthetic activity in terms of oxygen production in biofilm of the microalgae *Halochlorella rubescens*. **A**: Measured distribution of photosynthetic activities (empty squares, error bar represent standard deviation of triplicates) and the recovered actual distribution (solid black line). Grey solid line gives the values of the photosynthetic activity that should have been measured if the solid black line was the actual photosynthetic activity profile. **B**: ETR (electron transfer rate, empty circles are mean values from triplicates, solid line represents the smoothed curve) of the microalgal biofilm. Distribution of photosynthetic active radiation (PAR) intensity were given in both panels as dotted lines (in µmol photon m^{-2} s^{-1}).

Discussion

Generally, using data acquired directly from the light-dark shift method for estimating the photosynthetic activity in phototrophic biofilms can be inaccurate due to the change in mass transfer rates during the dark period and a loss of dissolved species because of surface removal of dissolved oxygen due to the advection in the phase above the biofilm (as described in introduction). The latter effect becomes even more pronounced when measurements are to be carried out on non-submerged biofilms. For submerged biofilms, to mitigate this inaccuracy, an agar layer has been applied onto the biofilm surface to stabilize the flow boundary layer (Glud et al., 1992). However, this procedure could change the structure or the mass transfer at the biofilm surface. For non-submerged biofilms, this agar treatment is inappropriate, since the biofilm will no longer be in direct contact with the gas phase above its surface. Light-dark shift measurements have been carried out previously on non-submerged biofilms, but no additional treatment of data was used (Bernstein et al., 2014). Such results, as shown by the comparison of original photosynthetic profiles and the simulated measured data points in Figure 3 (the effect of the surface removal), can be very misleading, especially for biofilms with both phototrophic and heterotrophic components (Glud et al., 1992; Lassen et al., 1998; Revsbech and Jorgensen, 1983; Revsbech et al., 1986).

To a certain degree, a better experimental set up (e.g. a shorter measurement time), can reduce the inaccuracy mentioned above. However, a mathematical treatment is required to improve the results further. And this requires the exact solution of the diffusion equation (Eq.7) (Glud et al., 1992; Revsbech et al., 1986). This can be derived using various methods (Crank, 1975; Polyanin, 2002). In the proposed mathematical treatment, the expression of Eq.8 was chosen so that the terms representing the effect of the process in the biofilm and the effect from the surface are separated (inner and surface terms in the square brackets). Eq.8 is a Fredholm integral equation of the first kind. Its solution requires the solution of an inversed diffusion equation, which has been discussed in detail since the 1960s and numerous solution methods have been developed (Hansen, 1992, 1994; Tikhonov et al., 1995). As described above, a generalized Tikhonov regularization with an approximated second derivative operator was chosen and the L-curve method was used for finding the best regularization parameter, which defines the balance point between the regularization error and the residue norm (Hansen and O'Leary, 1993). The regularization method, gives a smoothened approximated solution, and thus the recovery of the exact values should never be expected (Hansen, 1992). As a result, none of the sharp edges in the original distribution inside the biofilm was recovered (Figure. 3). Another problem caused by the smoothening is, as mentioned previously, a peak in the actual distribution near to the surface of a biofilm might be simply smoothened out if no precaution is taken to avoid this (e.g. direct solution of Eq.11). However since the Eq.8 separates the inner and surface terms, the minimization of Eq.11 can be transformed into the minimization of Eq.14. This yields a solution more accurately representing the original distribution, and the activity at the surface is always recovered when appropriate depth resolutions and n values were used (Figure 3). Following this approach, in the complete mathematical treatment procedure, the final approximated solution was solved using a previously calculated approximated solution (Step 3 and 4 in the last section of material and method). This did increase the numerical error compared to procedures that contain only a single approximated solution (Hansen, 1992; Tikhonov et al., 1995). However, in comparison to the solutions

acquired by directly solving Eq.10 (which could not recover the peaks near the biofilm surface in some cases, even though 5 μm depth resolution and $n = 500$ were used, results not shown), this increment in numerical error is acceptable.

For the simulated test problems using different measurement depth resolutions, accuracy of the recovered profile increases with a higher depth resolution, which, for a real measurement, would increase time consumed by experimental work. In all test problems presented here, a 20 μm depth resolution gave satisfactory results, and is considered as a reasonable resolution to perform experimental measurements.

The number of the discretion elements, the value n, is generally a very important parameter affecting the accuracy of a numerical method. With smaller n values, the solutions acquired generally become less accurate or even unstable, whereas a larger n value leads to higher computational cost (Hutton, 2003). In the simulated test problems, with $n < 50$, oscillating results were sometimes generated when low depth resolution was used. However, with $n = 50$, no oscillating solutions were generated, and an increase of n to values higher than 50 produced no significant improvement in the results acquired (not shown). Interpolation of data points is needed if an n larger than the number of measurement positions is used (as for a depth resolution of 20 μm and $n = 50$ for a 500 μm thick biofilm). This, as described above, was carried out by simply assuming that the value changes linearly between two adjacent points. Several curve fitting methods can be used to improve the quality of the interpolation, however, if this is to be used with lower measurement resolutions, caution must be taken, since the fitted curve might reflect the wrong trend (Guest, 1961; Motulsky and Ransnas, 1987; Wahba, 1990).

Microsensor data collected from a highly active non-submerged phototrophic biofilm of *Halochlorella rubescens* cultivated using a Twin-Layer photobioreactor system (Schultze et al., 2015) was chosen in this study to test the proposed mathematical treatment: The correction of direct microsensor data recovered the real photosynthesis profile in terms of ETR favourably compared to the uncorrected profile (directly measured). In the uncorrected profiles, a decrease of activity near the biofilm surface was observed, but this was not reflected by the ETR measurement. The ETR was used in several studies to estimate the gross photosynthetic activity in phototrophic biofilms (Banares-Espana et al., 2013; Barranguet and Kromkamp, 2000; Flameling and Kromkamp, 1998) and ETR values reported here are in the same ranges as observed e.g. by Kromkamp et al. (2001) in a biofilm dominated by a cyanobacterium. A direct comparison between the ETR and the recovered distribution from the light-dark shift method, however, has to be treated with caution: the microsensor method is generally recognized as a non-destructive and in-situ method (Nivens et al., 1995). In contrast, the ETR determination in combination with biofilm sectioning as applied in this work is neither in-situ nor non-destructive. Sectioning places cells at the biofilm surface, which previously have been located deeper inside the biofilm. This changes the concentrations of oxygen and CO_2 that the cells were originally exposed to. Nevertheless, a general comparison of the trends of the recovered photosynthesis and measured ETR profiles can be made. In this sense, the recovered profile reflects the photosynthetic activity distribution better than the uncorrected direct measurement data. The reason for this discrepancy between recovered and direct profiles was very likely, the removal of dissolved oxygen at the biofilm surface.

The accuracy of the proposed method depends strongly on the accurate determination of the effective diffusion coefficient and the advection rate in the biofilm. The effective diffusion coefficient in a biofilm depends on porosity and tortuosity, and the molecular size of the diffusing species as well as its affinity to biomass (IWA Task Group on Biofilm Modelling, 2006; Melo, 2005). Several methods have been developed for measuring or estimating the effective diffusion coefficient of dissolved oxygen in biofilms, however, all of these methods show individual weaknesses (Stewart, 1998; Wood et al., 2002). Considering a biofilm with a strongly depth-dependent structural heterogeneity, the situation becomes even more complex (Ramanan et al., 2013). In the simulated test problems shown here, the coefficient used to generate the simulated data points was the same as that used for recovery, thus no error is expected to originate from the effective diffusion coefficient. However, in a real situation, in which the true effective diffusion coefficient is unknown (e.g. effective diffusion coefficient has been estimated from porosity in the real biofilm test problems in this study, as described in section 2.5, since the observation during the sectioning suggested the cells in the biofilm behaved similarly to a densely packed porous medium), an inaccurate effective diffusion coefficient can lead to false estimations. On the other hand, the determination of the advection rate is relatively straightforward (using Eq.2), and, therefore, is no critical factor for the accuracy of the method.

We conclude that the proposed mathematical procedure can be applied with no further modification to microsensor data acquired by the light-dark shift method from biofilms with a very thin flow boundary layer as can be found in aerial biofilms or submerged biofilms subjected to a high flow rate in the bulk liquid. Furthermore, with minor modifications of the boundary conditions used for discretion, the method can also be used to recover the actual distribution of photosynthesis from measurements done on biofilms with a thicker boundary layer to overcome limitations of the currently used methods.

References:

Bachar A, Polerecky L, Fischer JP, Vamvakopoulos K, de Beer D, Jonkers HM. 2008. Two-dimensional mapping of photopigment distribution and activity of Chloroflexus-like bacteria in a hypersaline microbial mat. FEMS Microbiology Ecology 65(3):434-448.

Baker CTHs, Fox L, Mayers DF, Wright K. 1964. Numerical solution of Fredholm integral equations of first kind. The Computer Journal 02(7(2)):141-147.

Banares-Espana E, Kromkamp JC, Lopez-Rodas V, Costas E, Flores-Moya A. 2013. Photoacclimation of cultured strains of the cyanobacterium Microcystis aeruginosa to high-light and low-light conditions. FEMS Microbiology Ecology 83(3):700-710.

Barranguet C, Kromkamp J. 2000. Estimating primary production rates from photosynthetic electron transport in estuarine microphytobenthos. Marine Ecology Progress Series 204:39-52.

Bergman TL, Lavine AS, Incropera FP, DeWitt DP. 2011. Fundamentals of heat and mass transfer. Hoboken, New Jersey, USA: John Wiley & Sons.

Berner F, Heimann K, Sheehan M. 2014. Microalgal biofilms for biomass production. Journal of Applied Phycology:1-12.

Bernstein HC, Kesaano M, Moll K, Smith T, Gerlach R, Carlson RP, Miller CD, Peyton BM, Cooksey KE, Gardner RD and others. 2014. Direct measurement and characterization of active photosynthesis zones inside wastewater remediating and biofuel producing microalgal biofilms. Bioresource Technology 156:206-215.

Beutler M, Hinck S, de Beer D. 2009. A method for imaging of low pH in live cells based on excited state saturation. Journal of Microbiological Methods 77(1):98-101.

Bischoff HW, Bold HC. 1963. Some soil algae from Enchanted Rock and related algal species. Austin, Texas, USA: University of Texas Press. 95 p.

Calvetti D, Morigi S, Reichel L, Sgallari F. 2000. Tikhonov regularization and the L-curve for large discrete ill-posed problems. Journal of Computational and Applied Mathematics 123(1–2):423-446.

Courant R, Isaacson E, Rees M. 1952. On the solution of nonlinear hyperbolic differential equations by finite differences. Communications on Pure and Applied Mathematics 5(3):243-255.

Crank J, editor. 1975. Mathematics of diffusion. 2nd ed. Oxford, UK: Oxford University Press.

Flameling IA, Kromkamp J. 1998. Light dependence of quantum yields for PSII charge separation and oxygen evolution in eucaryotic algae. Limnology and Oceanography 43(2):284-297.

Genty B, Briantais J-M, Baker NR. 1989. The relationship between the quantum yield of photosynthetic electron transport and quenching of chlorophyll fluorescence. Biochimica et Biophysica Acta (BBA) - General Subjects 990(1):87-92.

Gieseke A, de Beer D. 2004. Use of microelectrodes to measure in situ microbial activities in biofilms, sediments, and microbial mats. In: Kowalchuk GA, de Bruijn FJ, Head IM, Akkermans AD, van Elsas JD, editors. Molecular Microbial Ecology Manual. The Netherlands: Springer. p 3483-3514.

Gill PE, Murray W, Wright MH. 1981. Practical optimization. Waltham, Massachusetts, USA: Academic Press. 401 p.

Glud RN, Ramsing NB, Revsbech NP. 1992. Photosynthesis and photosynthesis-coupled respiration in natural biofilms quantified with oxygen microsensors. Journal of Phycology 28(1):51-60.

Guest PG. 1961. Numerical methods of curve fitting. Cambridge, UK: Cambridge University Press. 438 p.

Hansen P. 1994. REGULARIZATION TOOLS: A Matlab package for analysis and solution of discrete ill-posed problems. Numerical Algorithms 6(1):1-35.

Hansen PC. 1992. Numerical tools for analysis and solution of fredholm integral-equations of the 1st kind. Inverse Problems 8(6):849-872.

Hansen PC, O'Leary DP. 1993. The Use of the L-Curve in the Regularization of Discrete Ill-Posed Problems. SIAM Journal on Scientific Computing 14(6):1487-1503.

Herlory O, Richard P, Blanchard GF. 2007. Methodology of light response curves: application of chlorophyll fluorescence to microphytobenthic biofilms. Marine Biology 153(1):91-101.

Hillebrand H, Durselen CD, Kirschtel D, Pollingher U, Zohary T. 1999. Biovolume calculation for pelagic and benthic microalgae. Journal of Phycology 35(2):403-424.

Hofstraat JW, Peeters JCH, Snel JFH, Geel C. 1994. Simple determination of photosynthetic efficiency and photoinhibition of dunaliella-tertiolecta by saturating pulse fluorescence measurements. Marine Ecology Progress Series 103(1-2):187-196.

Hutton DV. 2003. Fundamentals of finite element analysis. New York City, USA: McGraw-Hill. 512 p.

IWA Task Group on Biofilm Modelling. 2006. Mathematical modeling of biofilms. London, UK: IWA Publishing. 179 p.

Kress R, editor. 2014. Linear integral equations. 3rd ed. New York City, USA: Springer. 412 p.

Kromkamp JC, Domin A, Dubinsky Z, Lehmann C, Schanz F. 2001. Changes in photosynthetic properties measured by oxygen evolution and variable chlorophyll fluorescence in a simulated entrainment experiment with the cyanobacterium Planktothrix rubescens. Aquatic Sciences 63(3):363-382.

Kühl M, Lassen C, Jorgensen B. 1994a. Optical properties of microbial mats: Light measurements with fiber-optic microprobes. In: Stal L, Caumette P, editors. Microbial Mats. Berlin/Heidelberg, Germany: Springer. p 149-166.

Kühl M, Lassen C, Jorgensen BB. 1994b. Light penetration and light-intensity in sandy marine-sediments measured with irradiance and scalar irradiance fiberoptic microprobes. Marine Ecology Progress Series 105(1-2):139-148.

Kühl M, Polerecky L. 2008. Functional and structural imaging of phototrophic microbial communities and symbioses. Aquatic Microbial Ecology 53(1):99-118.

Lassen C, Glud RN, Ramsing NB, Revsbech NP. 1998. A method to improve the spatial resolution of photosynthetic rates obtained by oxygen microsensors. Journal of Phycology 34(1):89-93.

Melo LF. 2005. Biofilm physical structure, internal diffusivity and tortuosity. Water Science and Technology 52(7):77-84.

Motulsky HJ, Ransnas LA. 1987. Fitting curves to data using nonlinear-regression - a practical and nonmathematical review. FASEB Journal 1(5):365-374.

Murphy TE, Fleming E, Berberoglu H. 2014. Vascular Structure Design of an Artificial Tree for Microbial Cell Cultivation and Biofuel Production. Transport in Porous Media 104(1):25-41.

Naumann T, Cebi Z, Podola B, Melkonian M. 2013. Growing microalgae as aquaculture feeds on twin-layers: a novel solid-state photobioreactor (vol 25, pg 1413, 2013). Journal of Applied Phycology 25(5):1619-1619.

Neumaier A. 1998. Solving ill-conditioned and singular linear systems: A tutorial on regularization. SIAM Review 40(3):636-666.

Nivens DE, Palmer RJ, White DC. 1995. Continuous nondestructive monitoring of microbial biofilms - a review of analytical techniques. Journal of Industrial Microbiology 15(4):263-276.

Nowack ECM, Podola B, Melkonian M. 2005. The 96-Well Twin-Layer System: A Novel Approach in the Cultivation of Microalgae. Protist 156(2):239-251.

Pessarakli M, editor. 2005. Handbook of photosznthesis. 2nd ed. Boca Raton, Florida, USA: CRC Press. 952 p.

Platt T, Gallegos CL, Harrison WG. 1980. Photoinhibition of photosynthesis in natural assemblages of marine phytoplankton. Journal of Marine Research 38:687-701.

Polyanin AD. 2002. Handbook of linear partial differential equations for engineers and scientists. Boca Raton, Florida: Chapman&Hall/CRC Press.

Ralph PJ, Gademann R, Larkum AWD, Schreiber U. 1999. In situ underwater measurements of photosynthetic activity of coral zooxanthellae and other reef-dwelling dinoflagellate endosymbionts. Marine Ecology Progress Series 180:139-147.

Ramanan B, Holmes WM, Sloan WT, Phoenix VR. 2013. Magnetic Resonance Imaging of Mass Transport and Structure Inside a Phototrophic Biofilm. Current Microbiology 66(5):456-461.

Revsbech NP. 1983. In Situ Measurement of Oxygen Profiles of Sediments by use of Oxygen Microelectrodes. In: Gnaiger E, Forstner H, editors. Polarographic Oxygen Sensors. Berlin/Heidelberg, Germany: Springer. p 265-273.

Revsbech NP. 1989. An oxygen microsensor with a guard cathode. Limnology and Oceanography 34(2):4.

Revsbech NP, Jorgensen BB. 1983. Photosynthesis of benthic microflora measured with high spatial-resolution by the oxygen microprofile method - capabilities and limitations of the method. Limnology and Oceanography 28(4):749-756.

Revsbech NP, Jorgensen BB, Brix O. 1981. Primary production of microalgae in sediments measured by oxygen microprofile, $H^{14}CO_3^-$ fixation, and oxygen-exchange methods. Limnology and Oceanography 26(4):717-730.

Revsbech NP, Madsen B, Jorgensen BB. 1986. Oxygen production and consumption in sediments determined at high spatial-resolution by computer-simulation of oxygen microelectrode data. Limnology and Oceanography 31(2):293-304.

Roeselers G, Loosdrecht MCMv, Muyzer G. 2008. Phototrophic biofilms and their potential applications. Journal of Applied Phycology 20(3):227-235.

Schlichting H, Gersten K. 2000. Boundary-layer theory. Berlin/Heidelberg, Germany: Springer. 800 p.

Schultze LKP, Simon M-V, Li T, Langenbach D, Podola B, Melkonian M. 2015. High light and carbon dioxide optimize surface productivity in a Twin-Layer biofilm photobioreactor. Algal Research-Biomass Biofuels and Bioproducts 8:37-44.

Seckbach J, Oren A, editors. 2010. Microbial mats - modern and ancient microorganisms in stratified systems. the Netherlands: Springer. 606 p.

Shi J, Podola B, Melkonian M. 2007. Removal of nitrogen and phosphorus from wastewater using microalgae immobilized on twin layers: an experimental study. Journal of Applied Phycology 19(5):417-423.

Stewart G. 1973. Introduction to matrix computations. Waltham, Massachusetts, USA: Academic Press. 441 p.

Stewart PS. 1998. A review of experimental measurements of effective diffusive permeabilities and effective diffusion coefficients in biofilms. Biotechnology and Bioengineering 59(3):261-272.

Tikhonov AN, Goncharsky A, Stepanov VV, Yagola AG. 1995. Numerical methods for the solution of ill-posed problems. the Netherlands: Springer. 254 p.

Varah JM. 1983. Pitfalls in the numerical-solution of linear ill-posed problems. Siam Journal on Scientific and Statistical Computing 4(2):164-176.

Wahba G. 1990. Spline models for observational data. Philadelphia, Pennsylvania, USA: SIAM Press. 169 p.

Weissberg HL. 1963. Effective diffusion coefficient in porous media. Journal of Applied Physics 34(9):2636-2639.

Wolf G, Picioreanu C, van Loosdrecht MCM. 2007. Kinetic modeling of phototrophic biofilms: The PHOBIA model. Biotechnology and Bioengineering 97(5):1064-1079.

Wood BD, Quintard M, Whitaker S. 2002. Calculation of effective diffusivities for biofilms and tissues. Biotechnology and Bioengineering 77(5):495-516.

2.2. Microscale profiling of photosynthesis-related variables in a highly productive biofilm photobioreactor.

Presented here in the accepted version, reformatted for the presentation in this thesis.

Microscale profiling of photosynthesis-related variables in a highly productive biofilm photobioreactor

Tong Li[1*], Bastian Piltz[1], Björn Podola[1], Anthony Dron[2,3], Dirk de Beer[2] & Michael Melkonian[1]

[1]Universität zu Köln, Botanisches Institut, 50674 Köln, Germany;

[2]Max-Planck-Institut für Marine Mikrobiologie, 28359 Bremen, Germany

[3]Present address: Sustainable Energy, Air & Water Technology, Department of Bioscience

Engineering, University of Antwerp, Groenenborgerlaan 171, 2020 Antwerp, Belgium

*Corresponding Author: Tong Li

Universität zu Köln, Botanisches Institut, Biozentrum Köln, 50674 Köln, Germany

Phone: +49 (0)221-470 8090

Email: lit2@uni-koeln.de

Running head: Profiling biofilm in photobioreactor

Abstract

In the present study depth profiles of light, oxygen, pH and photosynthetic performance in an artificial biofilm of the green alga *Halochlorella rubescens* in a porous substrate photobioreactor were recorded with microsensors. Biofilms were exposed to different light intensities (50 – 1,000 µmol photons m^{-2} s^{-1}) and CO_2 levels (0.04 – 5 % v/v in air). The distribution of photosynthetically active radiation showed almost identical trends for different surface irradiances, namely: a relatively fast drop to a depth of about 250 µm, (to 5% of the incident), followed by a slower decrease. Light penetrated into the biofilm deeper than the Lambert-Beer Law predicted, which may be attributed to forward scattering of light, thus improving the overall light availability. Oxygen concentration profiles showed maxima at a depth between 50 and 150 µm, depending on the incident light intensity. A very fast gas exchange was observed at the biofilm surface. The highest oxygen concentration of 3.2 mM was measured with 1,000 µmol photons m^{-2} s^{-1} and 5% supplementary CO_2. Photosynthetic productivity increased with light intensity and/or CO_2 concentration and was always highest at the biofilm surface; the stimulating effect of elevated CO_2 concentration in the gas phase on photosynthesis was enhanced by higher light intensities. The dissolved inorganic carbon concentration profiles suggest that the availability of the dissolved free CO_2 has the strongest impact on photosynthetic productivity. The results suggest that dark respiration could explain previously observed decrease in growth rate over cultivation time in this type of PSBR.

Our results represent a basis for understanding the complex dynamics of environmental variables and metabolic processes in artificial phototrophic biofilms exposed to a gas phase and can be used to improve the design and operational parameters of PSBRs.

Key words

Phototrophic biofilm, Microalgae, Photobioreactor, Microsensor, Photosynthesis parameters

Introduction

Recent advances in the design of bioreactors for the cultivation of microalgae have focussed on immobilization of these organisms as a phototrophic biofilm (reviewed by Berner et al. 2014; Olivieri et al. 2014; Gross et al. 2015). An efficient type of biofilm bioreactor features a non-submerged biofilm exposed directly to light and a gas phase, and separated from the bulk of culture medium by a fine-porous sheet-like material (e.g., a microporous membrane). The principle of this biofilm bioreactor was introduced a decade ago by Podola and Melkonian (2003) as the 'Twin-Layer' (Nowack et al. 2005), now referred to in a more general term as 'porous substrate bioreactors' (PSBRs) (Murphy and Berberoglu 2014). Compared to other photobioreactors (e.g. suspension systems), PSBRs display fundamental advantages with respect to: biomass harvesting, water/energy consumption, the spectrum of applications and microalgal species that can be cultivated (e.g. Shi et al., 2007; Naumann et al., 2013; Benstein et al. 2014). Recent studies using high light and CO_2 levels and/or modifications of reactor design have documented high biomass productivities in PSBRs with respect to reactor surface (> 30 g *dw* m^{-2} d^{-1}; Schultze et al., 2015) as well as ground area (> 60 g *dw* m^{-2} d^{-1}; Liu et al., 2013; Zhang et al., 2015). Also, research performed at pilot-scale (Naumann et al., 2013; Shi et al., 2014; Zhang et al., 2015) demonstrated the proof of principle and a significant potential of PSBRs for commercial-scale microalgal cultivation.

Consequently, as a next step, more basic research is required to understand the dynamics of light, mass transfer, productivity and their interactions in PSBR biofilms, since this knowledge is essential for a systematic and comprehensive approach aimed at process optimization. For example, in several studies continuously decreasing growth rates were reported during prolonged cultivation of microalgae in PSBRs (Cheng et al., 2013; Ji et al., 2014; Schultze et al., 2015), possibly caused by respiration in the increasingly thicker non-illuminated zones of a growing biofilm. Moreover, oxygen generated by photosynthesis can accumulate to high concentrations in photosynthetic biofilms (Pringault and Garcia-Pichel, 2000). In suspension cultures oxygen accumulation is known to inhibit net productivity by photorespiration, or by formation of free oxygen radicals.

Several high resolution methods (Revsbech and Jorgensen, 1983; Wolf et al., 2007; Kühl and Polerecky, 2008; Ramanan et al., 2013) have been used on natural biofilms. Among others, microsensors offer direct, non-destructive and in-situ measurements and have been successfully applied to submerged phototrophic biofilms since the 1980s (Revsbech, 1983; Revsbech and Jorgensen, 1983). The data from these previous studies, however, does not apply to non-submerged artificial biofilms due to significant differences in the system setup (e.g. direct exposure to the atmosphere) and species composition of the biofilm (Tampion and Tampion, 1987; Podola and Melkonian, 2003; Seckbach and Oren, 2010).

In this study, we used microsensors to acquire depth profiles of light, oxygen, pH, and photosynthetic activity inside a highly active biofilm of the green alga *Halochlorella rubescens*, cultivated in a Twin-Layer PSBR at different light intensities and exposed to various CO_2 levels. The data obtained were used to describe the dynamics in a PSBR for the first time in detail. Based on the results obtained, we discuss the specific strengths of PSBRs and identify parameters for further optimization in these novel photobioreactors.

Materials and Methods

Microalgal cultivation

A suspension culture of the green alga *Halochlorella rubescens* (CCAC 0126; Culture Collection of Algae at the University of Cologne; www.ccac.uni-koeln.de) was used for biofilm inoculation and cultivation according to Schultze et al. (2015). The same strain has been used in previous studies, and is known to form a fast-growing phototrophic biofilm (Schultze et al., 2015). After inoculation, biofilms were pre-cultivated with a PAR light intensity of 300 µmol photons m^{-2} s^{-1} at the biofilm surface. After 14 days, filters were subjected to different PAR light intensities of 50, 300, and 1,000 µmol photons m^{-2} s^{-1} for 10 days. Microsensor measurements were then also conducted at these three light intensities. For cultivation and during measurements the temperature was kept at 23 ± 1 ºC, and Bold's Basal Medium (BBM; Bischoff and Bold, 1963) was used.

Microsensor measurements setup

The experimental setup and calibration of the microsensor system is based on the work of Gieseke and de Beer (2004) and the experimental setup is described in detail in the supplementary materials (Li et al., 2015). Oxygen microsensors with tip diameters < 10 µm and a response time ≤ 0.5 s were build and used as described previously (accurate to µM range, and with a stirring effect of less than 4%; Revsbech, 1989). Liquid ion exchange (LIX) type pH microsensors with accuracy of more than 0.01 pH unit and measurement range from pH 3 to 11 were used in the present study to measure pH profiles (Lee and de Beer, 1995). pH microsensors were calibrated according to de Beer et al. (2008). Irradiance profiles were recorded for all three incident light intensities with spherical tip irradiance microsensor with a tip diameter of 80 µm (Lassen et al, 1992), which was connected to a spectrophotometer (USB 4000, Ocean optics, Dunedin, USA). The measured irradiance data was integrated over wavelength bands to give estimations of the total, red, green and blue PAR intensities (400 – 700, 400 – 500, 500 – 600 and 600 – 700 nm, respectively). For each incident irradiance , the concentration of dissolved oxygen ([DO]), the pH and the photosynthetic activity profiles were recorded for different CO_2 levels in aeration applied onto the biofilm surface: 0.039 % (dry ambient air), and 1%, 3%, and 5 % CO_2 (dry ambient air with supplementary CO_2 v/v). When CO_2 levels were changed, biofilms in the measurement cell were adapted for 15 min prior to the microsensor measurements (which was sufficient for the biofilm to reach steady state, as measurements taken between 5 min to 1 hour after measurement conditions had been changed have produced profiles with no significant difference). Profiles were also recorded in biofilms subjected to darkness and aerated with dry ambient air (dark measurement). Prior to dark measurements, biofilms were incubated in the measurement cell for 3 hours without illumination.

All microsensor measurements were carried out with a 20 µm depth resolution. [DO] and pH profiles were acquired from 3 positions on the same biofilm sample (triplicates). Light and gross photosynthetic productivity profiles were acquired by using the method described in the supplementary materials (Li et al., 2015). Gross productivity measurements were carried out until a depth at which the shift from light to dark did not have significant effects on the [DO] within the measurement period (200, 400 and 500 µm for biofilms exposed to 50, 300 and 1,000 µmol m^{-2}

s^{-1}, respectively). Attenuation coefficients (extinction per unit depth, in mm^{-1}) of the PAR in the biofilms were calculated as described by Lassen et al. (1992).

Calculation for net productivity and dissolved inorganic carbon profiles

Net photosynthetic productivity was calculated from the steady state [DO] profiles using the mass balance equation (Bergman et al., 2011, Revsbech and Jorgensen, 1983):

$$P_n = -D_{e,O_2} \frac{\partial^2 [DO]}{\partial x^2} - u \frac{\partial [DO]}{\partial x}$$ (Eq. 1)

P_n is the net productivity, D_{e,O_2} is the effective diffusion coefficient of oxygen in biofilm, x is the depth and u is the convective flow rate in the biofilm perpendicular to its surface (due to surface evaporation). D_{e,O_2} and u were estimated from the measured biofilm porosity and the measured evaporation rate using the technique as described in supplementary materials (Li et al., 2015). The measurement showed no significant difference between biofilms exposed to different PAR light intensities and at different depths (Two-way ANOVA test). Porosity was measured to be 0.76 in *the H. rubescens* Twin-Layer biofilm, and D_{e,O_2} was calculated to be 0.68 of that in pure water, u was calculated to be 5.4 µm s^{-1} (Weissberg, 1963). To acquire the derivatives needed in Eq.1, 6th order polynomial curves were fitted to the steady state [DO] profiles (R^2 values $\geq$ 0.98; *curve fitting toolbox*, MATLAB, version 2013a, MathWorks, Ismaning, Germany).The derivatives were then calculated from the polynomial curves (de Beer, 2001). The thickness of the biofilms was estimated using a hand microtome as described in supplementary materials (Li et al., 2015). All statistical analysis were performed using GraphPad Prism v5.02 (GraphPad Software Inc., La Jolla, USA). For calculation, 1.99 × 10^{-9} m^2 s^{-1} was taken as diffusion coefficient of oxygen in water (Han and Bartels, 1996).

An estimation of the distribution of dissolved inorganic carbon concentrations ([DIC]) can be calculated using the DIC consumption rate distribution together with the CO_2 concentration in the gas phase and the measured pH profiles: Assuming DIC consumption to oxygen production has a 1:1 ratio (mole to mole), the photosynthetic productivity profiles can be used to estimate the consumption rate distribution of the [DIC]. Using the equation provided by Morel and Hering (1993), the total [DIC] at the biofilm surface can be calculated as (considering that the hydration of CO_2 at the biofilm surface is instantaneous, which is the ideal case):

$$DIC_{surface} = H_{CO_2} \cdot p_{CO_2} \cdot \left(1 + \frac{K_{a1}}{10^{-pH_{surface}}} + \frac{K_{a1} \cdot K_{a2}}{\left(10^{-pH_{surface}}\right)^2}\right)$$ (Eq.2),

H_{CO_2} is the Henry's constant for CO_2, and has a value of 0.304 mM kpa^{-1}; p_{CO_2} is the CO_2 partial pressure in the gas phase, K_{a1} and K_{a2} are the dissociation coefficients of carbonic acid and bicarbonate ion, with value of 10$^{-6.3}$ and 10$^{-10.3}$, respectively; $pH_{surface}$ is the measured pH value at the biofilm surface (Murphy and Berberoglu, 2014; Wolf et al., 2007). Distribution of the total [DIC] at depth x can be acquired from a transformation of mass balance equation:

$$[DIC]_x = [DIC]_{surface} - \frac{\int_0^x P_n \cdot dx}{\left(\frac{D_{e,DIC}}{x} - u\right)}$$ (Eq.3),

$D_{e,DIC}$ is the effective diffusion coefficient of DICs in biofilm, and was assumed to equal the value of bicarbonate ions, which has a value of 1.18×10^{-9} m^2 s^{-1} in pure water (Murphy and Berberoglu, 2014). DIC speciation at depth x was calculated from the measured pH profiles:

$$\begin{cases} [CO2]_x = [DIC]_x \cdot \dfrac{1}{1+\frac{K_{a1}}{10^{-pH_x}}+\frac{K_{a1} \cdot K_{a2}}{(10^{-pH_x})^2}} \\[2ex] [HCO3^-]_x = [DIC]_x \cdot \dfrac{K_{a1}/10^{-pH_x}}{1+\frac{K_{a1}}{10^{-pH_x}}+\frac{K_{a1} \cdot K_{a2}}{(10^{-pH_x})^2}} \\[2ex] [CO3^{2-}]_x = [DIC]_x \cdot \dfrac{K_{a1} \cdot K_{a2}/(10^{-pH_x})^2}{1+\frac{K_{a1}}{10^{-pH_x}}+\frac{K_{a1} \cdot K_{a2}}{(10^{-pH_x})^2}} \end{cases} \qquad (Eq.4).$$

Results

Biofilm thickness and appearance

The thickness of the biofilms grown at different light intensities was significantly different: around 320, 700 and 800 μm for biofilms exposed to 50, 300 and 1000 μmol photons m^{-2} s^{-1}, respectively. Visually, no color difference between the biofilms exposed to different light intensities could be observed.

Light

PAR profiles in *H. rubescens* biofilms exposed to different light intensities as the percentage of the total PAR measured at the biofilm surface and the calculated attenuation coefficients are presented in Fig. 1. Since spherical irradiance sensors with tip diameters of 80 μm were used, the irradiances of the first 80 μm were overestimated (Fig. 1), as the tip was not fully immersed in the biofilm. The PAR distributions from biofilms exposed to 50, 300 and 1000 μmol photons m^{-2} s^{-1} exhibit nearly identical trends: A relatively sharp decrease from the surface to about 250 μm depth, followed by a smoother reduction to less than 1% of the surface irradiance at a depth of around 350 μm. Irradiance in the blue, green and red ranges of the PAR also behaved similarly in biofilms exposed to different PAR intensities at the surface. In all cases, the intensity of blue light at the biofilm surface was the lowest and the first to be absorbed completely by the biomass. Attenuation coefficients showed similar tendencies for biofilms exposed to different light intensities: An increase from the biofilm surface to a maximal value (at around 200 μm), followed by a decrease. However, biofilms exposed to lower irradiance were observed to have higher attenuation coefficients (both the measured maximum and the average). Also, in Fig. 1, a 'dark zone' (non-illuminated region) can be observed in thicker biofilms (biofilm cultivated at 300 or 1000 μmol m^{-2} s^{-1}).
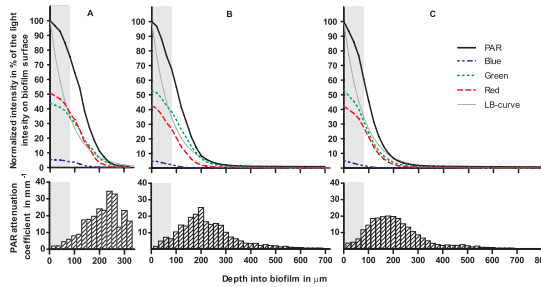
Figure 1: Intensity and attenuation coefficient of photosynthetically active radiation (PAR) in *Halochlorella rubescens* biofilms exposed to different light intensities. **A**: Biomass exposed to 50 µmol photons m^{-2} s^{-1}; **B**: Biomass exposed to 300 µmol photons m^{-2} s^{-1}; **C**: Biomass exposed to 1000 µmol photons m^{-2} s^{-1}. Intensities are presented in percentage of the total irradiance measured at the biofilm surface. Total PAR intensity, blue (400 to 500 nm), green (500 to 600 nm) and red (600 to 700 nm) are represented by different line styles; the lines represent average values measured in a 3 second period. Bars represent the attenuation coefficient of the complete PAR range. Lengths of x-axis indicates the thickness of the biofilm. The thin solid grey lines show the light distribution profile predicted by Lambert-Beer law with a fixed attenuation coefficient (denoted as LB-curve, and the absorption coefficient used for the calculation of the LB-curve was selected so, that the LB-curve have the same penetration depth as the measured profile). The grey areas indicate the depth in which the tip of the sensor was not fully immersed in the biofilm.

Oxygen and pH

[DO] profiles measured under illumination displayed similar shapes for all incident PAR and CO_2 levels (Fig. 2): Increasing from air saturation (0.274 mM) at the biofilm surface to a maximum at a depth between 50 and 150 µm, depending on light intensity and CO_2 levels. The maximum was followed by a decrease to values lower than the [DO] at the biofilm surface (from 180, 460 and 630 µm inwards for biofilms exposed to 50, 300 and 1000 µmol photons m^{-2} s^{-1}, respectively). The [DO] and its maximal value increased with light intensities and/or with an increase of CO_2 in the gas phase. The effect of CO_2 was more prominent when combined with higher PAR light intensities. The highest [DO] of 3.2 mM was measured in biofilms exposed to 1000 µmol photons m^{-2} s^{-1} aerated with 5% supplementary CO_2 (Fig. 2).
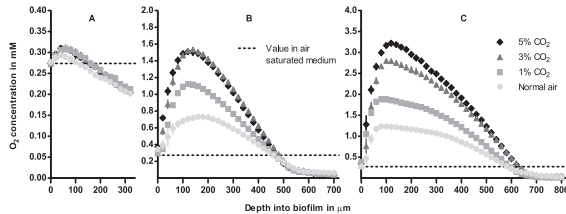
Figure 2: Concentration of dissolved oxygen ([DO]) profiles in *Halochlorella rubescens* biofilms exposed to different light intensities and aerated with different carbon dioxide concentrations. **A**: Biomass exposed to 50 µmol photons m^{-2} s^{-1}; **B**: Biomass exposed to 300 µmol photons m^{-2} s^{-1}; **C**: Biomass exposed to 1000 photons µmol m^{-2} s^{-1}. The marks and the error bars represent the means and standard deviations of triplicates; dotted line represents [DO] in BBM (Bold's Basal Medium) saturated with air. Lengths of x-axis indicates the thickness of the biofilm. Note the differences in oxygen concentration scales (y-axis) for different light intensities.

Fig. 3 shows pH profiles measured in illuminated biofilms. With 50 µmol photons m^{-2} s^{-1} PAR light intensity, the pH profiles displayed a maximum at the biofilm surface and decreased with depth. In biofilms exposed to 300 and 1,000 µmol photons m^{-2} s^{-1}, however, the pH first increased with depth, resulting in a maximum between 100 and 200 µm. Stronger PAR light intensities lead to higher pH values, whereas higher CO_2 concentrations reduced the

pH (Fig. 3). Furthermore, high CO_2 concentrations smoothened the peaks of the pH profiles in biofilms exposed to 300 and 1000 µmol photons m^{-2} s^{-1}. The maximal pH value measured was more than 10 (at 1,000 µmol photons m^{-2} s^{-1} with no additional CO_2), and was much higher than the pH value measured at the interface between biomass and support membrane (i.e. at the bottom) of the same biofilm.
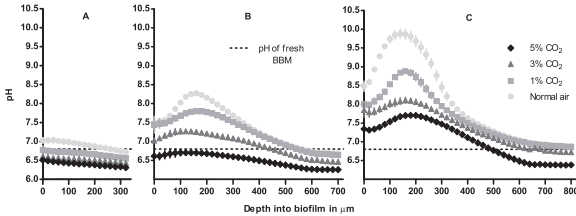
Figure 3: pH profiles in *Halochlorella rubescens* biofilms exposed to different light intensities and aerated with different carbon dioxide concentrations. **A**: Biomass exposed to 50 µmol m^{-2} s^{-1}; **B**: Biomass exposed to 300 µmol photons m^{-2} s^{-1}; **C**: Biomass exposed to 1000 photons µmol m^{-2} s^{-1}The marks and the error bars represent the means and standard deviations of triplicates; dotted line represents pH value of freshly prepared BBM (Bold's Basal Medium). Lengths of x-axis indicates the thickness of the biofilm.

Fig. 4 presents O_2 and pH profiles in biofilms in the absence of light and supplementary CO_2. Without illumination, the [DO] decreased with depth (Fig. 4 A). In thicker biofilms (biofilm pre-cultivated at 300 and 1000 µmol photons m^{-2} s^{-1}) this decrease reached values of nitrogen gas saturated medium (0 mM) at a depth of around 330 µm and was followed by an increase in deeper layers from 400 µm on. The pH values in the biofilm in the dark did not change with depth and were around 6.8 for all measured depths (Fig. 4 B).
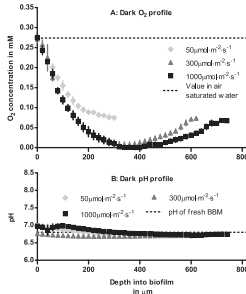
Figure 4: **A**: Dark oxygen profiles in *Halochlorella rubescens* biofilms exposed to different light intensities during cultivation and aerated with dry ambient air. Dotted line represents [DO] in BBM (Bold's Basal Medium) saturated with air. **B**: Dark pH profiles in *H. rubescens* biofilms exposed to different light intensities during cultivation and aerated with dry ambient air. Dashed line represents the pH value of freshly prepared BBM. The marks and the error bars represent the means and standard deviations of triplicates.

Photosynthetic activity

Fig. 5 describes the gross and the net productivity in the Twin-Layer biofilm. The trends of gross and net photosynthetic productivities were similar for all light intensities and CO_2 levels: A productivity maximum was found at the biofilm surface, which then decreased with depth. The net productivity dropped below 0 µmol oxygen m^{-3} s^{-1} in the deeper parts of the biofilms, where respiration was higher than gross photosynthesis. Increase in light intensity always led to an increase in both the maximal productivity and the total productivity (estimated from the total area under the productivity curve, Fig. 5). In contrast, an increase in CO_2 concentration alone did not necessarily lead to an increase in productivity. E.g. for biofilm exposed to 300 µmol m^{-2} s^{-1} an increase from 3% to

5% CO_2 did not lead to an increase in productivity. Generally, the positive effects of CO_2 concentrations on both the gross and net photosynthetic productivities were more pronounced at higher light intensities.

Dissolved inorganic carbon

The calculated [DIC] distributions are given in Fig. 6. Both light intensity and CO_2 in the gas phase influenced the total [DIC] and DIC speciation in the *H. rubescens* biofilms. Total [DIC] in biofilms aerated with additional CO_2 (> 1% v/v) remained almost constant along the depth gradient. Bicarbonate was the dominant DIC species in all measured biofilms, whereas carbonate was only significantly preset in biofilms subjected to high light intensity and low gas phase CO_2 levels (e.g. 1000 µmol photons m^{-2} s^{-1} and normal air). For all measured biofilms, the concentrations of dissolved free CO_2 were higher in the deeper part of the biofilm than near the biofilm surface. In biofilms subjected to 300 µmol photons m^{-2} s^{-1} and aerated with normal air, the total [DIC] dropped to almost 0 mM at around 200 µm depth. Generally, a higher gas phase CO_2 concentration led to higher dissolved free CO_2 levels in the biofilms, but not necessarily to a higher total [DIC] (3% and 5% CO_2 with 1000 µmol photons m^{-2} s^{-1}).
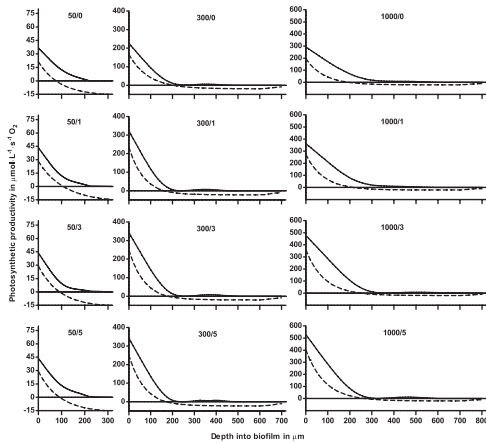
**Figure 5:** Photosynthetic productivity (measured as rates of change of [DO], for details, refer to the method for measuring gross productivity in the supplementary materials) profiles in *Halochlorella rubescens* biofilms exposed to different light intensities and aerated with different carbon dioxide concentrations. Solid line represents the corrected gross productivity; Dotted line gives the calculated net productivity (for graph clarity, SDs were calculated but not shown). The difference between gross productivity and net productivity gives light respiration. Lengths of x-axis indicates the thickness of the biofilm. Light intensities and aeration CO_2 concentrations are marked at the top of each panel (µmol photons m^{-2} s^{-1} / % v/v). Note the differences in photosynthetic productivity scales (y-axis) for different light intensities.
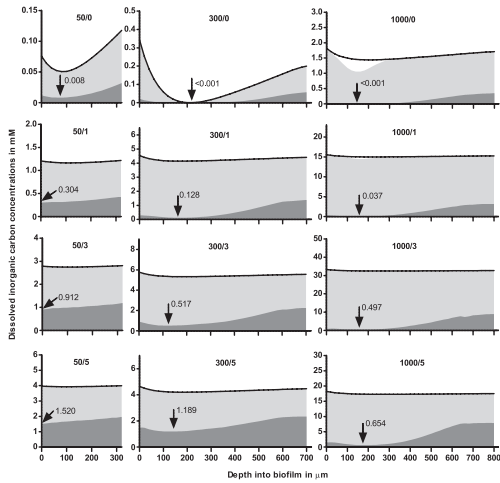
Figure 6: Calculated dissolved inorganic carbon concentration ([DIC]) distribution profiles in *Halochlorella rubescens* biofilms exposed to different light intensities and aerated with different carbon dioxide concentrations. Solid line represents the total [DIC] concentration; the speciation of DIC is represented by the bands under the solid line (Dark grey, light grey and white for free CO_2, bicarbonate and carbonate, respectively). Lengths of x-axis indicates the thickness of the biofilm. Light intensities and aeration CO2 concentrations are marked at the top of each panel (μmol photons m^{-2} s^{-1} / % v/v). The arrows give the position and value of the lowest free CO_2 concentration in biofilm. Note the differences in concentration scales (y-axis) for different panels; carbonate bands (white) are invisible in most of the panels due to very low concentrations.

Discussion

Light distribution as the driving factor for photosynthetic productivity

In the *H. rubescens* biofilms, light profiles did not follow the log distribution of the Lambert-Beer absorption curve (Fig. 1). In addition, no significant difference in the distribution of biomass density along the depth profile was found (see Materials and Methods). Wang et al. (2015) observed that the mass extinction (extinction per unit biomass) was lower in an algal biofilm than in suspension culture. These observations indicate that forward scattering of light by cells and/or adaptation of cellular pigment content plays an important role in light transfer in phototrophic biofilms, reducing the attenuation of light with depth (Kühl et al., 1994; Pringault and Garcia-Pichel, 2000; Berberoglu et al., 2007). As a result, light penetrates deeper into the biofilm, leading to a higher light dilution rate (photons available per cell) in the biofilm, which, in general, is favorable for photobioreactors (e.g. Olivieri et al., 2014). Our measured irradiance profiles showed similar trends for biofilms exposed to different light intensities, however, differences can be observed in the attenuation coefficients (Fig 1): The maximal attenuation coefficients decreased with increasing light intensity, which indicates that a more efficient light uptake was achieved by biofilms exposed to lower light intensities. This suggests an adaptation of the biomass to the light intensity it was exposed to, as it is well known that algal cells can adapt to different light intensities by regulating their pigment content (e.g. Jørgensen, 1969; Richardson et al., 1983). The observed increase of the attenuation coefficient with depth within about 200 μm from the biofilm surface can be a combined effect of this adaptation and the forward

scattering of light. Low irradiances in the deeper parts of the biofilm may lead to pigment degradation, and thus to lower attenuation coefficients. Attenuation distributions with similar trends have been observed by Pringault and Garcia-Pichel (2000) in a submerged artificial cyanobaterial biofilm.

Interactions between photosynthesis and chemical parameters

Since the results showed that the [DO] at the surface of all the measured biofilms were not significantly different from air saturated medium, it was assumed that [DO] at the surface of all biofilms was in equilibrium with the ambient gas phase. This supports the assumption of the existence of only a very thin mass transfer boundary layer in the gas phase adjacent to the biofilm surface that should only offer little resistance to gas transfer (Schlichting and Gersten, 2000). [DO] in the *H. rubescens* biofilm was controlled by photosynthesis, respiration, diffusion, advection inside the biofilm and the removal of dissolved gaseous species at the biofilm surface. Near the surface, [DO] increased with depth. This is due to an excess in production compared to consumption (see Eq. 1). At depths below the [DO] maximum, consumption of oxygen due to respiration and a reduced production (less light and/or CO_2) in the deeper parts of the biofilm led to decreasing [DO] with depth. Similar trends have been observed in submerged phototrophic biofilms (Glud et al., 1992; Pringault and Garcia-Pichel, 2000; Bernstein et al., 2014).

Despite the extremely thin boundary layer, and thus an effective exchange between the gas phase and the biofilm, high oxygen concentrations of up to 3.2 mM were observed in the biofilm (Fig. 2). This is more than 11 times higher than the [DO] in medium (BBM) saturated with air, and is equivalent to a partial pressure of oxygen of 2.4 atm. [DO] reaching a 6-fold concentration of air-saturated water has been measured by Pringault and Garcia-Pichel (2000) in a submerged artificial cyanobacterial biofilm exposed to similar light intensities. How biofilms and mats can establish this oversaturation, and why no development of gas bubbles was observed in the biofilm used in this study needs to be investigated further. Such high oxygen levels should inhibit net photosynthetic productivity, as they favor photorespiration (Spreitzer and Salvucci, 2002). This detrimental effect could be counteracted by carbon concentrating mechanisms (CCM), which elevate the CO_2/O_2 ratio around the RuBisCO (review by Raven et al., 2008).

In biofilms subjected to darkness, oxygen concentrations inside the biofilm were lower than at the surface of the biofilm, presumably due to respiration (Fig. 4). The slight increase of [DO] near the interface between the biofilm and substrate layer observed in thicker biofilms (biofilms grown at 300 and 1000 µmol photons m^{-2} s^{-1}, respectively) can be attributed to the dissolved oxygen supplied from culture medium through the membrane. This was presumably also responsible for the lower [DO] gradients observed in biofilms grown at 50 µmol photons m^{-2} s^{-1} during cultivation. During dark periods, biomass was consumed rather than produced. The loss of productivity due to respiration in the dark period is a known and undesired feature of microalgal mass cultivation (e. g. Grobbelaar and Soeder, 1985), and is particularly pronounced when large suspension volumes are used (e. g. in a raceway pond): the suspension stores the heat absorbed during the day, and due to the large liquid volume, the stored heat is released only relatively slowly (i.e. the temperature remains high for a relatively longer period after the onset of darkness), and thus resulting in higher respiration rates during the night. Since the lowest temperatures in open pond cultivation occur during the morning hours when light is already available for photosynthesis,

suboptimal photosynthetic productivity characterizes the performance of such systems during the first half of the day. Here, a biofilm-based bioreactor might be advantageous by offering a 100 to 1,000-fold lower water content compared to a suspension culture, leading to a significantly faster adoption of ambient temperature by the biomass. Another approach to increase productivity could be the application of continuous illumination. However, artificial illumination for biomass production is clearly uneconomical at a technical scale (e.g., Blanken et al., 2013).

The pH is an important variable regulating biomass productivity in phototrophic biofilms as it controls inorganic carbon speciation (free CO_2, bicarbonate and carbonate; Fig. 6). The pH, has been shown to influence the affinity of algal cells to free CO_2 (Azov, 1982). A high pH value represents a low dissolved free CO_2 concentration, as dissolved free CO_2 can only exist in large quantities in solutions with a pH value lower than 7.5. A further increase in pH in combination with high net oxygen production thus indicates uptake of bicarbonate ions for photosynthesis: at elevated pH, as CO_2 level decreases, it is more likely that organisms rely on uptake of bicarbonate (Fig. 6). Thus the role of carbonic anhydrase, that catalyzes the rapid interconversion of carbon dioxide to carbonic acid, is presumably important for DIC uptake in such biofilms. The uptake of nitrate and phosphate during growth can also elevate the pH. However, due to a slower uptake, the effect can be considered insignificant when compared to the effect of inorganic carbon uptake on pH.

For light intensities of 50 and 300 µmol photons m^{-2} s^{-1}, photosynthesis did not increase further at higher CO_2 levels (e.g. from 3% to 5% CO_2 at 300 µmol m^{-2} s^{-1}; Fig. 2), indicating that light rather than CO_2 was limiting photosynthesis. At 1000 µmol m^{-2} s^{-1}, increasing CO_2 from 3% to 5% did indeed lead to a further increase in photosynthetic activity, showing that the CO_2 supply should be tuned to light intensity to optimize the harvesting of light energy into biomass. In the dark, pH values were stable across the whole biofilm for biofilms exposed to all three light intensities during their cultivation period. This indicates that CO_2 production through respiration during the dark period was not strong enough to influence the local pH, and the phosphate buffer supplied in the medium was sufficient to stabilize the pH. In the 'dark zone' of a light exposed biofilm however, an elevation in pH above the value of the medium was observed. This, instead of being caused by direct CO_2 and/or HCO_3^- consumption by the biomass, may be caused by the shifting of the chemical equilibrium due to transport of CO_2 and/or HCO_3^- to the phototrophically active region, connected with the transport of protons in the opposite direction. With additional CO_2 in the gas phase, the total [DIC] stayed stable along the depth gradient of the biofilms. This indicates that with high CO_2 concentration in the gas phase (> 1% v/v), diffusion was not limiting the supply of DIC to the deeper part of the biofilm. However, the dissolved free CO_2 concentration changed significantly along the depth gradient and with the gas phase CO_2 levels. A higher dissolved free CO_2 resulted in higher productivity, even though a lower total [DIC] was observed (Fig. 5 and 6; biofilms exposed to1000 µmol photons m^{-2} s^{-1}, compare 3% and 5% CO_2). This shows that although the algal cells can utilize bicarbonate for photosynthesis, this is not as efficient as CO_2 assimilation (reviewed by Singh, 2014). By elevating the CO_2 level in the gas phase, the dissolved free CO_2 in the biofilm is increased through an increase in total [DIC] in the biofilm and/or by decreasing the pH in the biofilm.

Biological efficiency and photosynthetic productivity

Gross photosynthetic productivity decreased continuously with depth. Higher light intensities increased the maximum gross productivity, which was found at the surface of all biofilms (Fig. 5). Total gross photosynthetic productivity also increased with higher light intensity due to the increase in the maximum gross productivity as well as the increase in gross productivity in the deeper layers of the biofilm. The latter was caused by deeper light penetration and/or a higher light intensity at a given depth (Fig. 1). Gross photosynthetic productivity is a useful term for evaluating the functional status of a phototrophic biofilm (Gieseke and de Beer, 2004). However, it does not provide information on biomass net productivity, which is an important parameter for evaluating the overall performance of a phototrophic biofilm. Net photosynthetic productivity can be used for such estimations (Gieseke and de Beer, 2004). In a highly active biofilm grown in a porous substrate bioreactor under high light and CO_2 regimes, photorespiration may consume significant amounts of the oxygen as well as biomass produced by photosynthesis considering the very high [DO] (Fig. 2) (Pope, 1975; Birmingham et al., 1982; Larkum et al., 2003). As a result, the net photosynthetic productivities in such biofilms were lower compared to gross photosynthetic activities measured (Fig. 5). Our results show that both the net- and gross productivity integrated over the whole photosynthetic biofilm increased with light intensity, especially when supplementary CO_2 was available. However, when considering a realistic cultivation scenario, the effect of high light intensity and high CO_2 concentration on total biomass productivity would be much more prominent at the start of biofilm cultivation: The increase of the 'dark zone' with time (with biofilm thickness increase) would reduce the net productivity of the biofilm as a whole. Net productivity in these 'dark zones' was reduced to negative values, likely due to respiration. Moreover, for all biofilms, the net productivity dropped to negative values whenever the PAR intensity was below 25 µmol m-2 s-1 ('low light zones', Fig 1 and 5). In these 'low light zones', oxygen produced by photosynthesis was less than the consumption by respiration. This leads to biomass loss in both the 'low light zones' and the 'dark zones', and as a result, a reduction of the net productivity of the biofilm as a whole. This information can be used to determine the time point of biomass harvest, to maintain optimal productivity of the photobioreactor.

Interpretation of the calculated gross productivity data must be made with caution, because the calculation relies on an estimated effective diffusion coefficient of oxygen in the biofilm, which can be a source of error. For the calculation of the net productivity, in addition to the diffusion coefficients, a 6th order polynomial fit can be another source of inaccuracy, even though the R^2 value is high. In the studied biofilm system, the maximum net photosynthetic productivities were always found on the biofilm surface. In submerged biofilms, however, maxima usually occur deeper within the biofilms (Glud et al., 1992; Lassen et al., 1998; Pringault and Garcia-Pichel, 2000). This may be explained by the direct exposure of a non-submerged biofilm to the gas phase with a relatively high gas flow rate. Compared to a submerged surface, a non-submerged biofilm allows much faster removal rates of dissolved oxygen (produced in the biofilm) from its surface due to the very thin mass transfer/flow boundary layer (Schlichting and Gersten, 2000; Bergman et al., 2011). Compared to the deeper parts, cells near the biofilm surface of a non-submerged system had higher gross productivity, but were exposed to lower [DO], which leads to lower photorespiration rates (Larkum et al., 2003). Also, a higher dissolved free CO_2 was observed near the biofilm

surface (Fig. 6). This resulted in a higher net photosynthetic productivity near the biofilm surface. The increase in the net productivity (from negative values towards zero) near the bottom of the biofilm, as observed in thicker biofilms could be explained by limiting dark respiration due to very low oxygen concentrations in this part of the biofilm (Fig. 5).

Conclusions

The present study, using a highly productive *Halochlorella rubescens* biofilm grown in a Twin-Layer porous substrate photobioreactor (TL-PSBR), provides the first in-depth analysis of dynamic processes within such biofilms employing microsensors. The knowledge gained on the distribution of light, oxygen, pH and photosynthetic productivity within the Twin-Layer biofilms provides a sound basis to improve the design of this PSBR towards optimizing microalgal biomass productivity. The present study confirmed the existence of a 'dark zone' in PSBRs subjected to prolonged cultivation, and that its presence can reduce the productivity of PSBRs. However, a dedicated harvesting scheme can be used to minimize this problem (i.e. harvest before the biofilm reaches a thickness to develop 'dark zones'). Furthermore, the data presented could facilitate the modeling of growth in PSBR biofilms in general.

Acknowledgements

References:

Azov Y. 1982. Effect of pH on Inorganic Carbon Uptake in Algal Cultures. Applied and environmental microbiology 43(6):1300-1306.

Benstein RM, Çebi Z, Podola B, Melkonian M. 2014 Immobilized growth of the peridinin-producing marine dinoflagellate *Symbiodinium* in a simple biofilm photobioreactor. Mar. Biotechnol. 16:621-628.

Berberoglu H, Yin J, Pilon L. 2007. Light transfer in bubble sparged photobioreactors for H2 production and CO_2 mitigation. International Journal of Hydrogen Energy 32(13):2273-2285.

Bergman TL, Lavine AS, Incropera FP, DeWitt DP. 2011. Fundamentals of heat and mass transfer. Hoboken, New Jersey, USA: John Wiley & Sons. 1024 p.

Berner F, Heimann K, Sheehan M. 2014. Microalgal biofilms for biomass production. Journal of Applied Phycology:1-12.

Bernstein HC, Kesaano M, Moll K, Smith T, Gerlach R, Carlson RP, Miller CD, Peyton BM, Cooksey KE, Gardner RD and others. 2014. Direct measurement and characterization of active photosynthesis zones inside wastewater remediating and biofuel producing microalgal biofilms. Bioresource Technology 156:206-215.

Birmingham BC, Coleman JR, Colman B. 1982. Measurement of Photorespiration in Algae. Plant Physiology 69(1):259-262.

Bischoff HW, Bold HC. 1963. Some soil algae from Enchanted Rock and related algal species. Austin, Texas, USA: University of Texas Press. 95 p.

Blanken W, Cuaresma M, Wijffels RH, Janssen M. 2013. Cultivation of microalgae on artificial light comes at a cost. Algal Research 2(4):333-340.

Cheng P, Ji B, Gao L, Zhang W, Wang J, Liu T. 2013. The growth, lipid and hydrocarbon production of *Botryococcus braunii* with attached cultivation. Bioresource Technology 138(0):95-100.

de Beer D. 2001. Micro-electrodes. In: Rene H. W., editor. Immobilized Cells. Berlin/Heidelberg, Germany: Springer. p 85-100.

de Beer D, Bissett A, de Wit R, Jonkers H, Köhler-Rink S, Nam H, Kim BH, Eickert G, Grinstain M. 2008. A microsensor for carbonate ions suitable for microprofiling in freshwater and saline environments. Limnology and Oceanography: Methods 6(10):532-541.

Gieseke A, de Beer D. 2004. Use of microelectrodes to measure in situ microbial activities in biofilms, sediments, and microbial mats. In: Kowalchuk GA, de Bruijn FJ, Head IM, Akkermans AD, van Elsas JD, editors. Molecular Microbial Ecology Manual. the Netherlands: Springer. pp 3483-3514.

Glud RN, Ramsing NB, Revsbech NP. 1992. Photosynthesis and photosynthesis-coupled respiration in natural biofilms quantified with oxygen microsensors. Journal of Phycology 28(1):51-60.

Grobbelaar JU, Soeder CJ. 1985. Respiration losses in planktonic green algae cultivated in raceway ponds. J. Plankton Res. 7(4):497-506.

Gross M, Jarboe D, Wen Z. 2015 Biofilm-based algal cultivation systems. Appl. Microbiol. Biotechnol. 99:5781-5789.

Han P, Bartels DM. 1996. Temperature Dependence of Oxygen Diffusion in H_2O and D_2O. The Journal of Physical Chemistry 100(13):5597-5602.

Ji B, Zhang W, Zhang N, Wang J, Lutzu G, Liu T. 2014. Biofilm cultivation of the oleaginous microalgae *Pseudochlorococcum sp*. Bioprocess and Biosystems Engineering 37(7):1369-1375.

Jøsrgensen EG. 1969. The Adaptation of Plankton Algae IV. Light Adaptation in Different Algal Species. Physiologia Plantarum 22(6):1307-1315.

Kühl M, Lassen C, Jorgensen BB. 1994. Light penetration and light-intensity in sandy marine-sediments measured with irradiance and scalar irradiance fiberoptic microprobes. Marine Ecology Progress Series 105(1-2):139-148.

Kühl M, Polerecky L. 2008. Functional and structural imaging of phototrophic microbial communities and symbioses. Aquatic Microbial Ecology 53(1):99-118.

Larkum A, Douglas S, Raven JA, editors. 2003. Photosynthesis in Algae. 1st ed. Dordrecht, The Netherlands: Springer 480 p.

Lassen C, Glud RN, Ramsing NB, Revsbech NP. 1998. A method to improve the spatial resolution of photosynthetic rates obtained by oxygen microsensors. Journal of Phycology 34(1):89-93.

Lassen C, Ploug H, Jørgensen BB. 1992. A fibre-optic scalar irradiance microsensor: application for spectral light measurements in sediments. FEMS Microbiology Letters 86(3):247-254.

Lee WC, de Beer D. 1995. Oxygen and pH microprofiles above corroding mild-steel covered with a biofilm. Biofouling 8(4):273-280.

Li T, Podola B, de Beer D, Melkonian M. 2015. A method to determine photosynthetic activity from oxygen microsensor data in biofilms subjected to evaporation. Journal of Microbiological Methods 117:100-107.

Liu T, Wang J, Hu Q, Cheng P, Ji B, Liu J, Chen Y, Zhang W, Chen X, Chen L and others. 2013. Attached cultivation technology of microalgae for efficient biomass feedstock production. Bioresource Technology 127(0):216-222.

Morel FMM, Hering JG. 1993. Principles and applications of aquatic chemistry. Hoboken, New Jersey, USA: John Wiley & Sons. 588 p.

Murphy TE, Berberoglu H. 2014. Flux balancing of light and nutrients in a biofilm photobioreactor for maximizing photosynthetic productivity. Biotechnology Progress 30(2):348-359.

Naumann T, Cebi Z, Podola B, Melkonian M. 2013. Growing microalgae as aquaculture feeds on twin-layers: a novel solid-state photobioreactor. Journal of Applied Phycology 25(5):1413-1420.

Nowack ECM, Podola B, Melkonian M. 2005. The 96-well twin-layer system: a novel approach in the cultivation of microalgae. Protist 156: 239 -251.

Olivieri G, Salatino P, Marzocchella A. 2014. Advances in photobioreactors for intensive microalgal production: configurations, operating strategies and applications. Journal of Chemical Technology & Biotechnology 89(2):178-195.

Podola B, Melkonian M. 2003. A long-term operating algal biosensor for the rapid detection of volatile toxic compounds. Journal of Applied Phycology 15(5):415-424.

Pope D. 1975. Effects of light intensity, oxygen concentration, and carbon dioxide concentration on photosynthesis in algae. FEMS Microbial Ecology 2(1):1-16.

Pringault O, Garcia-Pichel F. 2000. Monitoring of oxygenic and anoxygenic photosynthesis in a unicyanobacterial biofilm, grown in benthic gradient chamber. FEMS Microbiol. Ecology 33(3):251-258.

Ramanan B, Holmes WM, Sloan WT, Phoenix VR. 2013. Magnetic Resonance Imaging of Mass Transport and Structure Inside a Phototrophic Biofilm. Current Microbiology 66(5):456-461.

Raven JA, Cockell CS, De La Rocha CL. 2008. The evolution of inorganic carbon concentrating mechanisms in photosynthesis. Philosophical transactions of the Royal Society of London. Series B, Biological sciences 363(1504):2641-2650.

Revsbech NP. 1983. In Situ Measurement of Oxygen Profiles of Sediments by use of Oxygen Microelectrodes. In: Gnaiger E, Forstner H, editors. Polarographic Oxygen Sensors. Berlin/Heidelberg, Germany: Springer. p 265-273.

Revsbech NP, Jorgensen BB. 1983. Photosynthesis of benthic microflora measured with high spatial-resolution by the oxygen microprofile method - capabilities and limitations of the method. Limnology and Oceanography 28(4):749-756.

Revsbech NP. 1989. An oxygen microsensor with a guard cathode. Limnology and Oceanography 34:4.

Richardson K, Beardall J, Raven JA. 1983. Adaptation of unicellular algae to irradiance: an analysis of strategies. New Phytologist 93(2):157-191.

Schlichting H, Gersten K. 2000. Boundary-layer theory. Berlin/Heidelberg, Germany: Springer. 800 p.

Schultze LKP, Simon M-V, Li T, Langenbach D, Podola B, Melkonian M. 2015. High light and carbon dioxide optimize surface productivity in a Twin-Layer biofilm photobioreactor. Algal Research-Biomass Biofuels and Bioproducts 8:37-44.

Seckbach J, Oren A, editors. 2010. Microbial mats - modern and ancient microorganisms in stratified systems. 1st ed. Dordrecht, The Netherlands: Springer. 606 p.

Shi J, Podola B, Melkonian M. 2007. Removal of nitrogen and phosphorus from wastewater using microalgae immobilized on twin layers: an experimental study. Journal of Applied Phycology 19(5):417-423.

Shi J, Podola B, Melkonian M. 2014. Application of a prototype-scale Twin-Layer photobioreactor for effective N and P removal from different process stages of municipal wastewater by immobilized microalgae. Bioresource Technology 154(0):260-266.

Singh S, Sundaram S, Kishor K. 2014. Photosynthetic microorganisms: mechanism for carbon concentration. 1st ed. Springer International Publishing. 123 p.

Spreitzer RJ, Salvucci ME. 2002. RuBisCO: structure, regulatory interactions, and possibilities for a better enzyme. Annual Review of Plant Biology 53:449-475.

Tampion J, Tampion MD. 1987. Immobilized Cells: Principles and Applications. 1st ed. Cambridge, UK: Cambridge University Press. 264 p.

Wang J, Liu J, Liu T. 2015. The difference in effective light penetration may explain the superiority in photosynthetic efficiency of attached cultivation over the conventional open pond for microalgae. Biotechnology for Biofuels 8(1):49.

Weissberg HL. 1963. Effective diffusion coefficient in porous media. Journal of Applied Physics 34(9):2636-2639.

Wolf G, Picioreanu C, van Loosdrecht MCM. 2007. Kinetic modeling of phototrophic biofilms: The PHOBIA model. Biotechnology and Bioengineering 97(5):1064-1079.

Zhang L, Chen L, Wang J, Chen Y, Gao X, Zhang Z, Liu T. 2015. Attached cultivation for improving the biomass productivity of *Spirulina platensis*. Bioresource Technology 181(0):136-142.

Supplementary materials

The method described here are described in detail by Li et al. (2015), for more detailed information, please refer to their publication.

Estimation of evaporation rate and effective diffusion coefficient in biofilm

The porosity of the biofilm (θ) was estimated from the volume of cells (biovolume) in the biofilm divided by the total biofilm volume. The biovolume was calculated as described by Hillebrand et al. (1999) from suspended biofilm samples with a 50 µm resolution by means of a custom-made hand microtome (Fig. S1). The biofilm immobilized on a polycarbonate membrane was placed onto a height-adjustable stage on a thin layer of culture medium. The stage allows levelling the biofilm sample into the sectioning plane by means of a micrometer screw. The sectioning plane was defined by a solid brass support over which a rigid microtome blade was passed manually to remove the overlying algal biofilm (Fig. S1).

Evaporation rate during the measurement was 0.68 mL min^{-1} (monitored by recording the change of the volume in the medium container, Fig S2), which corresponded to a convective flow rate of 5.4 µm s^{-1} inside the biofilm, which was calculated as:

$$u = q_e /(A_e \cdot \theta) \qquad \text{(Eq.S1)},$$

q_e is the rate of liquid volume lost, A_e is the exposed surface area of the biofilm.

Microsensor setup

A schematic representation of the experimental setup for microsensor measurements based on previous works by Gieseke and de Beer (2004) is given in Fig. S2: the biofilm immobilized on a polycarbonate membrane was placed onto a moist glass fiber inside the biofilm measurement cell under a controlled atmosphere of compressed air at a flow rate of 1 L min^{-1} (Fig. S2A). The non-inoculated area of the polycarbonate filter and glass fiber were covered with a black plastic foil to exclude light and gas exchange in this area. 50 mL of BBM culture medium were circulated though the measurement cell with a flow rate of 3 mL min^{-1} by means of a peristaltic pump and were exchanged every 1 hour during the measurement. Light was supplied from the front side by a halogen lamp (KL-1500, Schott, Mainz, Germany) equipped with a 3-fold splitter to ensure even distribution. The movement of the sensor was enabled by a computer-controlled micromanipulator (Pollux Drive, PI miCos, Eschbach, Germany).
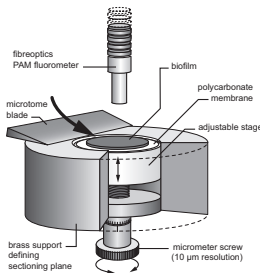
Figure S1: Schematic drawing of the experimental setup used for biofilm sectioning. The sample holder allows moving the biofilm in vertical direction by means of a micrometer screw (indicated by the thin solid arrows). The biomass above the sectioning plane was removed with a solid microtome blade. The cutting direction is indicated by the thick arrow.

Microsensor signals were amplified and converted into digital data (DAQpad 6015 and 6009, National Instruments,

Munich, Germany) prior to their further processing on a computer (Fig. S2B). Software used for system control and data acquisition was custom made (can be acquired upon request from Dr. Lubos Polerecky, Utrecht University, Netherlands, l.polerecky@uu.nl). Light-dark shift measurements (Revsbech, 1989) were carried out, and the data acquired was processed as described in the following section. Linear calibration of oxygen microsensor was carried out as described by Revsbech (1983) using BBM medium saturated with nitrogen gas or compressed air. A shutter connected to a timer was used to control light-dark cycling: the total dark period was 3 s, and a linear regression slope of oxygen concentration change between 0.7 and 2.1 s of the dark period was determined as the measured value. For each measurement depth, three light-dark cycles were performed after steady state was reached (this could be as long as 10 min), and these 3 values acquired were considered as triplicates. The PAR light intensity of a fixed depth was determined as the average value of a 3 s measurement period.
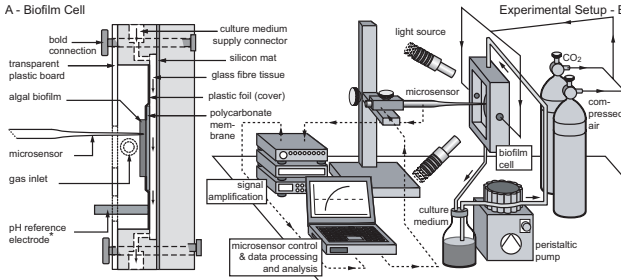
Figure S2: Experimental setup for microsensor studies in non-submerged microalgal biofilms. **A**: Schematic drawing of the vertical cross section of the measurement in artificial biofilms. Solid arrows in the glass fiber tissue indicate flow direction of the culture medium. **B**: Schematic drawing of the complete experimental setup, dotted lines with arrow indicate signal flow, whereas solid arrows represent medium and gas flows in the system.

Gross photosynthetic productivity calculation

Take the derivative of time on both sides of the dissolved oxygen mass transfer equation, and assume the time t and spatial variables x are not dependent (as during the measurement period, the thickness of the biofilm hardly changes) (Bergman et al., 2011, Revsbech and Jorgensen, 1983):

$$\partial\left(\frac{\partial C}{\partial t}\right)/\partial t = 0/\partial t - \partial R_l/\partial t + D_e \frac{\partial^2\left(\frac{\partial C}{\partial t}\right)}{\partial x^2} + u \frac{\partial\left(\frac{\partial C}{\partial t}\right)}{\partial x} - \partial R_s/\partial t \qquad (Eq.S2).$$

The term $\partial R_s/\partial t$ represents the rate change of the removal of dissolved gaseous species at the submerged biofilm surface due to the flow of bulk liquid, or, in this case, of the gas phase above the biofilm:

$$\partial R_s/\partial t = (D_e \frac{(C - C_s)}{x^2} + u \frac{(C - C_s)}{x})/\partial t$$

$$= \left(\frac{D_e}{x^2} + \frac{u}{x}\right) \cdot \partial C/\partial t \qquad (Eq.S3).$$

C_s represents the oxygen concentration on the very surface of the aerial biofilm, which is in equilibrium with the phase above and is considered to be a constant. Considering that the rate of respiration remains stable during the measurement period (Glud et al., 1992), and take $\partial C/\partial t = P(x, t)$, as $\partial C/\partial t$ is a function of depth x and time t. Substitute Eq.S3 into $\partial R_s/\partial t$ and $\partial C/\partial t$ to $P(x, t)$, Eq.S2 becomes:

$$\frac{\partial P(x,t)}{\partial t} = 0 - 0 + D_e \frac{\partial^2\big(P(x,t)\big)}{\partial x^2} + u \frac{\partial\big(P(x,t)\big)}{\partial x} - \left(\frac{D_e}{x^2} + \frac{u}{x}\right) \cdot P(x,t)$$

(Eq.S4).

Eq.S4 is a nonhomogeneous diffusion equation with a sink and can be solved by using any of the methods summarized by Crank or Polyanin (Crank, 1975; Polyanin, 2002). Using an initial condition $P(x, t = 0) = P(x, 0)$ and a boundary condition $\partial P(x = 0, t)/\partial t = 0$, the exact solution of Eq.S4 at $t = \tau$ can be expressed as:

$$P(x,\tau) = \int_0^\delta P(y,0) \cdot \left[e^{\left(\frac{-(y-x+u\cdot\tau)}{4\cdot D_e\cdot\tau}\right)} - e^{\left(\frac{-(y+u\cdot\tau)}{4\cdot D_e\cdot\tau}\right)} \cdot erfc\left(\frac{x}{\sqrt{4\cdot D_e\cdot\tau}}\right) \right] \cdot dy$$

(Eq.S5),

δ is the total depth of the biofilm, or, alternatively, the depth until which the shift from light to dark has an effect on the dissolved oxygen concentration. $P(x, \tau)$ is the measured value from the light-dark shift method with measurement time τ at measurement depth x, and $P(y, 0)$ is the actual photosynthetic activity at position y (the integrating variable), which is the desired term. For measurements taken at all depths, the measured value $P(x, \tau)$ at a depth x depends on the $P(y, 0)$ across the complete photosynthetically active region of the biofilm (surface to depth δ).

Eq.S5 is a Fredholm integral equation of the first kind (Kress, 2014), and its approximated solution can be calculated using Tikhonov regularization (Tikhonov et al., 1995) with a non-negative constrain applying the active-set algorithm purposed by Gill et al. (1981): Discrete δ by n, and let $P(x_j, \tau) = g_j$, $P(y_i, 0) = h_i$; $(i, j = 1, 2, \ldots, n)$ and write Eq.S5 in the discrete operator notion.

$$g_j = \sum_i^n k_{i,j} \cdot h_i$$

(Eq.S6),

$k_{i,j}$ is the operator term which contains both the term that reflects the effect of diffusion and advection of dissolved oxygen inside the biofilm (inner term, first term in square bracket in Eq.S5) and the term that reflects the effect of dissolved oxygen removal due to surface flow (surface term, second term in square bracket in Eq.S5). In matrix notion, let G be a vector containing g_j, H a vector containing h_i, and K a matrix containing the operator terms $k_{i,j}$:

$$G = K \cdot H$$

(Eq. S7).

Rewrite Eq.S7 as:

$$(G_{in} + G_{surf}) = (K_{in} + K_{surf}) \cdot H$$

(Eq.S9),

The subscripts in and $surf$ represent the effect from the inner term and the surface term in Eq.S5 respectively, operators K_{in}, K_{surf} can be calculated using Eq.S5, as well as g_{in} and G_{surf}, if an H is given. Apply the Tikhonov regularization, the problem in Eq.11 thus becomes:

$$\min_{F \geq 0} \left\{ \left\| (G_{in} + G_{surf}) - (K_{in} + K_{surf}) \cdot H \right\|^2 + \lambda^2 \cdot \| L \cdot H \|^2 \right\}$$

or,

$$\min_{F \geq 0} \left\{ \left\| (G_{in} - K_{in} \cdot H) + (G_{surf} - K_{surf} \cdot H) \right\|^2 + \lambda^2 \cdot \| L \cdot H \|^2 \right\}$$

(Eq.S10).

Observing the surface term in Eq.S5, notice the maximum value of the surface term is controlled by the position of the actual activity y, but a complement error function dependent solely on the position of the measurement taken (x) controls the final value. Furthermore, for a given G, under the same measurement conditions, G_{surf} always has the same set of values. Thus, for a given G, the minimization of the term $\left\|G_{surf} - K_{surf} \cdot H\right\|^2$ will always yield the same solution. As a result, the problem in Eq. S10 can be simplified to:

$$\min_{f \geq 0}\{\|G_{in} - K_{in} \cdot H\|^2 + \lambda^2 \cdot \|L \cdot H\|^2\} \tag{Eq.S11}.$$

Eq.S11 does not contain the surface term, but the solution of the problem still leads to H, which is the desired original profile. The L-curve method purposed by Hansen & O'Leary (1993) was used to find the best regularization parameter λ.

The treatment procedure was coded in MATLAB (version 2013a, MathWorks, Ismaning, Germany), and the inbuilt *quadprog* was used for solving the minimization problems. *L-curve* function from the regularization tools (Hansen, 1994) was used to find the λ value. The mean values of triplicates acquired from the microsensor measurement were randomly added or subtracted with a random value in range of the calculated standard deviation (SD) at the same position. These values were used as input for the calculation. The calculation procedure was repeated 3 times, and the mean value of the 3 results was taken as the final result (a SD can also be calculated). Data interpolation, if needed, was done by simply connecting two measured data points with a straight line (linear interpolation, using MATLAB inbuilt function *interp1*).

References for supplementary materials:

Bergman TL, Lavine AS, Incropera FP, DeWitt DP. 2011. Fundamentals of heat and mass transfer. 7th ed. Hoboken, New Jersey, USA: John Wiley & Sons. 1048 p.

Crank J, editor. 1975. Mathematics of diffusion. 2nd ed. Oxford, UK: Oxford University Press. 414 p.

Gieseke A, de Beer D. 2004. Use of microelectrodes to measure in situ microbial activities in biofilms, sediments, and microbial mats. In: Kowalchuk GA, de Bruijn FJ, Head IM, Akkermans AD, van Elsas JD, editors. Molecular Microbial Ecology Manual. The Netherlands: Springer. p 3483-3514.

Gill PE, Murray W, Wright MH. 1981. Practical optimization. Waltham, Massachusetts, USA: Academic Press. 401 p.

Glud RN, Ramsing NB, Revsbech NP. 1992. Photosynthesis and photosynthesis-coupled respiration in natural biofilms quantified with oxygen microsensors. Journal of Phycology 28(1):51-60.

Hansen P. 1994. REGULARIZATION TOOLS: A Matlab package for analysis and solution of discrete ill-posed problems. Numerical Algorithms 6(1):1-35.

Hansen PC, O'Leary DP. 1993. The Use of the L-Curve in the Regularization of Discrete Ill-Posed Problems. SIAM Journal on Scientific Computing 14(6):1487-1503.

Hillebrand H, Durselen CD, Kirschtel D, Pollingher U, Zohary T. 1999. Biovolume calculation for pelagic and benthic microalgae. Journal of Phycology 35(2):403-424.

Kress R, editor. 2014. Linear integral equations. 3rd ed. New York City, USA: Springer. 412 p.

Li T, Podola B, de Beer D, Melkonian M. 2015. A method to determine photosynthetic activity from oxygen microsensor data in biofilms subjected to evaporation. Journal of Microbiological Methods 117:100-107.

Polyanin AD. 2002. Handbook of linear partial differential equations for engineers and scientists. Boca Raton, Florida: Chapman&Hall/CRC Press. 800 p.

Revsbech NP. 1983. In Situ Measurement of Oxygen Profiles of Sediments by use of Oxygen Microelectrodes. In: Gnaiger E, Forstner H, editors. Polarographic Oxygen Sensors. Berlin/Heidelberg, Germany: Springer. p 265-273.

Revsbech NP, Jorgensen BB. 1983. Photosynthesis of benthic microflora measured with high spatial-resolution by the oxygen microprofile method - capabilities and limitations of the method. Limnology and Oceanography 28(4):749-756.

Tikhonov AN, Goncharsky A, Stepanov VV, Yagola AG. 1995. Numerical methods for the solution of ill-posed problems. Dordrecht, the Netherlands: Springer. 254 p.

2.3. Investigating dynamic processes in a porous substrate biofilm photobioreactor – A modeling approach.
Published in 'Algal Research', 2016(13):30-40.

Presented here in the original published version, reformatted for the presentation in this thesis (with section

numbers removed and corresponding changes).

Investigating dynamic processes in a porous substrate biofilm photobioreactor – A modeling approach

Tong Li[1*], Björn Podola[1] and Michael Melkonian[1]

[1]University of Cologne, Botanical Institute, 50674 Cologne, Germany;

*Corresponding Author: Tong Li

Universität zu Köln, Botanisches Institut, Biozentrum Köln, 50674 Köln, Germany

Phone: +49 (0)221-470 8090

Email: lit2@uni-koeln.de

Running head: Modeling of non-submerged algal biofilm

Abstract

In the present study, a one dimensional kinetic model was developed for a porous substrate biofilm photobioreator (PSBR), a biofilm bioreactor for the production of microalgae and other biotechnological applications. Light transfer was modeled with a radiative transfer equation (RTE), considering absorption, scattering and biomass pigment adaptation. Dissolved chemical species were modeled using mass balance equations (partial differential equations), with terms describing diffusion, convection, biomass growth, biomass consumption and chemical conversions. pH was modeled as a state variable, and a novel approach of modeling biomass increase in a phototrophic biofilm was introduced. The model was solved using numerical methods and model parameters were acquired either from literature or from experimental work carried out in the framework of this study. The proposed mode was applied to simulated gradients of light, dissolved oxygen concentration, pH etc. in a PSBR biofilm. The simulated results were compared with experimental data acquired in previous studies.

Our results show that the proposed model can accurately predict light intensity distribution in the modeled PSBR biofilm, provided the optical properties of the biomass were measured experimentally. The prediction of the concentration of dissolved oxygen and pH profiles also reflected experimental data with high fidelity. The results also strongly suggest that facilitated CO_2 transfer due to the presence of extracellular carbonic anhydrase in the biofilm matrix plays an important role in DIC transport in the modeled PSBR biofilm at low gas phase CO_2 concentration; and the pH gradient along the depth gradient of the modeled biofilm was mainly caused by the uptake of dissolved inorganic carbon. In addition, the simulation can predict biomass growth in the modeled PSBR with minimal error, thus, with minor modifications, the model can also be applied to predict biomass growth in larger-scale PSBRs.

Keywords

Introduction

Porous substrate photobioreactors (PSBRs) have been described in previous studies as highly productive systems for the cultivation of various microalgal species for biotechnological applications (e. g. Liu et al., 2013; Murphy et al., 2014; Schultze et al., 2015). One variety of PSBR, the Twin-Layer PSBR (TL-PSBR), has been shown in recent studies to have very high biomass productivity and a pilot-scale study showed its potential in large scale commercial operations (Naumann et al. 2013; Schultze et al. 2015; Shi et al. 2014). Until now, the dynamics behind these promising observations are still not well understood, however, such knowledge should be important for further optimization and up-scaling of the system.

In general, a model of such a biological system can help to improve its understanding, and may be particularly useful when designing, optimizing and controlling bioreactors based on a biological system in a prototype or larger scale (Dunn et al., 2003). Several models have already been developed for submerged phototrophic biofilms or other photobioreactors (e.g.,Berberoglu et al., 2007; Ogbonna et al., 1995; Olivieri et al., 2014; Wolf et al., 2007). However, only one model so far was developed specifically for PSBR biofilms: Murphy and Berberoglu (2014) described a two dimensional kinetic model, giving a first insight into the kinetic interactions inside the biofilm. However, this work focused more on the gradients in the direction of medium flow (i.e. gradient parallel to biofilm surface) rather than the gradients perpendicular to the medium flow (i.e. along the biofilm depth gradient), as pH was considered invariant along the depth gradient. This however, is not the case, as shown recently by microsensor measurements performed on a TL-PSBR biofilm (Li et al., 2015b).

In this study, a comprehensive kinetic model with respect to light and mass transfer, chemical equilibrium, biological processes and biomass production of a PSBR biofilm focusing on the gradients perpendicular to the biofilm surface (along a depth gradient) was developed. Several experiments were carried out in the framework of this study to determine the required parameters. The model was implemented using a numerical method. Simulated growth experiments were carried out in silico using the developed model with several growth condition scenarios, and the simulated results were compared with experimental data measured with microsensors from a previous study.

Materials and Methods

General assumptions and model setup

In the present study, gradients are assumed to exist in the direction perpendicular to the biofilm surface (along the depth gradient) only, thus are one dimensional (1D). Phototrophic growth is assumed to depend solely on irradiance, dissolved oxygen concentration, inorganic carbon availability and the availability of macro-nutrients (N and P). Trace elements are considered to be sufficiently supplied, and, therefore, their concentrations are supposed to have no effect on growth (e.g. Mg, Fe, Zn etc.). Biomass in the biofilm is assumed to be homogeneous: Dry biomass concentration (X_F) is considered as a constant; in consequence, porosity of the biofilm (θ) is also a constant (as was observed experimentally, see supplementary materials). The intracellular composition of the biomass is assumed to be constant over time and the depth gradient (i.e. biomass has a fixed C:N:P ratio, as it was observed experimentally, see supplementary materials).
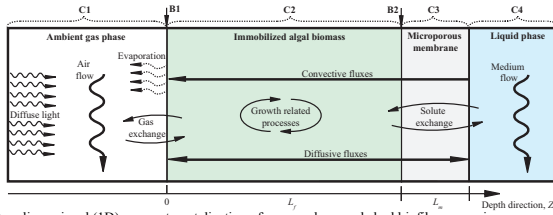
Figure 1: One-dimensional (1D) compartmentalization of a non-submerged algal biofilm grown in a porous substrate bioreactor as implemented in the proposed model. Compartments and boundaries are marked at the top of the figure. Direction of the depth gradient, Z, are given at the bottom. Growth related processes solely occur in the biofilm compartment. Arrow directions indicate the directions of the processes. L_f and $L_{membrane}$ are thicknesses of the biofilm and microporous substrate membrane, respectively. C1 to C4 represent: bulk gas compartment, biofilm compartment, boundary layer (BL) compartment and bulk liquid compartment, respectively. B1 and B2 represent the surface and bottom boundaries of the biofilm compartment.

Table I: [a]Nomenclature of symbols presented in Fig. 2.

Model parameters		State variables	
Symbol	**Definition**	**Symbol**	**Definition**
$D_{e,x}$	Effective diffusion coefficient of dissolved species x.	S_x	Concentration of dissolved species x in biofilm compartment.
u_z	Convective flow rate in biofilm due to evaporation.	I	Irradiance in the biofilm compartment.
p_x	Partial pressure of gas x in bulk gas.	μ	Growth rate of the biomass.
I_{in}	Incident irradiance.	L_F	Biofilm thickness.
$S_{x,surface}$	Concentration of dissolved species x at biofilm surface.	pH[b]	pH in biofilm.
$S_{x,medium}$	Concentration of dissolved species x in bulk liquid.		
pH_{medium}	pH in bulk liquid.		

[a]The subscript x representing species x are given in the subscripts in Fig. 2.
[b]pH itself is not a state variable, and is calculated from state variable S_H:

Since the proposed model focuses on modeling the kinetics of processes inside the biofilm rather than fluid dynamics at the interfaces, in the proposed model, the biofilm was simplified into 4 compartments without any flow boundary layer (Fig. 1): Bulk gas compartment (the ambient gas phase); biofilm compartment (the biomass, and the only compartment containing state variables); mass transfer boundary layer (BL) compartment (the micro-porous membrane) and bulk liquid compartment (the liquid phase in a macro porous material). Considering the fast mass transfer in bulk gas and bulk liquid compartments (displaying high convective flow rates), both compartments are assumed to be well-mixed (homogeneous). The micro-porous membrane is considered as a mass transfer boundary layer for dissolved species and is assumed to have a flow only in the direction parallel to the depth gradient. Growth related processes (e.g. consumption of nutrients, production of O_2 etc.) take place only in the biofilm compartment. Evaporation at the biofilm surface creates a convective flow in both the biofilm compartment and the boundary layer compartment. However, the gas flow boundary layer at the biofilm surface is neglected (Bergman et al., 2011; Schlichting and Gersten, 2000). Concentration gradients exist in both the biofilm compartment and the boundary layer compartment, and lead to diffusive fluxes in these compartments. Exchange of all dissolved species between biomass and bulk medium occurs through the BL compartment. In addition, direct exchange of dissolved gaseous specious (dissolution and/or escape of O_2 and CO_2) occurs at the biofilm surface (interface between bulk

gas and biofilm). Illumination at the biofilm surface is assumed to be emitted from a diffuse source (equal intensity in all directions). State variables only exist in the biofilm compartment, which has a surface/top boundary (interface between biomass and gas phase) and a bottom boundary (interface between biomass and the porous membrane). A schematic representation of the parameters, state variables and their interactions are given in Fig. 2 and Table I (Nomenclature of the symbols in Fig. 2 can be found in Tab. I). Processes included in the proposed model are:
1) Transport processes: Light transfer (absorption and scattering), mass transport process (diffusion of dissolved species and convection due to evaporation).

2) Biological processes: Photosynthesis (growth), respiration (both dark and photo-respiration), biomass pigment adaptation due to exposure to different light intensities and increase in biofilm thickness due to growth.

3) Chemical processes: Acid-base equilibrium (speciation of inorganic carbon and inorganic phosphate), and dissolution/release of gases (O_2 and CO_2) at biofilm surface.
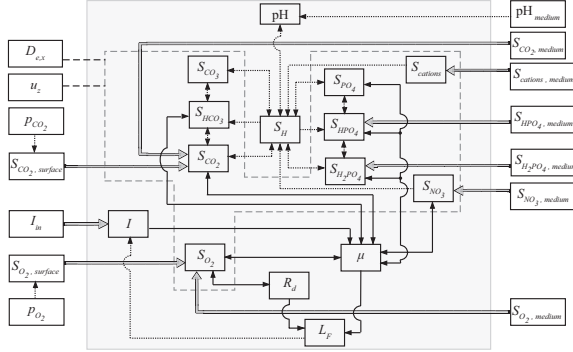
Figure 2: Schematic representation of the variables and parameters (text boxes) and their interactions (processes, indicated by arrows) considered in the proposed model. Grey box includes variables, parameters and interactions inside the biofilm compartment. The dash line box includes variables affected by the mass transfer processes: $D_{e,x}$ represents diffusion, and u_z represents advection caused by surface evaporation. Solid arrows represent growth-related interactions. Thick grey arrows show interactions that cross the boundaries (interaction between compartments). Notice interactions can be one-way or bi-directional (indicated by the arrow/arrows). Nomenclature of the symbols can be found in Tab. I. *Subscript *totalP* denote total inorganic phosphate.

Light transfer and phototrophic growth

The proposed model uses the radiative transfer equation (RTE) to model light transfer in the biofilm, as previous observations showed that the effect of scattering in densely packed suspension (here, a biofilm) cannot be neglected (Berberoglu et al., 2007). The 1D form of RTE is (Murphy and Berberoglu, 2014):

$$\frac{\partial I_\lambda(z,\hat{s}_a)}{\partial z} = -\left(\kappa_{\lambda,F,z} + \sigma_{\lambda,F},z\right) \cdot I_\lambda(z,\hat{s}_a) + \frac{\sigma_{\lambda,F,z}}{4\pi}\int_0^{4\pi} I_\lambda(z,\hat{s}_b)\cdot\Phi(\hat{s}_b,\hat{s}_a)\,d\Omega_b \qquad \text{(Eq.1)},$$

here, z represents the depth, $I_\lambda(z,\hat{s}_a)$ and $I_\lambda(z,\hat{s}_b)$ are the spectral radiant intensities of wavelength λ at depth z, travelling in the direction $\hat{s}_a$ and $\hat{s}_b$, respectively. $\kappa_{\lambda,F,z}$ and $\sigma_{\lambda,F,z}$ are the effective spectral absorption coefficient and the effective spectral scattering coefficient of the biofilm at depth z. $\Phi(\hat{s}_b,\hat{s}_a)$ is the scattering phase function from direction $\hat{s}_j$ to $\hat{s}_i$, and is estimated from Henry-Greenstein approximation as described by (Berberoglu et al., 2007); the scattering of algal cells was considered to be strongly forward, and an asymmetry factor of 0.98 was taken for calculation (Berberoglu et al., 2007). Ω_b is the solid angel surrounding direction $\hat{s}_b$. To simulate the effect of adaptation of the biomass by adjusting their cellular pigment content (verified experimentally, see supplementary materials), a simple linear function dependent on the position of the cell in the biofilm was used to estimate the absorption coefficient at an illuminated depth z in the biofilm for all photosynthetically active radiation (PAR) wavelengths:

$$\kappa_{\lambda,F,z} = \frac{z}{L_{F,light}} \cdot \kappa_{\lambda,F} \qquad (z \leq L_{F,light}) \qquad \text{(Eq.2)},$$

$L_{F,light}$ is the thickness of the illuminated part of the biofilm. $\kappa_{\lambda,F}$, which is the maximal absorption coefficient of the biomass, was determined experimentally together with the maximal scattering coefficient of the biomass $\sigma_{\lambda,F}$ (see supplementary materials; $\sigma_{\lambda,F}$ was considered to remain constant throughout the biofilm, i.e. $\sigma_{\lambda,F,z} = \sigma_{\lambda,F}$).
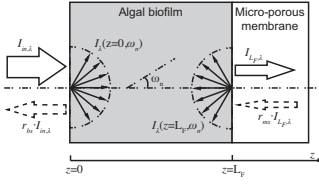
Figure 3: Schematic representation of the radiation transfer equation (RTE) boundary conditions considered in the proposed model (as described by Eq. 3 and 4). Thick solid line arrows: Total irradiance at the biofilm surface and the biofilm-membrane interface. Thick dotted line arrows: Reflected irradiance at the biofilm surface and the biofilm-membrane interface. Thin arrows: Directional irradiance inside the biofilm due to direct incident irradiance and/or reflected irradiance by the membrane surface.

At the biofilm surface (top boundary), light can be reflected before entering the biofilm. Assuming a diffuse light source, the boundary condition at the top boundary ($z = 0$) according to (Murphy and Berberoglu, 2014), and considering the vertical placement of the modeled biofilm (perpendicular to the ground as described by Shi et al., 2007) is:

$$I_\lambda(z = 0, \omega_n) = (1 - r_{bs}) \cdot \frac{I_{in,\lambda}}{\pi} \qquad \left(-\frac{\pi}{2} < \omega_n < \frac{\pi}{2}\right) \qquad \text{(Eq.3)}.$$

Similarly, light can be reflected by the microporous membrane before leaving the biofilm at the biofilm–membrane interface (bottom boundary). Thus, the boundary condition at the bottom boundary ($z = L_F$) following Murphy and Berberoglu (2014) is written as:

$$I_\lambda(z = L_F, \omega_n) = r_{ms} \cdot \frac{I_{L_F,\lambda}}{\pi} \qquad \left(-\pi < \omega_n < -\frac{\pi}{2} \; and \; \frac{\pi}{2} < \omega_n < \pi\right) \qquad \text{(Eq.4)}.$$

In Eq.3 and 4, ω_n is the angle relative to the normal of the biofilm surface; L_f is biofilm thickness; r_{bs} and r_{ms} are the reflectance of the biofilm and membrane surface, respectively (Fig. 3).

The proposed model does not differentiate the efficiency of PARs with different wavelengths in photosynthesis. In consequence, at any depth z, the calculated intensities in all directions and all bands in PAR range are integrated into total PAR (I_z):

$$I_z = \int_{400nm}^{700nm} \int_0^{4\pi} I_\lambda(z, \hat{s}_a) \, d\Omega_a \, d\lambda \qquad \text{(Eq.5)}$$

Irradiance for one discrete element was calculated as the average value of its left and right nodes, and this was fed into an equation (P-I curve) describing the kinetics of phototrophic growth as described by (Platt et al. 1980):

$$f_I = \left(1 - e^{\frac{-\alpha \cdot I_z}{ETR_{max}}}\right) \cdot e^{\frac{-\beta \cdot I_z}{ETR_{max}}} \qquad \text{(Eq.6)},$$

whereas f_I represents the effect of irradiance on photosynthetic growth. ETR_{max} is the maximal electron transfer rate (ETR), α is the initial slope of the ETR-irradiance curve and β is a term representing the degree of photo-inhibition (In the present study, ETR_{max}, α and β were determined experimentally, see supplementary materials).

The effect of oxygen on phototrophic growth was expressed as an inhibition term dependent on the concentration of dissolved oxygen ([DO], denoted as S_{O_2}), similar to the approach used by Murphy and Berberoglu (2014) for inorganic carbon and phosphate but without the saturation term (i.e. only inhibition is considered, as observed experimentally by Pope, 1975 and by Grötzschel and de Beer, 2002):

$$f_{O_2} = \frac{S_{O_2}}{S_{O_2} + S_{O_2}^2 / K_{O_2,In}} \qquad \text{(Eq. 7)}.$$

f_{O_2} represents the effect of [DO] on phototrophic growth, and $K_{O_2,In}$ is the inhibition constant for [DO] on photosynthesis. In the present study, this inhibition was considered as an effect of photorespiration. $K_{O_2,In}$ is a dependent variable controlled by the CO_2 to O_2 ratio, R_{CO_2/O_2}, and follow a Monod type kinetic, as suggested by the data presented by Ku and Edwards (1978):

$$K_{O_2,In} = K_{O_2,In,max} \frac{R_{CO_2/O_2}}{R_{CO_2/O_2} + K_{R_{CO_2/O_2},S}} \qquad \text{(Eq.8)}$$

$K_{O_2,In,max}$ is the assumed maximal inhibition (i.e. photorespiration) coefficient of [DO] on phototrophic growth, and $K_{R_{CO_2/O_2},S}$ is the assumed half saturation constant of the CO_2 to O_2 ratio on photorespiration.

The effects of dissolved macro-nutrients (N as nitrate; S_{NO_3}; P as total phosphate: sum of monohydrogenphosphate, S_{HPO_4} and dihydrogenphosphate, $S_{H_2PO_4}$ and phosphate ion S_{PO_4}) on growth were modeled using Monod type kinetics (IWA Task Group on Biofilm Modelling 2006), the effect of inhibition by high CO2 concentration and high nutrients concentration are not considered in the present study, as suggested by the data presented by Schultze et al. (2015) and in the supplementary material (Fig. S9):

$$f_x = \frac{S_x}{K_{x,S} + S_x}$$ (Eq. 9).

f_x represents the effect of S_{NO_3} (f_{NO_3}) or $S_{PO_4,total}$ (f_{PO_4}) on phototrophic growth, and their saturation constants are represented by $K_{x,S}$. However, only monohydrogenphosphate and dihydrogenphosphate ions were modeled as diffusive species in the present study, as significant concentrations of phosphate ions were not expected in such biofilms as suggested by previous investigations (Li et al., 2015b).

In the present study, carbon concentrating mechanisms (CCMs) were taken into account by assuming that both CO_2 and HCO_3^- (direct uptake of bicarbonate and conversion of bicarbonate to CO_2 at the cell surface before uptake were not distinguished in the present study, and are considered to have the same effect) are able to support phototrophic growth (Raven et al. 2008), and an approach similar to that described by Wolf et al. (2007) is used: Monod type kinetics are applied to describe phototrophic growth on CO_2 and HCO_3 expressed as

$$f_{CO_2} = \frac{S_{CO_2}}{K_{CO_2,S} + S_{CO_2}}$$ (Eq. 10),

and

$$f_{HCO_3} = \frac{S_{HCO_3}}{K_{HCO_3,S} + S_{HCO_3}} \cdot \frac{S_{CO_2}}{S_{CO_2}/K_{CO_2,in}^2 + S_{CO_2}}$$ (Eq. 11),

respectively. S_{CO_2} and S_{HCO_3} represent concentrations of dissolved CO_2 and HCO_3^-. $K_{CO_2,S}$ and $K_{HCO_3,S}$ are the saturation constants for CO_2 and HCO_3^- growth, respectively. $K_{CO_2,in}$ is the assumed inhibition constant of CO_2 on growth using bicarbonate as carbon source.

Finally, the phototrophic growth rate was calculated using a similar method as described by Wolf et al. (2007), however, irradiance and [DO] are considered to have an influence on the growth rate (μ) independently of the nutrient concentrations:

$$\mu = \mu_{max} \cdot f_I \cdot f_{o_2} \cdot \left[\min(f_{NO_3}, f_{PO_4}, f_{CO_2}) + \min(f_{NO_3}, f_{PO_4}, f_{HCO_3}) \right]$$ (Eq. 12).

The maximal growth rate of the biomass is represented by μ_{max} (estimated experimentally, see supplementary materials). Another effect of the CCM is the production of extracellular carbonic anhydrase (CA) at low dissolved free CO_2 concentrations (Raven et al., 2008). This results in an increased interconversion rate of CO_2 – bicarbonate (increased to identical value as dehydration of carbonic acid). Another effect of the extracellular CA is a facilitated CO_2 transport in the biofilm, which leads to significantly accelerated CO_2 transport (Bao and Trachtenberg, 2006; Gros et al., 1976; Trachtenberg et al., 1999). In the present study, this effect was modeled by multiplying the effective diffusion coefficient of CO_2 with a simple exponential function dependent on local dissolved free CO_2 concentration, as suggested by the results from Gros et al. (1976):

$$D_{e,CO_2}^* = D_{e,CO_2} \cdot \left(f_a \cdot e^{f_b \cdot S_{CO_2}} + 1 \right)$$ (Eq. 13).

f_a and f_b are two pre-determined factors, and D_{e,CO_2} is the calculated effective diffusion coefficient of CO_2 in the biofilm (see section below). Eq. 13 describes a function influencing the effective diffusion coefficient of CO_2 in biofilm, at low CO_2 concentrations the effective diffusion coefficient of CO_2 can be increased significantly (several fold), whereas at high CO_2 concentrations the effective diffusion coefficient of CO_2 is hardly affected, as suggested by the data presented in previous studies (Bao and Trachtenberg, 2006; Gros et al., 1976; Trachtenberg et al., 1999).

Dark respiration rate was considered to be [DO] dependent and follows the Monod kinetic (Wolf et al., 2007):

$$R_d = R_{d,max} \cdot \frac{S_{O_2}}{S_{O_2} + K_{O_2,Sa}}$$ (Eq. 14),

in which $K_{O_2,Sa}$ is the saturation constant, and $R_{d,max}$ is the maximal dark respiration rate (determined experimentally, see supplementary materials). The biofilm thickness (L_F) is a pseudo-state variable in the proposed mode, and the rate of biofilm thickness change is calculated as (Wolf et al., 2007; the approach for modeling change in biofilm thickness is described   in detail below):

$$u_{L_F} = \frac{dL_F}{dt} = \int_0^{L_F} (\mu - R_d) \, dz \qquad \text{(Eq.15).}$$

It is possible, that besides aerobic respiration, the algal cells respire anaerobically (Atteia et al., 2013), however, due to a lack of knowledge on this topic, this process was not included in the present study.

The consumption/production of dissolved species by biological processes are calculated based on biomass growth, as described in detail by (IWA Task Group on Biofilm Modelling 2006), and generally:

$$\gamma_{x,F} = (\mu - R_d) \cdot X_F \cdot \frac{1}{Y_x} \qquad \text{(Eq.16).}$$

$\gamma_{x,F}$ is the consumption/production rate of the dissolved species x due to growth, X_F is the biomass concentration of the biofilm (dry weight per volume). Y_x is the yield of species x with respect to biomass production or consumption. For inorganic carbon, nitrogen and phosphorus, the yields are calculated as the reciprocal of their contents in biomass (IWA Task Group on Biofilm Modelling, 2006). In the present study, it is assumed that photosynthesis utilizing CO_2 and bicarbonate have identical yields on oxygen (O_2:C = 1.3:1; Atkinson and Smith, 1983; Raven et al., 2014) and biomass.

Mass balance and chemical equilibrium

Mass transfer in the proposed model is described by the 1D mass balance equation (Bergman et al., 2011):

$$\frac{dS_x}{dt} = D_{e,x} \frac{d^2 S_x}{dz^2} + u_z \frac{dS_x}{dz} + \gamma_{x,F} + \gamma_{x,Che} \qquad \text{(Eq.17),}$$

S_x is the concentration of dissolve species x, $D_{e,x}$ is the effective diffusion coefficient of species x in the biofilm and u_z is the convective flow rate in the biofilm caused by evaporation at the biofilm surface. $\gamma_{x,F}$ and $\gamma_{x,Che}$ are production/consumption due to biomass growth/respiration and chemical conversion, respectively. Chemical conversions in the present study are controlled by the rate constant (k) and the equilibrium constant (K) of the reaction, e.g., for reaction A↔B+C, the conversion rate of A is expressed as:

$$\gamma_{A,Che} = k_{A/BC} \cdot \left(S_A - \frac{S_B \cdot S_C}{K_{A/BC}} \right) \qquad \text{(Eq.18).}$$

Values of rate and equilibrium constants can be found in Tab. III.

The boundary conditions required to solve Eq.17 are given below (IWA Task Group on Biofilm Modelling, 2006):

1) At the bottom boundary ($z = L_F$, biofilm – membrane interface), for all dissolved species, the flux of the species x across the BL compartment equals the flux at the bottom of the biofilm compartment ($j_{m,x}$):

$$j_{m,x} = D_{membrane,x} \cdot \frac{S_{x,medium} - S_{x,L_F}}{L_m} + u_z \cdot S_{x,medium} \qquad \text{(Eq.19).}$$

$D_{membrane,x}$ is the effective diffusion coefficient of x in the porous membrane, $S_{x,medium}$ is the concentration of species x in the liquid phase (bulk liquid compartment), and L_m is the thickness of the membrane (BL compartment).

2) At the surface boundary ($z = 0$, biofilm surface), for gaseous species, the concentrations of O_2 and CO_2 are assumed to be constant, and are governed by Henry's law. For oxygen:

$$S_{O_2,z=0} = p_{O_2} \cdot K_{Hen,O_2} \qquad \text{(Eq.20),}$$

and for dissolved inorganic carbons (DICs):

$$S_{DIC,z=0} = p_{CO_2} \cdot K_{Hen,CO_2} \cdot \left(1 + \frac{K_{a1,H_2CO_3}}{S_{H,z=0}} + \frac{K_{a1,H_2CO_3} \cdot K_{a2,H_2CO_3}}{S_{H,z=0}^2} \right) \qquad \text{(Eq.21),}$$

in which $S_{O_2,z=0}$ and $S_{DIC,z=0}$ ($S_{x,surface}$ in Fig. 2) are the concentration of dissolved O_2 and DIC at the biofilm surface, p_x is the partial pressure of x in the gas phase, and $K_{Hen,x}$ is the Henry's constant for species x (For CO_2, chemical equilibria of the dissolved inorganic carbons are also taken into consideration. As described by Murphy and Berberoglu (2014), K_{a1,H_2CO_3}, K_{a2,H_2CO_3} and $S_{H,z=0}$ are the dissociation constants for H_2CO_3 and the proton concentration at biofilm surface, respectively.). For non-gaseous dissolved species however, the surface boundary is considered as a no flux boundary ($J_x = 0$). This simulates the increase in concentration of a dissolved species as a result of evaporation at the biofilm surface.

For initial conditions (at $t = 0$), an initial biofilm thickness is given as $L_{F,t=0}$; the concentrations of non-gaseous dissolved species were set to identical values as found in freshly prepared medium; for dissolved gaseous species, the concentrations throughout the biofilm at $t = 0$ were assumed to be identical to their concentration at the biofilm

surface. In the present study, effective diffusion coefficients were determined as described by Li et al. (2015a; see also supplementary materials).

The pH in the biofilm compartment is modeled using the charge balance equation by (Wolf et al., 2007), considering the concentration of protons (S_H) only depending on the charge balance (assumed to be a non-diffusive species). The speciation of inorganic carbon and inorganic phosphate are assumed to be pH dependent, only. The charge balance equation applied in the present study is:

$$S_{H^+} - S_{OH^-} = S_{HCO_3^-} + 2 \cdot S_{CO_3^{2-}} + S_{H_2PO_4^-} + 2 \cdot S_{HPO_4^{2-}} + 3 \cdot S_{PO_4^{3-}} - S_{cations} \quad \text{(Eq.22).}$$

S represents concentration of the different species, and K_w is the disassociation constant of water. In the present study, Na$^+$ is considered to be the sole cation present. Define $Ch(\text{pH}) = S_H - S_{OH}$ (a pH dependent parameter), according to (Campos and Flotats, 2003), S_H can be calculated as:

$$S_H = \begin{cases} \frac{Ch(\text{pH}) + \sqrt{Ch(\text{pH})^2 + 4 \cdot K_w}}{2}, & ch(\text{pH}) \geq 0 \\ \frac{2 \cdot K_w}{-Ch(\text{pH}) + \sqrt{Ch(\text{pH})^2 + 4 \cdot K_w}}, & ch(\text{pH}) < 0 \end{cases} \quad \text{(Eq.23).}$$

However, in the proposed model, instead of calculating S_H at the end of each numerical integration step, S_H is considered to be a state variable, and, therefore is calculated using the algorithms described by (Campos and Flotats, 2003):

$$\frac{dS_H}{dt} = \frac{dCh(\text{pH})}{dt} \cdot \begin{cases} \frac{1}{2} \cdot \left(\frac{Ch(\text{pH})}{\sqrt{Ch(\text{pH})^2 + 4 \cdot K_w}} + 1 \right), & ch(\text{pH}) \geq 0 \\ -\frac{S_H}{2 \cdot K_w} \left(\frac{Ch(\text{pH})}{\sqrt{Ch(\text{pH})^2 + 4 \cdot K_w}} - 1 \right), & ch(\text{pH}) < 0 \end{cases} \quad \text{(Eq.24).}$$

Model implementation and parameters

In the proposed model, the biofilm compartment is divided into discrete elements using a simple upwind scheme (Courant et al., 1952) into n elements (for the ith element: $I = 1, 2, \ldots, n$), with the 1st element being the biofilm surface (top boundary) and the nth element representing the biofilm–membrane interface (bottom boundary). In the present study, the model was coded using MATLAB (version 2013a, MathWorks, Ismaning, Germany; the code can be acquired from the first author upon request).

To implement the RTE into the proposed model, the discrete ordinate method (DOM) was applied to divide the solid angle (4π) into two hemispheres, each with 24 distinct directions (Berberoglu et al., 2007). This generated for each discrete element a system of ordinary differential equations (ODEs), which were then solved using the method provided by Colomer et al. (2000) with the MATLAB *linsolve* function. A grid sensitivity study was carried out and 1 discrete elements per 5 µm simulated biofilm was determined to be numerically sufficient (< 1% change with a further increase in number of discrete elements; Berberoglu et al., 2007).

Partial differential equations (PDEs) describing the mass balances were transformed into systems of ODEs using the method of lines (MOL; Schiesser, 1991). The acquired ODE systems were solved using a variable order numerical differentiation formula (*ode15s*, MATLAB). The biofilm thickness (L_F) is a pseudo-state variable in the proposed model: All non-surface (non-top boundary) discrete elements are set to contain the same amount of biomass, and, hence, have the same thickness ($L_{F,i\neq1} = dL_F$) during the simulated growth period, and were kept constant. Increase in biofilm thickness is modeled as the addition of a new layer of biomass onto the surface of the existing biomass (into the surface discrete element, $L_{F,i=1}$, which has an initial thickness of 0). Addition of the new surface element is triggered when the increase in thickness reached dL_F (detected by the *event* function of the *ode15s* solver) (Fig. 4). Directly after addition of this new discrete element, the variables in new discrete element are assumed to have the same value as the element below ($S_{x,i=1} = S_{x,i=2}$) and the system was solved again using this as the new initial condition. A grid sensitivity study showed one discrete element per 10 µm of the simulated biofilm thickness was numerically sufficient (< 1% change with a further increase in number of discrete elements).
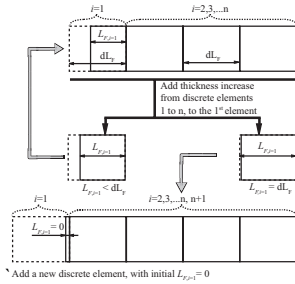
Figure 4: Schematic representation of the implementation of biofilm thickness (L_F) as a pseudo-state variable. dL_F is the pre-defined biofilm thickness for the non-surface discrete element (i = 2, …, n). $L_{F,i=1}$ is the biofilm thickness of the surface discrete element (i = 1). The sum of biofilm thickness increase from all discrete elements ($\sum_i^n L_{F,i}$) is added to $L_{F,i=1}$. Once $L_{F,i=1}$ reached dL_F, a new discrete element was added on top of the former $L_{F,i=1}$

In the present study, the parameters used in the model were adjusted to a *Halochlorella rubescens* (CCAC 0126; Culture Collection of Algae at the University of Cologne; www.ccac.uni-koeln.de) TL-PSBR biofilm cultivated with Bold's basal medium (BBM; Bischoff and Bold 1963), which served as a model system in previous experimental PSBR biofilm studies (Schultze et al., 2015; Li et al, 2015; Li et al 2015).

In the present study, in order to achieve a realistic representation of the investigated system, experiments were carried out in the framework of this study to acquire the parameters required in the model equations (coefficients and constants found in Eq. 1 to Eq. 24). However, it was not possible to acquire all the parameters experimentally, as a result, some of the parameters were taken from previously published studies, and others had to be assumed due to lack of knowledge (e.g. the biomass was assumed to be able to utilize bicarbonate directly as a carbon source). The assumed parameters were acquired by running the model with different sets of unknown parameters (within a theoretically reasonable range) and selecting the parameter set that produced results that fitted the experimental observations. Model parameters used in the present study, their value and their methods of determination or references can be found in Tab. II and III (for detailed experimental method see supplementary materials, as indicated in the text above).

Table III: [a]Chemical reactions integrated into the proposed model and their rate and equilibrium constants.

Reaction	Equilibrium constant, K	Rate constant, k, in d^{-1}	Source
$H_2O \leftrightarrow H^+ + OH^-$	10^{-14}	Instantaneous	Morales-Rodriguez et al., 2011
$CO_2 + H_2O \leftrightarrow HCO_3^- + H^+$	$10^{-6.35}$	$10^{7.54}$	Gibbson and Edsall, 1963
$CO_2 + OH^- \leftrightarrow HCO_3^-$	$10^{-6.35}$	$10^{8.86}$	Wolf et al., 2000
$HCO_3^- \leftrightarrow CO3^{2-} + H^+$	$10^{-10.33}$	$10^{4.6}$	Morales-Rodriguez et al., 2011
$H_3PO_3 \leftrightarrow H_2PO_3^{2-} + H^+$	$10^{-2.15}$	Instantaneous	Morales-Rodriguez et al., 2011
$H_2PO_3^- \leftrightarrow HPO_3^{2-} + H^+$	$10^{-7.2}$	$10^{9.74}$	Morales-Rodriguez et al., 2011
$HPO_3^{2-} \leftrightarrow PO3^{3-} + H^+$	$10^{-12.1}$	Instantaneous	Morales-Rodriguez et al., 2011

[a]At 25°C.

Table II: [a]Model parameters applied in the present study.

Symbol	Definition	Value/Unit		Source
ETR_{max}	Maximal electron transfer rate	49.6	mole m^{-2} s^{-1}	b
$D_{cations}$	Considered here as diffusion coefficient of Na$^+$ in water	1.15×10^{-4}	m^2 d^{-1}	Morales-Rodriguez et al. 2011
D_{CO_2}	Diffusion coefficient of CO_2 in water	1.65×10^{-4}	m^2 d^{-1}	Morales-Rodriguez et al. 2011
D_{CO_3}	Diffusion coefficient of CO_3^{2-} in water	1.02×10^{-4}	m^2 d^{-1}	Morales-Rodriguez et al. 2011
D_{HCO_3}	Diffusion coefficient of HCO_3^- in water	7.9×10^{-5}	m^2 d^{-1}	Morales-Rodriguez et al. 2011
D_{NO_3}	Diffusion coefficient of NO_3^- in water	1.47×10^{-4}	m^2 d^{-1}	Morales-Rodriguez et al. 2011
D_{O_2}	Diffusion coefficient of O_2 in water	1.73×10^{-4}	m^2 d^{-1}	Morales-Rodriguez et al. 2011

Table II (*continued*)

Symbols	Definition	Value/Unit		Source
$D_{H_2PO_4}$	Diffusion coefficient of $H_2PO_4^-$ in water	6.2×10^{-5}	$m^2\ d^{-1}$	Morales-Rodriguez et al. 2011
f_a	Factor determining facilitated CO_2 transfer	100	/	c
f_b	Factor determining facilitated CO_2 transfer	10^{-4}	/	c
K_{Hen,CO_2}	Henry's constant of CO_2 dissolution in water	3.04×10^{-7}	$m^2\ d^{-1}$	Morales-Rodriguez et al. 2011
K_{Hen,O_2}	Henry's constant of oxygen dissolution in water	1.3×10^{-8}	$m^2\ d^{-1}$	Morales-Rodriguez et al. 2011
$K_{R_{CO_2/O_2,S}}$	Saturation coefficient representing effect of CO_2 to O_2 ration on O_2 inhibition	0.35	/	c
$K_{O_2,In,max}$	Maximal inhibition coefficient of oxygen on net photosynthetic productivity	1×10^{-3}	M	c
$K_{CO_2,S}$	Half saturation coefficient of CO_2 on photosynthetic productivity	4×10^{-4}	M	[c]Goldman et al. 1974
$K_{CO_2,in}$	Inhibition coefficient of CO_2 on photosynthetic productivity using bicarbonate	5×10^{-4}	M	c
$K_{HCO_3,S}$	Half saturation coefficient of HCO_3^- on photosynthetic productivity	4×10^{-5}	M	[c]Goldman et al. 1974
$K_{NO_3,S}$	Half saturation coefficient of NO_3^- on photosynthetic productivity	1×10^{-4}	M	Wolf et al. 2000
$K_{O_2,S}$	Half saturation coefficient of O_2 on dark respiration	1×10^{-4}	M	Wolf et al. 2000
$K_{PO_4,total,S}$	Half saturation coefficient of total phosphate on photosynthetic productivity	1.7×10^{-5}	M	Wolf et al. 2000
L_m	Substrate membrane thickness	5×10^{-5}	m	c
p_{O_2}	O_2 partial pressure at the biofilm surface	21000	Pa	/
$p_{CO_2,medium}$	Dissolved CO_2 partial pressure in medium	41	Pa	/
$p_{CO_2,surface}$	Dissolved CO_2 partial pressure at biofilm surface	41	Pa	/
pH_{medium}	pH of the medium	6.8	/	Bischoff and Bold, 1963
$R_{d,max}$	Maximal biomass dark respiration rate	0.133	d^{-1}	b
r_{bs}	Surface reflectance of the biofilm	0.1	/	c
r_{ms}	Surface reflectance of the membrane	0.5	/	c
$S_{cations,medium}$	Sum of cations concentrations in medium, here considered as Na^+ (calculated as $[NO_3^-]$ + $2 \cdot [HPO_4^{2-}] + [H_2PO_4^-]$ in fresh medium)	5.1×10^{-4}	M	[c]Bischoff and Bold, 1963
$S_{CO_2,medium}$	Dissolved CO_2 concentration in medium	/	M	e
$S_{CO_3,medium}$	Dissolved bicarbonate ion concentration in medium	/	M	e
$S_{HCO_3,medium}$	Dissolved carbonate ion concentration in medium	/	M	e
$S_{O_2,medium}$	Dissolved oxygen concentration in medium	0	M	c
$S_{NO_3,medium}$	NO_3^- concentration in medium	2.94×10^{-3}	M	Bischoff and Bold, 1963
$S_{HPO_4,medium}$	HPO_4^{3-} concentration in medium	4.31×10^{-4}	M	Bischoff and Bold, 1963
$S_{H_2PO_4,medium}$	$H_2PO_4^{3-}$ concentration in medium	1.29×10^{-3}	M	Bischoff and Bold, 1963
u_z	Convection rate due to evaporation on the biofilm surface	0.23	$m\ d^{-1}$	Li et al., 2015

[a]At 23°C. [b]Determined experimentally, see supplementary materials. [c]Assumed. [d]Product data sheet. [e]Calculated from chemical equilirium.

Results and Discussion

Light transfer in TL-PSBR

Simulated irradiance distributions in a 1,000 μm thick TL-PSBR biofilm subjected to 300 μmol photon m^{-2} s^{-1} are presented in Fig. 5: Comparison between irradiance profile modeled, considering neither forward scattering nor pigment adaptation, with forward scattering but no pigment adaptation and in-scattering plus pigment adaptation are given in Fig. 5A. Fig. 5B compares the modeled results and experimental data as measured by Li et al. (2015b). The results show that both forward scattering and pigment adaptation of the biomass have significant effects on the distribution of PAR in a PSBR biofilm. By adding the forward scattering term and/or the term describing the pigment adaptation of the biomass, the PAR penetrates deeper into the biofilm (Fig. 5A). Comparison between the simulated results with both forward scattering and biomass pigment adaptation taken into consideration showed that the proposed model can very accurately describe the PAR distribution in *H. rubescens* TL-PSBR (Fig. 5B).

Based on the model developed by Murphy and Berberoglu (2014), it is concluded that the intensity distributions calculated from optical thickness with a fixed mass extinction coefficient are a sufficient modeling approximation. Our results, however, show that both forward scattering and adaption of the biomass (changing the absorption coefficient along the depth gradient, i.e. lowering biomass absorption coefficient in the part of the biofilm near the surface) increased the penetration depth of the PAR (as shown by the high fit of modeled data to the experimental data). Thus, light penetration depth and light dilution rate (i.e. available photons per cell) would be significantly underestimated if the in-scattering and/or biomass pigment adaptation were not taken into consideration in such biofilm models, as could be suspected from previous studies as reviewed by (Richardson et al., 1983).
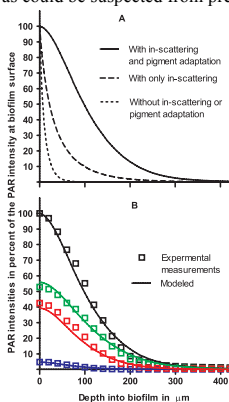
Figure 5: Light intensity distributions presented as percent of the surface irradiance in *Halochlorella rubescens* biofilms exposed to 300 μmol photon m^{-2} s^{-1}. **A**: Simulated total photosynthetic active radiation (PAR) distributions under different scenarios (without both in-scattering and pigment adaptation, dotted line; with in-scattering only, dashed line; and with both in-scattering and pigment adaptation, solid line). **B**: Comparison between simulated distribution considering both in-scattering and biomass pigment adaptation (solid lines) and experimental data (empty squares) measured by Li et al. (2015b). Different colors indicate different spectrum bands (red 600 – 700 nm, green 500 – 600 nm, blue 400 – 500 nm, respectively).

Delivery of dissolved inorganic carbon

Figure 6 compares the simulated results (with and without taking facilitated CO$_2$ transport due to extracellular CA into account) of biofilms exposed to 300 μmol photon m^{-2} s^{-1} surface irradiance and different additional gas phase CO$_2$ concentrations (0% and 5% v/v). Compared to the modeled result without considering facilitated CO$_2$ transfer in the model, when no additional CO$_2$ was supplied in the gas phase, the simulated results with a term describing facilitated CO$_2$ transfer reflected the experimental data presented by Li et al. (2015b) more faithfully.   In contrast to these findings, at high CO$_2$ concentration (5% supplementary CO$_2$ in the gas phase), no significant effect of the implementation of facilitated CO$_2$ transfer could be observed (Fig. 6B).

The phenomenon of facilitated CO$_2$ transport in solutions with CA is well documented, and known to accelerate intracellular CO$_2$ transfer and CO$_2$ transfer in liquid membranes up to 200-fold (Bao and Trachtenberg, 2006; Trachtenberg et al., 1999). Our results strongly suggest that this is also the case in *H. rubescens* biofilms: Without taking into account facilitated CO$_2$ transfer, the simulated results predict a much lower dissolved oxygen

concentration ([DO]) compared to the experimental data, which is also valid for pH values. Thus, the results suggest that facilitated CO_2 transport plays an important role in supplying DIC into the biofilm at low gas phase CO_2 concentrations. In the present study, the facilitated CO_2 transport was modeled using an exponential function dependent on the local CO_2 concentration, However, previous studies suggested that this phenomenon also depends on the concentration of CA, the concentration of other dissolved species and/or their structures as well (Bao and Trachtenberg, 2006; Gros et al., 1976; Trachtenberg et al., 1999). In contrast, the approach used here appears to be crude. Nevertheless, under the assumption of all other factors being constant, a CO_2 concentration-dependent relationship as found here has been previously observed by other researchers (Gros et al., 1976). It can be expected, that this facilitated CO_2 transport exists also in submerged phototrophic biofilms. However, due to a significantly thicker boundary layer at the biofilm surface and the liquid phase instead of a gas phase covering the biofilm, the effect of the facilitated CO_2 transport would be much less pronounced in submerged biofilms due to limited transport at the biofilm surface compared to a PSBR biofilm.
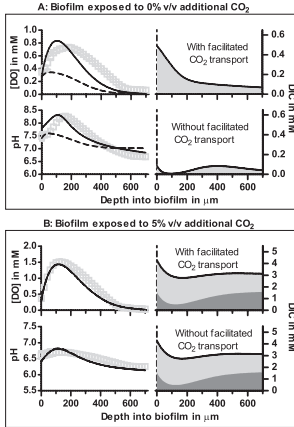
Figure 6: Dissolved oxygen concentration ([DO]), pH and dissolved inorganic carbon (DIC) profiles in *Halochlorella rubescens* biofilms exposed to 300 μmol photon m^{-2} s^{-1}. Panel **A** and **B** present data simulated/measured with 0% and 5% additional CO_2 in the gas phase. In each panel: [DO] profiles are presented in top-left subplots, whereas bottom-left subplots give pH profiles (in both left subplots, solid lines: simulated distribution with facilitated CO_2 transfer; dashed lines: simulated distribution without facilitated CO_2 transfer; empty squares: experimental data measured by Li et al., 2015b). The two subplots on the right present simulated DIC distributions with profiles considering facilitated transfer on top (solid lines: total [DIC]; light gray area: bicarbonate; dark gray area: dissolved free CO_2). Notice at 5% CO_2, no significant difference can be observed between simulated distributions with and without considering facilitated CO_2 transfer.

Nutrient supply in TL biofilms subjected to high irradiance

Gradients in simulated *H. rubescens* PSBR biofilms exposed to 1,000 μmol photon m^{-2} s^{-1} and different CO_2 concentrations in the gas phase are presented in Fig. 7. The simulated [DO] and pH profiles are compared with the experimental data measured by Li et al. (2015b): The simulated profiles generally reflect the experimental data with a good fit. However, at 5% additional CO_2 in the gas phase, the simulated [DO] are about 20% lower than the measured values. The simulated results also show that the supply of N and P to the growing region of the biofilm (illuminated zone) is not limiting at irradiances and CO_2 concentrations used for the simulation.

The observed lower [DO] in the simulated results using 5% supplementary gas phase CO_2 compared to the experimental data might be explained by the determination of the model parameters from biomass grown at a lower light intensity (300 μmol photon m^{-2} s^{-1}), which may lead to an inaccurate set of input parameters (e.g. a higher ETR_{max} and/or different Monod constants) for this specific growth conditions.

Figure 7: Dissolved oxygen concentration ([DO]), pH, dissolved inorganic carbon (DIC) and macronutrients (N as nitrate and P as total inorganic phosphate) profiles in *Halochlorella rubescens* biofilms exposed to 1,000 µmol photon m^{-2} s^{-1}, and considering facilitated CO_2 transfer. Panel **A** and **B** present data simulated/measured with 0% and 5% additional CO_2 in the gas phase, respectively. In each panel: [DO] profiles are presented in top-left subplots and bottom-left subplots give the pH profiles (in both left subplots, solid lines: simulated distribution; empty squares: experimental data measured by Li et al., 2015b). The top-right subplots present simulated DIC profiles (solid lines: total [DIC]; light gray area: bicarbonate; dark gray area: dissolved free CO_2). The bottom-right subplots show the simulated macronutrient profiles (dark gray solid lines: N; light gray solid lines: P).
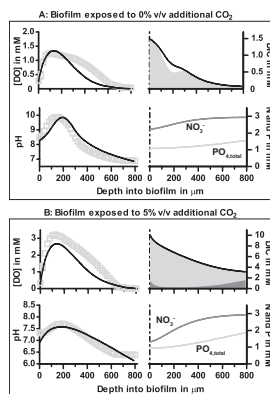
At 0% CO_2, the concentrations of macro-nutrients N and P decreased only slightly at the biofilm surface compared to the biofilm–membrane interface, whereas the [DIC] changed dramatically along the depth gradient. At 5% CO_2, the concentrations of N and P, especially nitrate, changed significantly along the depth gradient, however, this was a minor change compared to the change in [DIC] (5-fold greater difference than NO_3). Thus, it is very likely that the change of N and P concentrations along the depth gradient in the modeled biofilm has only a minor effect on the pH gradient. The main contributor shaping the pH gradient is the consumption of DIC.

Our data suggest that supply of N and P to the growing region of the biofilm was also not limiting at high irradiances and high CO_2 concentrations, even when the 20% underestimation of [DO] in the modeled results was taken into account (assuming a lower [DO] directly translates into lower productivity), provided that the nutrient concentrations in the bulk liquid phase remain constant. Thus, a direct upscaling of the model to 2D should be avoided (as the nutrient concentrations change with vertical distance from the medium outlet). Nevertheless, a pseudo-2D model based on the proposed model can be easily developed (IWA Task Group on Biofilm Modelling 2006), that can be used to predict growth along a vertically oriented cultivation area.

Effect of buffering on growth and DIC distribution

Fig. 8 presents the simulated growth rates and [DIC] profiles in *H. rubescens* PSBR biofilms exposed to 300 µmol photon m^{-2} s^{-1} and three supplementary CO_2 concentrations (0%, 1% and 5% v/v, respectively), as well as medium with different buffering capacities (BBM without additional buffer and BBM with excessive buffering capacity, the latter was achieved by modeling the pH as a constant with a value of 6.8). The results show that the medium buffering capacity can influence both total [DIC] and its speciation in the biofilm. At 0% supplementary CO_2 in the gas phase, the growth for both well buffered and normal medium is mostly due to bicarbonate assimilation. The additional buffering of the medium actually decreased the [DIC]. At 1% supplementary CO_2, the growth based on bicarbonate surpasses growth based on CO_2 slightly. The buffered medium causes a decrease in [DIC] near the biofilm surface, however, this has no significant impact on growth rate. At 5% CO_2, growth utilizing CO_2 exceeds bicarbonate-mediated growth and the buffering of the medium increases the concentrations of both CO_2 and bicarbonate.

Figure 8: Simulated growth and dissolved inorganic carbon (DIC) profiles in *Halochlorella rubescens* biofilms exposed to 300 µmol photon m^{-2} s^{-1}, and considering facilitated CO_2 transfer. Panel **A**, **B** and **C** present data simulated/measured with 0%, 1% and 5% additional CO_2 in the gas phase, respectively. In each panel: The left subplots present simulated growth profiles (black solid lines: CO_2 growth with normal medium; black dashed lines: bicarbonate growth with normal medium; gray solid lines: CO_2 growth with excessively buffered medium; gray dashed lines: bicarbonate growth with excessively buffered medium). DIC profiles are presented in the right subplots with the profiles simulated with normal medium on top (solid lines: total [DIC]; light gray area: bicarbonate; dark gray area: dissolved free CO_2).
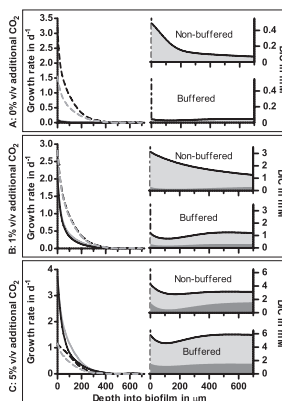
The results suggest that at low gas phase CO_2 concentration (no additional CO_2 supplied in the gas phase), by buffering the medium excessively, the pH at the biofilm surface is lowered. Thus, less bicarbonate is formed at the biofilm surface, leading to less DIC entering the biofilm. Finally, this results in reduced growth rates in buffered medium compared to normal medium (photosynthesis using bicarbonate is reduced). At 1% supplementary CO_2 in the gas phase, the buffering of the medium produces no significant change in growth rate distribution, even though the DIC distribution was affected. This might be caused by the limitation of growth by other factors (such as the $CO_2:O_2$ ratio) rather than by the limiting supply of DIC at the given CO_2 concentration in the gas phase. By increasing the ambient CO_2 concentration to 5%, a slight increase in CO_2-mediated growth was observed, most likely induced by an increase in the $CO_2:O_2$ ratio. However, this was countered by the inhibiting effect of a high CO_2 concentration on bicarbonate utilization. As a result, the total growth rate (sum of CO_2 and bicarbonate growth) was not affected.

In the present study, the *H. rubescens* strain used for simulation is assumed to be pH insensitive (i.e. pH has no direct influence on growth) and can utilize bicarbonate for photosynthesis with relatively high efficiency. Thus, the buffering of the medium generally does not have a large effect on growth. However, if a more pH-sensitive strain and/or a strain with less efficient bicarbonate uptake mechanisms would be considered, the effect of medium buffering would be much more pronounced.

Long term biomass growth and effect of dark respiration

Figure 9 presents biomass growth data using continuous illumination (as the model currently is numerically unstable when a light/dark circle is considered) from both experimental (Schultze et al., 2015) and simulated data. In this growth simulation, the effect of temperature is taken into consideration: Algal growth was simulated with both the dark respiration rate measured at 23°C (see supplementary materials) and an adjusted dark respiration rate increased by a factor of 1.5, as the temperature in the growth experiments was elevated by about 5°C (Schultze et al., 2015). Here, the elevated temperature was assumed to have the same impact on gross photosynthetic production and photorespiration, thus the net growth (i.e. gross photosynthetic production minus photorespiration and dark respiration) was considered to be not temperature dependent, and thus, only the dark respiration rate is affected by the elevated temperature (i.e. increase with increasing temperature) in the proposed model. And the correction factor for the increase of dark respiration rate with elevated temperature was estimated based on the observation of Hancke and Glud (2004). The simulated results show that biomass growth of *H. rubescens* was significantly affected by the dark respiration rate (i.e. temperature). Considering a higher dark respiration rate adjusted to the modified experimental conditions, simulated values fit the experimental data with very high fidelity.
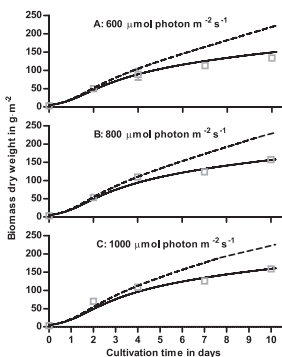
Figure 9: Experimental (Schultze et al., 2015) and simulated growth data of *Halochlorella rubescens* biomass in a Twin-Layer porous substrate bioreactor using continuous illumination. Panel **A**, **B** and **C** give growth data from biofilms cultivated at 600, 800 and 1000 µmol photon m^{-2} s^{-1} surface irradiance, respectively. In all panels: Grey squares represent previously measured experimental data; solid lines gives the simulated data using an adjusted dark respiration rate to match the experimental temperature of 28 °C. Dashed line show the simulated data using dark respiration rate measured at 23°C.

Another possible reason for the increased dark respiration rate could be: in their experimental setup, Schultze et al. did not exclude gas transfer between the macro-porous material and the ambient air (Schltze et al., 2015), thus oxygen was supplied from the bottom of the biofilm to the non-illuminated region of the biofilm, and this presumably led to an increase in dark respiration. However, this effect affects only the bottom part of the biofilm, and its influence was small compared to the overall effect of temperature (data not shown).

The results presented here simulate growth of continuously illuminated *H. rubescens* biofilms, and thus should not be directly applied to systems with a light/dark cycle. The results strongly suggest that the dark respiration rate, during the dark phase or in the non-illuminated region of the biofilm, has a strong impact on biomass productivity of the TL-PBSR. In practice, by reducing this dark respiration (e.g. reduced temperature during the dark period), a higher total biomass productivity can be achieved.

Conclusions

Our results show that the proposed model in the present study can accurately predict the distribution of light intensity in TL-PSBR biofilms, provided the optical properties of the biomass are measured experimentally. With other model parameters acquired both from the literature and from experiments, the prediction of [DO] and pH profiles also reflect experimental data with high fidelity. Also, the simulated biomass growth reflexes the experimental results with high accuracy.

In the present study, the model was used to simulate TL-PBSR subjected to several growth scenarios for one algal strain by applying different sets of model parameters. The model can be used to predict the distribution of gradients under any given culture condition and/or for different algal strains, provided experiments are carried out to determine different parameters. Improvement of the model can be made in several aspects, e.g. a better description for the facilitated CO_2 transport and/or the effect of temperature; or, a more accurate description of the pigment adaptation mechanism. However, such improvements require more experimental observations and will increase the complexity of the model considerably. By presenting this approach, we have proven that our model considering various complex dynamics in a biofilm does have the capability to predict total biofilm growth rates with considerable accuracy. Therefore, with some further modification, it may be a valuable tool in system optimization in PSBR and process design

Acknowledgements

References:

Atteia A, van Lis R, Tielens AG, Martin WF. 2013. Anaerobic energy metabolism in unicellular photosynthetic eukaryotes. Biochimca et Biophysica Acta - Bioenergetics 1827(2):210-223.

Atkinson MJ, Smith SV. 1983. C:N:P ratios of benthic marine plants1. Limnology and Oceanography 28(3):568-574.

Bao L, Trachtenberg MC. 2006. Facilitated transport of CO_2 across a liquid membrane: Comparing enzyme, amine, and alkaline. Journal of Membrane Science 280(1–2):330-334.

Berberoglu H, Yin J, Pilon L. 2007. Light transfer in bubble sparged photobioreactors for H2 production and CO2 mitigation. International Journal of Hydrogen Energy 32(13):2273-2285.

Bergman TL, Lavine AS, Incropera FP, DeWitt DP. 2011. Fundamentals of heat and mass transfer. Hoboken, New Jersey, USA: John Wiley & Sons.

Bischoff HW, Bold HC. 1963. Some soil algae from Enchanted Rock and related algal species. Austin, Texas, USA: University of Texas Press. 95 p.

Campos E, Flotats X. 2003. Dynamic simulation of pH in anaerobic processes. Applied Biochemistry and Biotechnology 109(1-3):63-76.

Colomer G, Costa M, Consul R, Oliva A. 2000. Radiant exchange in domains with obstacles using the discrete ordinates method. European Congress on Computational Methods in Applied Sciences and Engineering. Barcelona.

Courant R, Isaacson E, Rees M. 1952. On the solution of nonlinear hyperbolic differential equations by finite differences. Communications on Pure and Applied Mathematics 5(3):243-255.

Dunn IJ, Heinzle E, Ingham J, Prenosil JE. 2003. Biological reaction engineering. Weinheim: Wiley-VCH Verlag.

Gibbons BH, Edsall JT. 1963. Rate of hydration of carbon dioxide and dehydration of carbonic acid at 25 degrees. Journal of Biological Chemistry 238:3502-7.

Goldman JC, Oswald WJ, Jenkins D. 1974. The kinetics of inorganic carbon limited algal growth. Journal Water Pollution Control Federation 46(3):554-574.

Gros G, Moll W, Hoppe H, Gros H. 1976. Proton transport by phosphate diffusion - a mechanism of facilitated CO_2 transfer. The Journal of General Physiology 67(6):18.

Grötzschel S, de Beer D. 2002. Effect of oxygen concentration on photosynthesis and respiration in two hypersaline microbial mats. Microbial Ecology 44(3):208-216.

Hancke K, Glud RN. 2004. Temperature effects on respiration and photosynthesis in three diatom-dominated benthic communities. Aquatic Microbial Ecology 37(3):265-281.

IWA Task Group on Biofilm Modelling. 2006. Mathematical modeling of biofilms. London, UK: IWA Publishing. 179 p.

Ku S-B, Edwards G. 1978. Oxygen inhibition of photosynthesis. Planta 140(1):1-6.

[a]Li T, Podola B, de Beer D, Melkonian M. 2015. A method to determine photosynthetic activity from oxygen microsensor data in biofilms subjected to evaporation. Journal of Microbiological Methods 117:100-107.

[b]Li T, Piltz B, Podola B, Dron A, de Beer D, Melkonian M. Microscale profiling of photosynthesis-related variables in a highly productive biofilm photobioreactor. Biotechnology and Bioengineering, accepted manuscript online: 24 OCT 2015

Liu T, Wang J, Hu Q, Cheng P, Ji B, Liu J, Chen Y, Zhang W, Chen X, Chen L and others. 2013. Attached cultivation technology of microalgae for efficient biomass feedstock production. Bioresource Technology 127(0):216-222.

Morales-Rodriguez R, Singh R, Cameron I, Gani R. 2011. Chapter 12 - Modelling for Bio-,Agro- and Pharma Applications. In: Gani IC, editor. Product and Process Modelling. Amsterdam: Elsevier. p 363-432.

Murphy TE, Berberoglu H. 2014. Flux balancing of light and nutrients in a biofilm photobioreactor for maximizing photosynthetic productivity. Biotechnology Progress 30(2):348-359.

Murphy TE, Fleming E, Berberoglu H. 2014. Vascular structure design of an artificial tree for microbial cell cultivation and biofuel production. Transport in Porous Media 104(1):25-41.

Naumann T, Cebi Z, Podola B, Melkonian M. 2013. Growing microalgae as aquaculture feeds on twin-layers: a novel solid-state photobioreactor (vol 25, pg 1413, 2013). Journal of Applied Phycology 25(5):1619-1619.

Nowack ECM, Podola B, Melkonian M. 2005. The 96-Well Twin-Layer System: A novel approach in the cultivation of microalgae. Protist 156(2):239-251.

Ogbonna JC, Yada H, Tanaka H. 1995. Kinetic study on light-limited batch cultivation of photosynthetic cells. Journal of Fermentation and Bioengineering 80(3):259-264.

Olivieri G, Salatino P, Marzocchella A. 2014. Advances in photobioreactors for intensive microalgal production: configurations, operating strategies and applications. Journal of Chemical Technology & Biotechnology 89(2):178-195.

Platt T, Gallegos CL, Harrison WG. 1980. Photoinhibition of photosynthesis in natural assemblages of marine phytoplankton. Journal of Marine Research 38:687-701.

Pope DH. 1975. Effects of light intensity, oxygen concentration, and carbon dioxide concentration on photosynthesis in algae. Microbial Ecology 2(1):1-16.

Raven JA, Beardall J, Giordano M. 2014. Energy costs of carbon dioxide concentrating mechanisms in aquatic organisms. Photosynthesis Research 121(2):111-124.

Raven JA, Cockell CS, De La Rocha CL. 2008. The evolution of inorganic carbon concentrating mechanisms in photosynthesis. Philosophical transactions of the Royal Society of London. Series B, Biological sciences 363(1504):2641-2650.

Richardson K, Beardall J, Raven JA. 1983. Adaptation of unicellular algae to irradiance: an analysis of strategies. New Phytologist 93(2):157-191.

Schiesser WE. 1991. The Numerical Method of Lines: Integration of Partial Differential Equations. Waltham, Massachusetts: Academic Press. 326 p.

Schlichting H, Gersten K. 2000. Boundary-layer theory. Berlin/Heidelberg: Springer-Verlag. 800 p.

Schultze LKP, Simon M-V, Li T, Langenbach D, Podola B, Melkonian M. 2015. High light and carbon dioxide optimize surface productivity in a Twin-Layer biofilm photobioreactor. Algal Research-Biomass Biofuels and Bioproducts 8:37-44.

Shi J, Podola B, Melkonian M. 2014. Application of a prototype-scale Twin-Layer photobioreactor for effective N and P removal from different process stages of municipal wastewater by immobilized microalgae. Bioresource Technology 154(0):260-266.

Trachtenberg MC, Tu CK, Landers RA, Willson RC, McGregor ML, Laipis PJ, Kennedy JF, Paterson M, Silverman DN, Thomas D and others. 1999. Carbon dioxide transport by proteic and facilitated transport membranes. Life Support Biosph Sci 6(4):293-302.

Wolf G, Picioreanu C, van Loosdrecht MCM. 2007. Kinetic modeling of phototrophic biofilms: The PHOBIA model. Biotechnology and Bioengineering 97(5):1064-1079.

Supplementary materials

General information

In this study, a Twin-Layer biofilm of the green alga *Halochlorella rubescens* (CCAC 0126; Culture Collection of Algae at the University of Cologne; www.ccac.uni-koeln.de) was modeled. Some of the parameters used in the present study were acquired experimentally, as described below. All statistical analysis of the experimental results presented here were carried out using Prism (version 5.1, Graphpad, GraphPad Software Inc., La Jolla, USA).

Experimental studies

Biofilm cultivation

To investigate the growth of the biofilm and to characterize the biomass, H. rubescens biofilms with an inoculation biomass concentration of 5 g m-2 were produced and cultivated as described by Li et al. (2015) (batch setup, with circulating medium): BBM culture medium (Bischoff and Bold, 1963)   and a light intensity of 300 µmol photons m-2 s-1 with a 14/10 light/dark cycle were used for the whole cultivation period, and the biofilms were aerated with 0.75 L min-1 ambient air.

The freshly harvested biofilm samples were measured for fresh weight, and biofilm thickness was measured using a hand microtome as described by Li et al. (2015). The biofilm volume was estimated by multiplying biofilm area and thickness. The samples were then dried at 105 ℃ for 2 hours prior to dry weight (DW) determination.

Long term growth experiment

To investigate the growth of the biofilm and to characterize the biomass, *H. rubescens* biofilms were cultivated for 100 days, and triplicate samples were taken twice a week. Subsequently, biomass was digested, and its N and P contents were determined using the method by   (Hu and Barker, 1999). Finally, to achieve a more accurate determination, the nitrogen and phosphorus contents (w/w) of the N and P contents of samples from 100 day were also determined using an elemental analyzer (Flash 1112, Interscience, Rockland, MA, USA). Biomass concentration (X_F) was calculated as dry biomass per fresh biofilm volume (in kg m^{-3}). In the present study, the biomass concentration is considered to be constant, as: A linear regression of the data does yield a line with a slope significantly different from zero. However, after day 40, most of the dry biomass concentration data points were not significantly different from each other, as suggested by ANOVA test. Thus, we suspect that the significant different at the beginning of the cultivation is caused by error in biofilm thickness measurements, as the biofilm is too thin to be measured accurately. Even if the biomass concentration change observed was caused by reasons other than inaccurate biofilm thickness measurements, the exact reason and mechanism are unclear to us. From our point of view, and also for the simplicity of the model the assumption that the biomass concentration remains constant during the cultivation period was made. The results are present in Fig. S1, S2 and S3. Biomass yield on C, N and P are calculated as the reciprocal of their respective biomass contents. A C:N:P ratio of 40:7:1 was used for the present study (for calculated yields, refer to Tab. II).
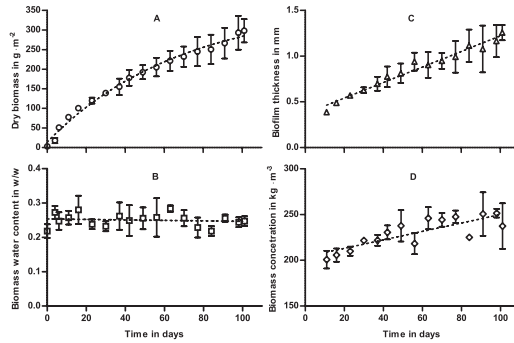
`Figure S1:** Biomass of *Halochlorella rubescens* biofilms during 100 days of cultivation. **A**: Biomass dry weight (DW), the dotted line is a one-phase association curve fitted to the data. **B**: Biomass water content in w/w (DW/fresh weight), dotted line represents the linear regression line of the data. **C**: Biofilm thickness, dotted line represents a linear regression. **D**: Biomass concentration (DW/fresh volume), dotted line represents a linear regression. In all panels, error bars represent the standard deviations of triplicates.
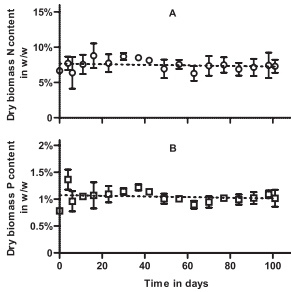
Figure S2: Biomass N and P contents of *Halochlorella rubescens* biofilms during 100 days of cultivation. **A**: Biomass N content (w/w), empty circles and error bars represent the means and standard deviations of triplicates; dotted line represents the linear regression line of the data. **B**: Biomass P content (w/w), empty squares and error bars represent the means and standard deviations of triplicates; dotted line represents the linear regression line of the data.

Figure S3: Carbon, nitrogen and phosphorus content of dry biomass of *Halochlorella rubescens* measured with an elemental analyzer. The grey bars and error bars represent means and standard deviations of 6 replicates. The horizontal dot-dash lines and the numbers next to the bars give the C, N and P contents of biomass used in the proposed model.
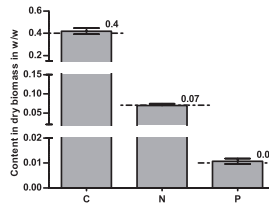
Experiments investigating effects of nutrient concentrations on biomass

To investigate the effects of different nitrogen and phosphorus concentrations in culture medium on biomass N and P content, a separate growth experiment with the same cultivation conditions except using a continuous system (medium was pump only once through the system, instead of circulating, as described by Li et al. (2015), was carried out. In this experiment, after inoculation, BBM medium with modified N or P concentrations was supplied to the Twin-Layer system. The biofilms were cultivated for 4 days, and 6 parallel samples were analyzed. The

samples were first dried for DW determination and the N and P contents were then determined with digestion (as described above). The results are shown in Fig. S4. The biomass composition is considered stable during the simulated growth (i.e. the N, P concentrations do not have impact on biomass composition), as indicated by the experimental results.
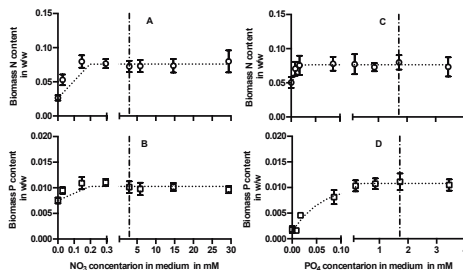
Figure S4: N and P contents of *Halochlorella rubescens* biomass from biofilms cultivated using medium with modified N or P concentrations. **A**: N content (w/w) of biofilms cultivated using medium with modified N concentrations. **B**: P content (w/w) of biofilms cultivated using medium with modified N concentrations. **C**: N content (w/w) of biofilms cultivated using medium with modified P concentrations. **D**: P content (w/w) of biofilms cultivated using medium with modified P concentrations. In all panels, error bars represent the standard deviation of triplicates and dotted lines are one-phase association curves fitted to the data. The vertical dot-dash lines give the concentration of N or P in non-modified standard Bold's basal medium (BBM).

Determination of dark respiration rate

For estimating the dark respiration rate, 24 samples were harvested on day 12 of the 100 day growth experiment (see section below). 12 samples were dried for DW determination, the other 12 were put into a bioreactor system under the same cultivation conditions but covered with aluminum foil to exclude light. After 24 hours, these 12 samples were removed from the system and their DW was determined. The dark respiration rate (in d^{-1}) was determined as:

$$R_d = \ln\left(\frac{DW_{t=1}}{DW_{t=0}}\right) \tag{Eq. S1},$$

$DW_{t=0}$ and $DW_{t=1}$ are the mean DWs of samples dried before and after the dark incubation in darkness, respectively. An R_d of 0.13 d^{-1} was calculated for the present study.

Measurement of the electron transfer rate

A depth profile of the electron transfer rate (ETR, in µmol electrons m^{-2} s^{-1}) of the 100 days old *H. rubescens* biofilms (3 parallels, i.e. 3 independent samples) was acquired between 0-600 µm using the pulse amplitude modulation (PAM) method described by Li et al. (2015). The data acquired were fitted with a P-I model (Platt et al., 1980). Based in the fitted model the maximal ETR (ETR_{max}) and the initial ETR curve slope (α) were determined. The results of the ETR measurement are presented in Fig. S5 and S6. In the present study, ETR_{max} and α was set to be 49.6 mole m^{-2} s^{-1} and 0.24, respectively (the average value of the 'illuminated zone'; as suggested by data presented by Li et al., 2015, Fig S5). The maximal biomass growth rate (μ_{max}) was estimated from the ETR_{max}: Assuming 1 mole of electron transferred corresponds to 0.16 mole of O_2 production (Morris and Kromkamp, 2003); and the ratio of O_2 production to inorganic carbon consumption is 1:1.3 (Atkinson and Smith, 1983). In the present study, the calculation yielded a maximal growth rate of 8 d^{-1}.
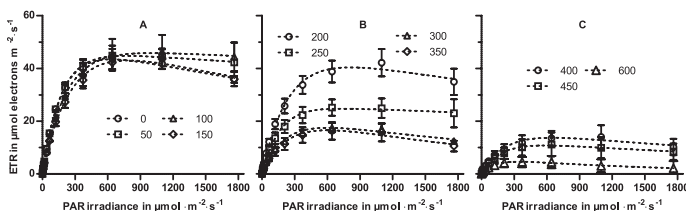
Figure S5: Electron transfer rate (ETR) measured at different depths in *Halochlorella rubescens* biofilms grown at a surface irradiance of 300 µmol photons m^{-2} s^{-1}. **A**: ETR at 0 (biofilm surface, empty circles), 50 (empty squares), 100 (empty triangles) and 150 µm depth (empty diamonds). **B**: ETR at 200 (empty circles), 250 (empty squares), 300 (empty triangles) and 350 µm depth (empty diamonds). **C**: ETR at 400 (empty circles), 450 (empty squares) and 600 (empty triangles). In all panels, the symbols and error bars give the means and standard deviations of triplicates, and the dotted lines represent the fit curve of a P-I model (see text).
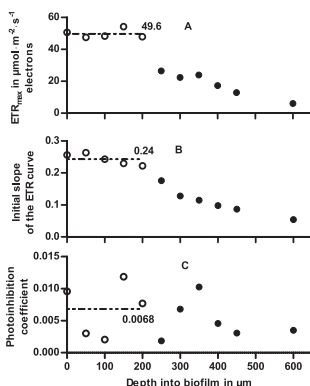
Figure S6: Maximal electron transfer rate (ETR) and initial slope of the ETR curve plotted as a depth profile in the *Halochlorella rubescens* biofilms. Values were calculated from the P-I model fitted to the ETR curve (see Fig. S3 and text). **A**: Maximal electron transfer rate (*ETR$_{max}$*). **B**: Initial slope of the ETR curve (*α*). **C**: Inhibition coefficient estimated from ETR curve (*β*). The biofilms were separated into two sections according to the results presented by Li et al. (2015): A well illuminated section (empty circles, ≥ 5 µmol photons m^{-2} s^{-1}) and a section subjected to low light (solid circles, < 5 µmol photons m^{-2} s^{-1}). In all panels, the dot-dash lines and numbers represent the average values (values used in the present study as model parameters) in well illuminated sections.

Determination of optical properties of biomass

To measure the optical properties of the biomass, fresh biomass samples (triplicate, i.e. 3 samples) from a 3 days old Twin-Layer biofilm were suspended in BBM to obtain a biomass concentration of 0.05 g L^{-1}. Ultrasonication was carried out to separate the cells. The specific extinction, absorption and scattering coefficients (β_λ, κ_λ and σ_λ; extinction = absorption + scattering) of the cell suspension were measured as described by (Berberoglu and Pilon, 2007): A photospectrometer (UV-2450, Shimadzu, Duisburg, Germany) equipped with an integrating sphere (ISR-240A, Shimadzu, Duisburg, Germany) were used; and a flow cell with 0.1 mm light path (FT04-06, Thermo, Duisburg, Germany) was employed to keep the cells in suspension during the measurements. The mass extinction, mass absorption ($M_{absorption}$ and $M_{scattering}$) and mass scattering were calculated according to (Berberoglu et al., 2007) with 1 nm wavelength resolution (coefficient divided by biomass concentration, m^2 kg^{-1}). The results of the measurements of the optical properties are given in Fig. S7. The absorption and scattering coefficient of the *H. rubescens* Twin-layer biomass in the present study ($\kappa_{\lambda,F}$ and $\sigma_{\lambda,F}$), are calculated from $M_{absorption}$, $M_{scattering}$ and X_F:

$$\kappa_{\lambda,F} = M_{absorption} \cdot X_F \tag{Eq. S2}$$

and,

$$\sigma_{\lambda,F} = M_{scattering} \cdot X_F \tag{Eq. S3}.$$
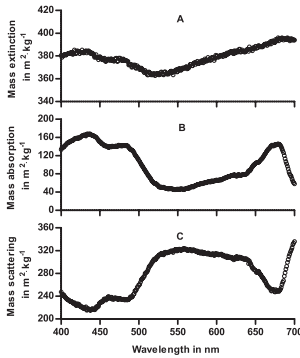
Figure S7: Optical properties of biomass from *Halochlorella rubescens* biofilms grown at a surface irradiance of 300 µmol photons m⁻² s⁻¹. **A**: Biomass mass extinction in the photosynthetically active radiation (PAR) region. **B**: Biomass mass absorption in the PAR region. **C**: Biomass mass scattering in the PAR region. In all panels, empty circles represent mean values of triplicates. Notice the differences in y-axis scales.

Determination of effective diffusion coefficients in biofilm

In present study, the X_F was set to 220 kg m⁻³ and assumed to be a constant both over time and biofilm depth (even though the linear regression showed a slope significantly different from 0, Fig. S1); Biomass C, N and P content are also considered to be stable over time and biofilm depth (as experimental results indicated little effect of both different medium nutrient concentrations and cultivation time on biomass composition). The effective diffusion coefficients (of a species x) in biofilm and membrane ($D_{e,x}$ and $D_{m,x}$) are estimated from biomass and membrane porosity (θ =0.76 and 0.35, respectively, Whatman PC-40, Whatman, Freiburg, Germany; Li et al., 2015) using the formula:

$$D_{x,e} = D_x \cdot \frac{\theta}{1+0.5\cdot(1-\theta)} \tag{Eq. S4}$$

(Weissberg, 1963). In Eq. S4, D_x represents the diffusion coefficient of species x in water, whose values can be found in Tab. II.

Experimental verification of biomass pigment adaptation

In order to verify biomass pigment adaptation, an experiment was carried out to determine the effect of light intensity on biomass chlorophyll content. *H. rubescens* biofilms were cultivated using the batch setup with identical cultivation conditions as previously described (see 0). However, instead of using only one light intensity, several light intensities were used (50 – 1000 µmol photons m⁻² s⁻¹ surface irradiance). Biofilms were harvest after 3 days and the biomass resuspened in BBM prior to mass absorption determination. Chlorophyll a content of biomass was estimated with the mass absorption as 675 nm. The results are presented in Fig. S8, which shows a significant effect of irradiance on mass absorption at 675 nm (One-way ANOVA).
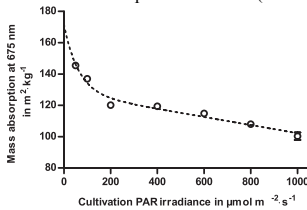
Figure S8: Mass absorption at 675 nm measured from suspended biomass cultivated at different irradiances. Empty circles and error bars represent mean values and standard deviations of triplicates. Dotted line represents a two-phase decay fit curve of the data.

Effect of nutrients concentrations on biomass growth rate

Using a similar approach as described in supplementary material section 2.3, and with identical cultivation conditions, the growth rates of *H. rubescens* biofilms using BBM medium with different nitrate and phosphate concentrations were determined. The biomass growth was observed from day 2 to day 6 after inoculation, and the

growth rates were taken as the slope of biomass increase between day 2 and day 6. The results are present in Fig. S9. The data suggest that at the concentrations encountered in normal cultivation conditions, N and P do not inhibit biomass growth.
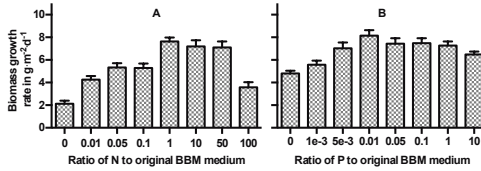
Figure S9: Effect of BBM medium with modified nutrient concentrations on the growth of *Halochlorella rubescens* biofilms. **A**: Growth of *H. rubescens* biofilms using BBM medium with modified nitrate concentrations (as indicated in the x-axis label). **B**: Growth of *H. rubescens* biofilms using BBM medium with modified phosphate concentrations (as indicated in the x-axis label). Filled bars and error bars represent the mean values and standard deviations of 6 replicates.

References for supplementary materials

Atkinson MJ, Smith SV. 1983. C:N:P ratios of benthic marine plants1. Limnology and Oceanography 28(3):568-574.

Berberoglu H, Pilon L. 2007. Experimental measurements of the radiation characteristics of Anabaena variabilis ATCC 29413-U and Rhodobacter sphaeroides ATCC 49419. International Journal of Hydrogen Energy 32(18):4772-4785.

Berberoglu H, Yin J, Pilon L. 2007. Light transfer in bubble sparged photobioreactors for H2 production and CO2 mitigation. International Journal of Hydrogen Energy 32(13):2273-2285.

Bischoff HW, Bold HC. 1963. Some soil algae from Enchanted Rock and related algal species. Austin, Texas, USA: University of Texas Press. 95 p.

Hu Y, Barker AV. 1999. A single plant tissue digestion for macronutrient analysis. Communications in Soil Science and Plant Analysis 30(5-6):677-687.

Li T, Podola B, de Beer D, Melkonian M. 2015. A method to determine photosynthetic activity from oxygen microsensor data in biofilms subjected to evaporation. Journal of Microbiological Methods 117:100-107.

Morris EP, Kromkamp JC. 2003. Influence of temperature on the relationship between oxygen- and fluorescence-based estimates of photosynthetic parameters in a marine benthic diatom (Cylindrotheca closterium). European Journal of Phycology 38(2):133-142.

Platt T, Gallegos CL, Harrison WG. 1980. Photoinhibition of photosynthesis in natural assemblages of marine phytoplankton. Journal of Marine Research 38:687-701.

Weissberg HL. 1963. Effective Diffusion Coefficient in Porous Media. Journal of Applied Physics 34(9):2636-2639.

3. Discussion

As the first step in this study, a new experimental setup and new mathematical method were developed to analyze the data acquired during the experimental studies. Then, a comprehensive and systematic investigation was carried out to study the dynamic processes inside a PSBR. In this second part, both experimental investigations with microsensors and modeling of the PSBR phototrophic biofilm were carried out. The present study established a solid basis for future investigations of the PSBR biofilms. The results acquired by this study offer the first deep insight into the PSBR biofilm. From the results, several valuable conclusions on previously established hypotheses and new hypotheses have been made.

3.1. Improvement of data analysis through the new method

As discussed previously (see manuscript 1; Li et al. 2015c), the drawbacks of the gross photosynthetic productivity measurement with oxygen microsensors in phototrophic biofilms have been known since the early 1980s, and various methods have been developed to improve its accuracy (Glud et al. 1992; Lassen et al. 1998; Revsbech 1983). However, all the methods developed until now require an assumed 'true' distribution or modification of the biofilm surface (e.g. application of a thin agar layer onto the biofilm surface), and cannot be applied if the shape of the 'true' (i.e. original gross productivity distribution) is unknown. In general, the data treatment in such measurements tries to correct the inaccuracy caused by the loss of dissolved oxygen (DO) through the biofilm surface to the phase above during the measurement period (Revsbech 1983). In a biofilm whose surface is directly exposed to a gas phase, the inaccuracy caused by this phenomenon leads to a large error when the data was analyzed directly or when previously developed methods were applied to correct the raw data.

As a result, a new mathematical method was developed in the framework of this study to correct for this effect. The results (both numerical and experimental) show the effectiveness of the proposed method. The results show clearly the significant impact that an exposed biofilm surface has on gas exchange. An important point made in the present study is that, in order to effectively apply this new data treatment method, a fine measurement resolution (≤ 20 μm) has to be used. The establishment of this method paved the way for the photosynthetic productivity measurements of the investigated PSBR biofilm using microsensors, and deepened the understanding of the transport processes (especially DO) in such biofilms. The proposed method was developed to analyze data acquired using the light-dark shift method for a non-submerged biofilm, however, with minor modifications of the boundary conditions applied (as discussed in manuscript 1), the method can also be used for data acquired using the same light-dark shift method from submerged biofilms.

3.2. Light transfer in phototrophic biofilms

As observed by Wang et al. (2015), the immobilization of algal cells in biofilms increases the light dilution rate of the total biovolume (i.e. photons available per cell) compared to that in a suspension culture. It has been long suspected, that in a phototrophic biofilm, besides adsorption, both forward-scattering of light and the adaptation of biomass (e.g. changes in pigment contents) can have significant impact on light transfer (Berberoglu and Pilon 2007; Jøsrgensen 1969). It has also been suspected, that these effects would result in a more efficient light utilization by cells immobilized in biofilms.

In this study, a direct verification of this hypothesis was carried out for the first time, by comparing modeled results using three different scenarios: 1) incorporating only extinction (no forward-scattering or biomass pigment adaptation); 2) with forward-scattering but no biomass pigment adaptation and 3) with both forward-scattering and pigment adaptation taken into account to experimental data measured with irradiance microsensors. The high accuracy of the model prediction when both forward-scattering and pigment adaptation were taken into consideration proved clearly, that the above mentioned hypothesis is correct. Thus, in future studies investigating radiative transfer (i.e. light transfer) in phototrophic biofilms, the effects of both forward-scattering and biomass pigment adaptation have to be taken into account. However, to achieve an accurate evaluation of the effects of forward-scattering and cell pigment adaptation, experiments similar to that conducted in this study have to be

carried out in order to determine the algal strain and/or cultivation condition specific parameters (e.g. scattering coefficient).

An important point that has not been addressed in this study is the effect of photosynthetically active radiation (PAR) of different wavelengths. The solution of the radiative transfer equation (RTE) applied in the model as proposed in the present study does consider the effects of different wavelengths on light transfer. However, in this study, the PAR with different wavelengths is considered to have the same effect on photosynthetic productivity, hence the term 'total PAR' was used. However, it is general knowledge, that different PAR wavelengths have different effects on photosynthetic efficiency. Thus, in future studies, one should consider incorporating this effect, and experimental studies have to be carried out to determine strain and/or cultivation condition dependent cellular pigment composition. The results can be then used to evaluate the efficiency of PAR with different wavelengths.

3.3. Effects of surface evaporation of a non-submerged biofilm surface

The analysis reveals that the fundamental processes in a PSBR biofilm and a 'traditional' (i.e. submerged) phototrophic biofilm are very similar, as both are subjected to diffusion, convection and have identical biological processes (e.g. photosynthesis and respiration; Murphy and Berberoglu 2014; Wolf et al. 2007). However, due to their essential differences in system configuration, compared to a submerged biofilm, some processes in PSBR biofilms are enhanced (e.g. gas transfer at the biofilm surface), and others weakened (e.g. accumulation of DO inside the biofilm). A marked difference between a PSBR biofilm and a submerged biofilm is that the former is subjected to surface evaporation, as in a PSBR the biofilm surface is exposed directly to the ambient gas phase. This surface evaporation creates an outward flow of liquid in the PSBR biofilm perpendicular to the biofilm surface. This, in effect, adds a flux inside the PSBR biofilm towards the biofilm surface (Bergman et al. 2011). The effect of this additional flux is an enhanced mass transfer in the direction perpendicular to the biofilm surface towards the surface of the biofilm. This leads to an enhanced nutrients transfer from the bottom of the biofilm to its surface. Also, due to an extremely thin mass transfer boundary layer at the biofilm surface, an enhanced gas exchange between the biofilm and the phase above (a gas phase for a PSBR biofilm and a liquid phase for a submerged biofilms) is achieved (Bergman et al. 2011; Schlichting and Gersten 2000). The combined effect of the additional flux and the enhanced gas exchange is an increased removal rate of oxygen produced by photosynthesis from the inside of the biofilm. The effect on [DO] in the biofilm is quite significant, as has been concluded in the first manuscript (Li et al. 2015c) presented in this thesis. However, even with this enhanced gas transfer, exceptionally high [DO] has been measured in the studied biofilm (equals to 12 times of the normal oxygen partial pressure in air under normal condition). Results from the modeling study proved that it is theoretically possible to achieve such high DO level in the investigated biofilm, but only if no oxygen is released as gas from the liquid phase inside the biofilm. However, the mechanism behind this over-saturation of oxygen in the investigated biofilm without the formation of gas bubbles is still not completely clear. Also, it is not clear how the investigated algal cells still maintained relatively high photosynthetic activity at this high level of DO. This phenomenon should be investigated further in future studies. Nevertheless, this over-saturation of oxygen could prove useful in biotechnological applications (e.g. oxygenation and/or odor removal in wastewater treatment), if this over-saturation would be transferred to the bulk liquid phase (i.e. culture medium).

Similar to oxygen, the exchange of CO_2 between the biofilm and the phase above is enhanced in a PSBR biofilm. However, this enhanced CO_2 exchange alone is not sufficient to supplied enough dissolved inorganic carbon into the deeper part of the biofilm to support the high photosynthetic activity (i.e. fast growth) that has been observed in investigations conducted both in the framework of this study (e.g. comparing the modeled data with measured data) and elsewhere (Schultze et al. 2015). A new hypothesis has been developed based on the findings made in the present study, which is discussed in the following section.

3.4. Supply of inorganic carbons in phototrophic biofilms

In this study, the following is hypothesized: At low CO_2 concentrations (i.e. without additional CO_2 in the gas phase) the facilitated CO_2 transfer in the investigated biofilm significantly increased the DIC transport efficiency

inside the PSBR biofilms. The phenomenon of facilitated CO_2 in solutions when carbonic anhydrase (CA) is present have long been observed, and has already been applied to enhance CO_2 transfer in artificial membrane systems (Bao and Trachtenberg 2006; Gros et al. 1976; Trachtenberg et al. 1999). Thus, it can also be expected in the studied biofilm. It is further hypothesized: in phototrophic biofilm, both the liquid between the cells and the surface of the cells serves as 'carrier' for the facilitated CO_2 transport, thus leading to a very strong DIC transport enhancement at low CO_2 concentrations (Bao and Trachtenberg 2006; Gros et al. 1976).

Until now, facilitated CO_2 transfer has not been reported in phototrophic biofilms. This study presents the first evidence of the existence of facilitated CO_2 transfer, and its effect on dissolved inorganic carbon (DIC) transport in a highly active phototrophic biofilm. The lack of reports on observed facilitated CO_2 transport in such biofilms until now might be due to several reasons: Firstly, the most extensively studied phototrophic biofilms are natural phototrophic biofilms, and most of these biofilms are mixed biofilms (containing significant portion of both heterotrophic and phototrophic components) as defined by Wolf et al. (2007). As CO_2 is produced by heterotrophic components inside the biofilm, which is then provided to the phototrophic organisms (i.e. increases the inorganic carbon availability inside the biofilm), the effect of the facilitated CO_2 from biofilm surface into the inside of the biofilm becomes less significant. Secondly, it is very likely, as discussed in the 2nd manuscript (Li et al. 2015b) presented in this thesis, that the DIC supply in a submerged biofilm is limited due the liquid phase above the biofilm (i.e. compared to a direct exposure to the ambient gas phase) and not by the transport inside the biofilm itself. Nevertheless, this hypothesis has to be verified independently, and additional experimental studies have to be carried out (e.g. direct determination of DIC profiles in PSBR biofilms, or verification of extracellular CA in the biofilm).

3.5. Carbon availability and pH

As suggested by the results, the facilitated CO_2 transfer plays an important role in transporting DIC to the deeper part of the biofilm when CO_2 is supplied in very low concentration in the gas phase. However, as the algal cells can only take up DIC in free CO_2, and some strains also in bicarbonate form (as assumed in the present study), the total [DIC] in the biofilm does not equal to the available DIC (e.g. when carbonate dominates, the biologically available carbon is much less than total [DIC]). As discussion previously (see manuscript 2 and 3, Li et al., 2015b and Li et al. Manuscript under review), the speciation of DIC is pH dependent, and their relationship can be estimated using a standard textbook DIC speciation chart: Generally, the higher the pH, the higher the proportion of carbonate in the total DIC, which is not available for uptake by the algal cells. However, in a phototrophic biofilm system, the interaction between pH and DIC speciation and consumption is a bidirectional process: DIC uptake (i.e. free dissolved CO_2 and bicarbonate) increases the local pH, this leads to less CO_2 and bicarbonate in the total DIC, which again influence the DIC uptake rate. In the present study, the proposed model can describe this process with relatively high accuracy, as indicated by the results.

Also, contrary to previous assumptions, the results show that uptake of macronutrients (i.e. N as nitrate and P as total phosphate) has no significant or only very small influence on local pH. Results from both experimental and modeling investigations show, that the pH in the investigated PSBR biofilm can reach high values even when a buffered medium (e.g. BBM, buffered with phosphate buffer in the present study) is used for cultivation. This indicates the existence of a cellular level pH regulation mechanism, at least in the case of *H. rubescens* used in the study, which sustained the photochemical activity of the cell at very high pH values. This pH regulation mechanism is possibly related to the carbon concentrating mechanism, as reviewed by Raven et al. (2008). And as has been shown in the present study, this mechanism plays a very important role in the investigated PSBR biofilms.

In the present study, the concentrations of solutes (e.g. macronutrients and DIC) in the medium (i.e. the bulk liquid phase, see manuscript 3) were considered to be time-independent. This was experimentally achieved by two different approaches: 1) By changing the medium very often and assumes the minor change in solute concentrations which occurs between each change had no significant influence on the results (as in all experimental investigations carried out in this study using a batch setup) or, 2) by keeping the concentrations in the medium constant (as in experiments using a continuous setup and in the model). In a real cultivation situation however,

when the medium is circulated in the system for a longer period of time, the cumulative effect of nutrients uptake, as observed by (Shi et al. 2007), and its effect on pH of the medium have to be taken into account.

3.6. Long term growth of PSBR biofilm

As discussed previously, due to the absence of a moving liquid layer above the PSBR biofilm, PSBR biofilms are not subjected to biofilm detachment. However, a reduction of growth rate with time in prolonged cultivation has been observed both in this study and in other studies (Liu et al. 2013; Li et al, 2015; Schultze et al. 2015). In the present study, the proposed model was used to predict the growth of the investigated biofilm in a 10 days period under continuous illumination. The results show that the shape of the growth curve was directly influenced by the dark respiration rate. The analysis of results indicates, it is very likely, that this reduction in growth observed during prolonged cultivations is due to the thickening of the 'dark region' (i.e. region of the biofilm that is not illuminated) as a result of the increase of the thickness of the biofilm. As in these dark regions, the biomass is consumed (i.e. respired) rather than produced. In the present study, growth simulation with a light/dark circle was not performed due to the instability of the model. When a light/dark circle is applied however, a thicker biofilm would consume more biomass during the dark period due to respiration compared to a thinner biofilm, thus resulting also in a reduced daily growth rate of the thicker biofilm compared to the thinner one under identical cultivation conditions.

3.7. Closing remarks

Through this study, important new insights into the dynamic processes in PSBR biofilms have been acquired (as discussed in the sections above). A solid basis for investigation together with powerful tools (microsensor measurements, the proposed model etc.) has been developed to help understand the processes inside such biofilms. By modifying the model parameters, the model can easily be applied to BSPR biofilms with other algal strains and/or different cultivation conditions (e.g. medium, temperature). However, experimental investigations similar to that performed in this study have to be carried out in order to acquire the parameters required by the model to achieve a more accurate prediction. With minor modifications, the model can also be applied for system optimization in large-scale operations. The present study provides several interesting and important topics that should be investigated in the future: E.g., the effect of irradiance spectrum on photosynthetic activity, investigations into the facilitated CO_2 transfer in the studied biofilm; the mechanism behind the exceptionally high [DO] measured in the biofilm and a more comprehensive modeling study aimed at system optimization.

References

Abdel-Raouf N, Al-Homaidan AA, Ibraheem IBM. 2012. Microalgae and wastewater treatment. Saudi Journal of Biological Sciences 19(3):257-275.

Bao L, Trachtenberg MC. 2006. Facilitated transport of CO_2 across a liquid membrane: Comparing enzyme, amine, and alkaline. Journal of Membrane Science 280(1–2):330-334.

Becker EW. 1994. Microalgae: biotechnology and microbiology. Cambridge: University Press. 304 p.

Berberoglu H, Pilon L. 2007. Experimental measurements of the radiation characteristics of *Anabaena variabilis* ATCC 29413-U and *Rhodobacter sphaeroides* ATCC 49419. International Journal of Hydrogen Energy 32(18):4772-4785.

Berberoglu H, Yin J, Pilon L. 2007. Light transfer in bubble sparged photobioreactors for H2 production and CO_2 mitigation. International Journal of Hydrogen Energy 32(13):2273-2285.

Bergman TL, Lavine AS, Incropera FP, DeWitt DP. 2011. Fundamentals of heat and mass transfer. Hoboken, New Jersey, USA: John Wiley & Sons. 1048 p.

Berner F, Heimann K, Sheehan M. 2015. Microalgal biofilms for biomass production. Journal of Applied Phycology. 27(5):1793-1804.

Boelee NC, Janssen M, Temmink H, Shrestha R, Buisman CJN, Wijffels RH. 2014. Nutrient removal and biomass production in an outdoor pilot-scale phototrophic biofilm reactor for effluent polishing. Applied Biochemistry and Biotechnology 172(1):405-422.

Borowitzka M, Huisman J, Osborn A. 1991. Culture of the astaxanthin-producing green alga *Haematococcus pluvialis* 1. Effects of nutrients on growth and cell type. Journal of Applied Phycology 3(4):295-304.

Cardozo KHM, Guaratini T, Barros MP, Falcão VR, Tonon AP, Lopes NP, Campos S, Torres MA, Souza AO, Colepicolo P and others. 2007. Metabolites from algae with economical impact. Comparative Biochemistry and Physiology Part C: Toxicology & Pharmacology 146(1–2):60-78.

Carlozzi P, Pushparaj B, Degl'Innocenti A, Capperucci A. 2006. Growth characteristics of Rhodopseudomonas palustris cultured outdoors, in an underwater tubular photobioreactor, and investigation on photosynthetic efficiency. Applied Microbiology and Biotechnology 73(4):789-795.

Ciferri O. 1983. *Spirulina*, the edible microorganism. Microbiological reviews 47(4):551-578.

Converti A, Lodi A, Del Borghi A, Solisio C. 2006. Cultivation of *Spirulina platensis* in a combined airlift-tubular reactor system. Biochemical Engineering Journal 32(1):13-18.

Crowe B, Attalah S, Agrawal S, Waller P, Ryan R, Wagenen JV, Chavis A, Kyndt J, Kacira M, Ogden KL and others. 2012. A comparison of *Nannochloropsis salina* growth performance in two outdoor pond designs: conventional raceways versus the arid pond with superior temperature management. International Journal of Chemical Engineering. 2012:p9

Danilov RA, Ekelund NG. 2001. Effects of pH on the growth rate, motility and photosynthesis in *Euglena gracilis*. Folia Microbiol (Praha) 46(6):549-554.

Davis R, Aden A, Pienkos PT. 2011. Techno-economic analysis of autotrophic microalgae for fuel production. Applied Energy 88(10):3524-3531.

Davis TA, Volesky B, Mucci A. 2003. A review of the biochemistry of heavy metal biosorption by brown algae. Water Research 37(18):4311-4330.

de la Noüe J, Laliberté G, Proulx D. 1992. Algae and waste water. Journal of Applied Phycology 4(3):247-254.

Douglas SE. 1998. Plastid evolution: origins, diversity, trends. Current Opinion in Genetics & Development 8(6):655-661.

Glud RN, Ramsing NB, Revsbech NP. 1992. Photosynthesis and photosynthesis-coupled respiration in natural biofilms quantified with oxygen microsensors. Journal of Phycology 28(1):51-60.

Gros G, Moll W, Hoppe H, Gros H. 1976. Proton transport by phosphate diffusion - a mechanism of facilitated CO_2 transfer. The Journal of General Physiology 67(6):773-790.

Gross M, Jarboe D, Wen Z. 2015. Biofilm-based algal cultivation systems. Applied Microbiology and Biotechnology 99(14):5781-5789.

Heber U, Andrews TJ, Boardman NK. 1976. Effects of ph and oxygen on photosynthetic reactions of intact chloroplasts. Plant Physiology 57(2):277-283.

Jøsrgensen EG. 1969. The Adaptation of Plankton Algae IV. Light adaptation in different algal species. Physiologia Plantarum 22(6):1307-1315.

Ketheesan B, Nirmalakhandan N. 2012. Feasibility of microalgal cultivation in a pilot-scale airlift-driven raceway reactor. Bioresource Technology 108:196-202.

Lassen C, Glud RN, Ramsing NB, Revsbech NP. 1998. A method to improve the spatial resolution of photosynthetic rates obtained by oxygen microsensors. Journal of Phycology 34(1):89-93.

Li T, Lin G, Podola B, Melkonian M. 2015a. Continuous removal of zinc from wastewater and mine dump leachate by a microalgal biofilm PSBR. Journal of Hazardous Materials 297:112-118.

Li T, Piltz B, Podola B, Dron A, de Beer D, Melkonian M. 2015b. Microscale profiling of photosynthesis-related variables in a highly productive biofilm photobioreactor. Biotechnology and Bioengineering:n/a-n/a.

Li T, Podola B, de Beer D, Melkonian M. 2015c. A method to determine photosynthetic activity from oxygen microsensor data in biofilms subjected to evaporation. Journal of Microbiological Methods 117:100-107.

Liu T, Wang J, Hu Q, Cheng P, Ji B, Liu J, Chen Y, Zhang W, Chen X, Chen L and others. 2013. Attached cultivation technology of microalgae for efficient biomass feedstock production. Bioresource Technology 127(0):216-222.

Moore A. 2001. Blooming prospects? EMBO reports 2(6):462-464.

Moreira D, Philippe H. 2001. Sure facts and open questions about the origin and evolution of photosynthetic plastids. Research in Microbiology 152(9):771-780.

Muller-Feuga A. 2000. The role of microalgae in aquaculture: Situation and trends. J. Appl. Phycol. 12(3-5):527-534.

Murphy TE, Berberoglu H. 2014. Flux balancing of light and nutrients in a biofilm photobioreactor for maximizing photosynthetic productivity. Biotechnology Progress 30(2):348-359.

Naumann T, Cebi Z, Podola B, Melkonian M. 2013. Growing microalgae as aquaculture feeds on twin-layers: a novel solid-state photobioreactor. Journal of Applied Phycology 25(5):1413-1420.

Norton TA, Melkonian M, Andersen RA. 1996. Algal biodiversity. Phycologia 35(4):308-326.

Nowack ECM, Podola B, Melkonian M. 2005. The 96-Well Twin-Layer System: A Novel Approach in the Cultivation of Microalgae. Protist 156(2):239-251.

Olivieri G, Salatino P, Marzocchella A. 2014. Advances in photobioreactors for intensive microalgal production: configurations, operating strategies and applications. Journal of Chemical Technology & Biotechnology 89(2):178-195.

Park JBK, Craggs RJ, Shilton AN. 2011. Wastewater treatment high rate algal ponds for biofuel production. Bioresource Technology 102(1):35-42.

Podola B, Melkonian M. 2003. A long-term operating algal biosensor for the rapid detection of volatile toxic compounds. Journal of Applied Phycology 15(5):415-424.

Pringault O, Garcia-Pichel F. 2000. Monitoring of oxygenic and anoxygenic photosynthesis in a unicyanobacterial biofilm, grown in benthic gradient chamber. FEMS Microbiol. Ecol. 33(3):251-258.

Raven JA, Cockell CS, De La Rocha CL. 2008. The evolution of inorganic carbon concentrating mechanisms in photosynthesis. Philosophical transactions of the Royal Society of London. Series B, Biological sciences 363(1504):2641-2650.

Revsbech NP. 1983. In Situ Measurement of Oxygen Profiles of Sediments by use of Oxygen Microelectrodes. In: Gnaiger E, Forstner H, editors. Polarographic Oxygen Sensors. Berlin/Heidelberg, Germany: Springer. p 265-273.

Richardson K, Beardall J, Raven JA. 1983. Adaptation of unicellular algae to irradiance: an analysis of strategies. New Phytologist 93(2):157-191.

Schlichting H, Gersten K. 2000. Boundary-layer theory. Berlin/Heidelberg: Springer-Verlag. 800 p.

Schultze LKP, Simon M-V, Li T, Langenbach D, Podola B, Melkonian M. 2015. High light and carbon dioxide optimize surface productivity in a Twin-Layer biofilm photobioreactor. Algal Research-Biomass Biofuels and Bioproducts 8:37-44.

Shi J, Podola B, Melkonian M. 2007. Removal of nitrogen and phosphorus from wastewater using microalgae immobilized on twin layers: an experimental study. Journal of Applied Phycology 19(5):417-423.

Shi J, Podola B, Melkonian M. 2014. Application of a prototype-scale Twin-Layer photobioreactor for effective N and P removal from different process stages of municipal wastewater by immobilized microalgae. Bioresource Technology 154(0):260-266.

Shimizu Y. 1996. Microalgal metabolites: a new perspective. Annual Review of Microbiology 50(1):431-465.

Trachtenberg MC, Tu CK, Landers RA, Willson RC, McGregor ML, Laipis PJ, Kennedy JF, Paterson M, Silverman DN, Thomas D and others. 1999. Carbon dioxide transport by proteic and facilitated transport membranes. Life Support Biosph Sci 6(4):293-302.

Wang J, Liu J, Liu T. 2015. The difference in effective light penetration may explain the superiority in photosynthetic efficiency of attached cultivation over the conventional open pond for microalgae. Biotechnology for Biofuels 8(1):49.

Whatley JM. 1993. The endosymbiotic origin of chloroplasts. International Review of Cytology - A Survey of Cell Biology (Hrsg.) 144:259-299.

Wolf G, Picioreanu C, van Loosdrecht MCM. 2007. Kinetic modeling of phototrophic biofilms: The PHOBIA model. Biotechnology and Bioengineering 97(5):1064-1079.

Summary

In the present study, a comprehensive investigation of the dynamic processes in an artificial algal biofilm immobilized on a porous substrate has been conducted. Experimental investigations including microsensor measurements were carried out. For this purpose, the microsensor setup used for profiling submerged biofilms was modified to enable measurement on the investigated biofilms. To achieve an accurate evaluation of the data acquired through microsensor measurements, a new mathematical method was developed, and a 20 μm depth resolution has been suggested for future photosynthetic activity measurements.

After the establishment of the microsensor methods, a systematic microsenser investigation was carried out: the distribution of dissolved oxygen, pH value and photosynthetic productivity profiles of algal biofilms in a porous substrate biofilm photobioreactor (Twin-Layer photobioreactor) exposed to different surface irradiance and/or exposed to different gas phase CO_2 concentrations were measured. The results acquired from these experiments offered important insights into the processes in such biofilms: E.g. light penetration depth, maximal dissolved oxygen concentration and pH distribution. The results show, as expected, photosynthesis in the biofilms occurs only near the biofilms surface (i.e. in the illuminated zones), and dark respiration in the inner part of the biofilm could be the reason of the observed biomass productivity decrease with prolonged cultivation. Also, increases in surface irradiance and/or gas phase CO_2 concentrations led to an increase in photosynthetic productivity of the investigated biofilm. No photoinhibition was observed in the studied biofilms, although exceptionally high dissolved oxygen concentrations (12 times of that in normal atmosphere) have been recorded.

The model (as described in the 3rd manuscript, Li et al. 2015d) developed in the study has proven to be very effective in predicting experimental observations. The results show clearly the importance of taking into account not only adsorption and scattering, but also the adaptation of the pigment content of the biomass for investigating radiative transfer in PSBR biofilms. Also, through the development of the model, important insights into the dynamic processes in the investigated biofilm were acquired: E.g., it is very likely that the facilitated CO_2 transfer plays an important role in inorganic carbon transport in the studied biofilms when the CO_2 concentration supplied in the gas phase is low; macronutrients (N and P) do not limit growth even at high surface irradiance and high gas phase CO_2 concentrations as long as they are sufficiently supplied in the medium; and the buffering of the medium with a strong buffer will have significant effects on the inorganic carbon availability in the studied biofilm.

Through this study, a solid basis has been established for future investigation on PSBR biofilms. The methods and model developed in this study are established specifically for investigating biofilms grown in the Twin-Layer porous substrate biofilm photobioreactor. However, with minor modifications and/or additional experimental measurements, they can be easily applied to other phototrophic biofilm systems or for investigation and/or optimization of commercial scale systems.

Zusammenfassung

In der vorgelegten Studie wurden die dynamischen Prozesse in einem auf porösem Substrate künstlich gezüchteten Algenbiofilm umfassend untersucht. Experimentelle Untersuchungen, u.a. Mikrosensormessungen, wurden durchgeführt. Zu diesem Zweck wurde ein neuer Versuchsaufbau, sowie eine neue mathematische Berechnungsmethode zur Auswertung der durch Mikrosensormessungen aufgenommenen Daten entwickelt. Die Untersuchungen zeigten, dass um die Daten sinnvoll auswerten zu können, zukünftige Mikrosensormesungen am untersuchten Biofilm mit einer Tiefenauflösung von 20 μm durchgeführt werden sollten.

In nachfolgende systematische Mikrosensormessungen wurden die Profile von gelöstem Sauerstoff, pH und photosynetischer Produktivität an Biofilmen gemessen. Die Messungen wurden an bei vieschiedenen Lichtintensitäten gezüchtet und/oder verschiedenen CO_2 Konzentrationen ausgesetzt Biofilmen durchgeführt. Die Ergebnisse ermöglichen wichtige Einsichten in den obengenannten Biofilm, wie: z.B. Lichtverfügbarkeit, maximale Konzentration von gelöstem Sauerstoff und pH Werte. Die Ergebnisse zeigen, dass die Photosynthese wie erwartet nur nahe der Biofilm-Oberfläche, beziehungsweise in der beleuchteten Region des Biofilms, stattfindet. Außerdem trägt die Dunkelresipration in der tieferen Schicht, beziehungsweise der nicht oder nur schwach beleuchteten Region des Biofilms zu der beobachteten Abnahme von Biomassewachstum bei längerer Kutivierungszeit bei. Die Daten zeigen ebenfalls, dass die photosynthetische Produktivität im untersuchten Biofilm mit erhöter Lichtintensität und/oder erhöter CO_2 Konzentration ansteigt. Photoinhibition der Algenzellen wurden trotz der gemessenen außgewöhnlich hohen gelöste Sauerstoffkonzentration (12 fach der Konzentration in normaler Luft) nicht beobachtet.

Die Ergebnisse beweisen, dass das in dieser Studie vorgelegte Model die experimentellen Beobachtungen mit angemessener Präzision vorhersagen kann. Um das Transferverhältnis des Lichts in dem untersuchten Biofilm präzise modellieren oder untersuchen zu können, sind nicht nur die Absorption des Lichts sondern auch dessen Streuung, sowie die Anpassung der Algenzellen an verschiedene Lichtstärken zu berücksichtigen. Das Model offenbart weiterhin wichtige Einsichten in die dynamischen Prozesse des untersuchten Biofilms: z.B. 1) Es wurde festgestellt, dass der sogenannte "Facilitated CO_2 Transfer" eine sehr wichtige Rolle für den Transport des gelösten anorganischen Kohlenstoffs in dem untersuchten Biofilm, insbesondere bei geringem CO_2 Gehalt in der Gasphase spielt; 2) Wenn ausreichend Makro-Nährstoffe (Stickstoff und Phosphor) im Kuturemedium vorhanden sind, stellt der Transport (z.B. Diffusion) der Makro-Nährstoffe kein Hindernis für das Wachstum dar, d.h. Makro-Nährstoffe werden durch die Transportprozesse ausreichend bereitgestellt; 3) Die Pufferung des Mediums kann die Verfügbarkeit des gelösten anorganischen Kohlenstoff in deutlichem Maße beeinflussen.

Die vorgelegte Studie hat eine solide Basis für zukünftige Untersuchungen am PSBR Biofilm geschaffen. Die im Rahmen dieser Studie entwickelten Methoden eignen sich für die Untersuchungen des obengenannten Biofilms. Allerdings können mit geringfügigen Modifikationen und ggf. mit zusätzlichen experimentellen Untersuchungen die hier vorgelegten Methoden auch für andere phototrophische Biofilme und/oder für die Optimierung kommerzieller Systeme, die auf die untersuchten Biofilm basieren, verwendet werden.

Appendix I: MATLAB code for measured photosynthetic productivity data treatment

The MATLAB code presented here was written as described and applied in the 1st manuscript presented in this thesis.

```matlab
function [
xfinal,Measured,STD,calback]=
PIcorrectNN( testX, testLfcum
,realdata,nLf,dataSTD )
%input data: testX, testLfcum: measured
value in, thickness of in test problem.
realdata: Real data in matrix form, nLf:
thickness of the biofilm in discrete
form, dataSTD: STD of the measured data

if nargin<3 || realdata==0,
    realdata=0;

testXSTD=zeros(1,length(testLfcum));
    nLf=length(testX);
    originaldata=[];
end,
%% parameters input
DO2=1.97e-9; %diffusion coefficient of
O2 in water in m^2/sec
Poro=0.32; %volumetric porosity
%
DO2bio=DO2.*(ones(size(testLfcum)).*
Poro^1);  %Diffsion coefficient
inside biofilm
DO2bio=DO2.*Poro^1;
%
uz=4.5E-06./(ones(size(testLfcum)).*
Poro^(1/3));         %advection rate
caused by evaporation on the surface
uz=4.5E-06/Poro^(1/3);
t=1;                %t

%% fit curve to the realdata
if realdata==1,
    if nargin<4 && realdata==1,
        error('For real data enter
number discretion points'),
    end,
    if nargin<5 && realdata==1,
        warning('No STD input for real
data, set to 5% of the realdata'),
        dataSTD=testX.*0.01;
    end,

originaldata=[testLfcum;testX;dataST
D];
    [-,-,dCdtcurvefit ,STDcurvefit] =
dCdtcurvetestSlm(
testX,testLfcum,dataSTD ,nLf); %use
Slm tool for data curve fitting

testLfcum=linspace(0,testLfcum(end),
nLf);
    testX=dCdtcurvefit;
    testXSTD=STDcurvefit;
end,

%% calculation
[ xfinal,Measured,STD,calback] =
testGtikhonovopsNN( testX, testLfcum
,realdata,testXSTD,DO2bio,uz,t,origi
naldata);
end

function [
xfinal,Btotal1,BSTD,Recoverdfx2] =
testGtikhonovopsNN( testX, testLfcum
,realdata,testXSTD,DO2bio,uz,t,origi
naldata)
DO2bio: effective diffusion
coefficient of DO, uz: evaporation
caused convection rate, t: measurement
time
%% calculation
[L,~] = get_l(length(testLfcum),2);
%data input, here a test problem or real
data if realdata==1
x2sum=zeros(length(testX),1);
Btotal1sum=x2sum;
```

```matlab
BSTDsum=x2sum;
if  realdata == 1,
    ncal=3;
else
    ncal=1;
end,
for i=1:ncal,
    if realdata == 1,
        [ Atotal1, Ain1, ~, ~ , ~, ~ ] =
testABgeneration
(testX,testLfcum,DO2bio,uz,t);
        Btotal0=testX'; % real data
input
        [UU1cal,smcal,XXcal] = cgsvd
(Atotal1,L);
        lambdacal =
l_curvenoP(UU1cal,smcal,Btotal0);
        [xcal]
=tikhonov(UU1cal,smcal,XXcal,Btotal0,
lambdacal);
        [ ~, ~, ~, Btotal0, Bin0, ~ ] =
testABgeneration
(xcal',testLfcum,DO2bio,uz,t);
        % error input

BSTD=((testXSTD)'-(-(testXSTD)')).*r
and(size((testXSTD)'))+(-(testXSTD)'
); %add artificial random error
representing noising data
        Btotal1=Btotal0+BSTD;
        Btotal1(Btotal1<0)=0;
        Bin1=Bin0+BSTD;
        Bin1(Bin1<0)=0;
    else
        [ ~, Ain1, ~, Btotal0, Bin0, ~ ]
= testABgeneration
(testX,testLfcum,DO2bio,uz,t);
        % error input
        BSTD=max(Btotal0)/50*randn
(size(Btotal0));%.*(Btotal0./max(Bto
tal0)); %add artificial random error
representing noising data
        Btotal1=Btotal0+BSTD;
        Btotal1(Btotal1<0)=0;
        Bin1=Bin0+BSTD;
        Bin1(Bin1<0)=0;
    end
    %
    [UU1,sm1,XX1] = cgsvd (Ain1,L);
    lambda1 = l_curvenoP
(UU1,sm1,Bin1);
    [x1]
=tikhonov(UU1,sm1,XX1,Bin1,lambda1);
    x1(x1<0)=0; %projected
non-constrain tikhonov

    % solve for non-negative solution
    x0=x1;%zeros(size(testLfcum));

Lcal=[zeros(1,length(testLfcum));zer
os(1,length(testLfcum));L];

H=(Ain1'*Ain1+lambda1^2.*Lcal'*Lcal)
;
    f=(-Ain1'*Bin1)';
    opts3 =
optimoptions('quadprog','Algorithm',
'active-set','Display','iter');
    lb=ones(size(Bin1)).*0;
    ub=[];
    x2 =
quadprog(H,f,[],[],[],[],lb,ub,x0,op
ts3);

    x2sum=x2sum+x2;
    Btotal1sum=Btotal1sum+Btotal1;
    BSTDsum=BSTDsum+abs(BSTD);
end,
if  realdata == 1,
    x2=x2sum./ncal;
```

```matlab
    Btotal1=Btotal1sum./ncal;
    BSTD=BSTDsum./ncal;
else
    BSTD=abs(BSTD);
end

if max(x2)<=max(Btotal1),
    warning('May yield false result,
try change regularization
parameters'),
end

if max(x2)>=1e2*max(Btotal1),
    warning('yielding false result,
regularization parameters have to be
changed'),
end,

%% calculate recovered f(x,0)
xfinal2=x2';
[ ~,~,~,
Recoverdfx2,~,~]=testABgeneration
(x2',testLfcum,DO2bio,uz,t);

%% plotting
figure('name','test problem, Tikhonov
regulerization')
hold on,
if realdata~=1,

plot(testLfcum,testX,'black--','line
width',3);

plot(testLfcum,Btotal1(:,end),'bo');
else
errorbar(originaldata(1,:),originald
ata(2,:),originaldata(3,:),'blacks',
'linewidth',2);
end
plot(testLfcum,xfinal2,'-b','linewid
th',3);
plot(testLfcum,Recoverdfx2,'-r','lin
ewidth',3);
if realdata~=1,
    legend('Real f(x,0)'...
    ,'measured g(x,T) '...
    ,'Calculated f(x,0) with
non-negative' ...
    ,'recoverd g(x,T) with
non-negative');
else
    legend('Measured data points, mean
& STD' ...
    ,'Calculated f(x,0) with
non-negative' ...
    ,'recoverd g(x,T) with
non-negative');

set(gca,'children',flipud(get(gca,'c
hildren')));
end
xlim([0 testLfcum(end)]);
ylim([0
ceil(max(max(testX),max(xfinal2))*10
)/10]);
set(gca,'XTick',0:testLfcum(end)/10:
testLfcum(end), ...

'YTick',0:ceil(max(max(testX),max(xf
inal2))*10)/10/5:ceil(max(max(testX)
,max(xfinal2))*10)/10)
title('Mathematical treatment of the
measured data')
xlabel('Depth into biofilm');
ylabel('Photosynthetic activity in
mole/m^3/sec O2')
set(gca,'XGrid','on');

end
```

```
function [ Atotal, Ain, Asurf, Btotal,
Bin, Bsurf ] = testABgeneration
(testX,testLfcum,DO2bio,uz,t)
%UNTITLED Summary of this function goes
here
%   Detailed explanation goes here

%% constructe the known kernel, matrix
of Ai
xcal=testLfcum;
acal=(4*pi*DO2bio*t)^0.5;
%a=(4*pi*D*t)^0.5 in meter
bcal=acal.^2/pi;        %b=4*D*t
deltay=xcal(2)-xcal(1);      %deltax,
weighing factor
xcal1=repmat(xcal,length(xcal),1);
%y or x0 in nLf discretion
xcal2=repmat(xcal',1,length(xcal))-0
.*deltay;  %x in nLf discretion

xend=xcal2./bcal.^0.5;
erfx=erf(xend);

Ain=(exp(-(xcal2-xcal1+uz.*t).^2./bc
al))./acal.*deltay; %y or x0 position
dependent
Ain(xcal2<0)=0;
Asurf=(exp(-(0-xcal1+uz*t).^2./bcal)
.*(1-erfx))./acal.*deltay; %x or x0
position dependent
Asurf(xcal2<0)=0;
Atotal=Ain-Asurf;

%% constructe the known lefthand side,
matrix of B, measured dCdt using
Splinefit

Bin=sum(repmat(testX,length(testLfcu
m),1).*(Ain),2);%y or x0 position
dependent
Bsurf=sum(repmat(testX,length(testLf
cum),1).*(Asurf),2);
Btotal=sum(repmat(testX,length(testL
fcum),1).*(Atotal),2);

end


function
[reg_corner,rho,eta,reg_param] =
l_curvenoP(U,sm,b,method,L,V)
%L_CURVE Plot the L-curve and find its
"corner".
%
% [reg_corner,rho,eta,reg_param] =
%
l_curve(U,s,b,method)
%
l_curve(U,sm,b,method)  , sm =
[sigma,mu]
%
l_curve(U,s,b,method,L,V)
%
% Plots the L-shaped curve of eta, the
solution norm || x || or
% semi-norm || L x ||, as a function of
rho, the residual norm
% || A x - b ||, for the following
methods:
%    method = 'Tikh'  : Tikhonov
regularization   (solid line )
%    method = 'tsvd'  : truncated SVD or
GSVD    (o markers )
%    method = 'dsvd'  : damped SVD or
GSVD      (dotted line)
%    method = 'mtsvd' : modified TSVD
(x markers )
% The corresponding reg. parameters are
returned in reg_param. If no
% method is specified then 'Tikh' is
default.  For other methods use
plot_lc.
%
% Note that 'Tikh', 'tsvd' and 'dsvd'
require either U and s (standard-
% form regularization) computed by the
function csvd, or U and sm (general-
% form regularization) computed by the
function cgsvd, while 'mtsvd'
% requires U and s as well as L and V
computed by the function csvd.
%
% If any output arguments are specified,
then the corner of the L-curve
```

```
% is identified and the corresponding
reg. parameter reg_corner is
% returned.  Use routine l_corner if an
upper bound on eta is required.

% Reference: P. C. Hansen & D. P.
O'Leary, "The use of the L-curve in
% the regularization of discrete
ill-posed problems",  SIAM J. Sci.
% Comput. 14 (1993), pp. 1487-1503.

% Modified from code by Per Christian
Hansen, DTU Compute, October 27, 2010.

% Set defaults.
if (nargin==3), method='Tikh'; end  %
Tikhonov reg. is default.
npoints = 200;  % Number of points on the
L-curve for Tikh and dsvd.
smin_ratio = 16*eps;  % Smallest
regularization parameter.

% Initialization.
[m,n] = size(U); [p,ps] = size(sm);
if (nargout > 0), locate = 1; else locate
= 0; end
beta = U'*b; beta2 = norm(b)^2 -
norm(beta)^2;
if (ps==1)
  s = sm; beta = beta(1:p);
else
  s = sm(p:-1:1,1)./sm(p:-1:1,2); beta
= beta(p:-1:1);
end
xi = beta(1:p)./s;
xi( isinf(xi) ) = 0;

if (strncmp(method,'Tikh',4) |
strncmp(method,'tikh',4))

  eta = zeros(npoints,1); rho = eta;
reg_param = eta; s2 = s.^2;
  reg_param(npoints) =
max([s(p),s(1)*smin_ratio]);
  ratio =
(s(1)/reg_param(npoints))^(1/(npoint
s-1));
  for i=npoints-1:-1:1, reg_param(i) =
ratio*reg_param(i+1); end
  for i=1:npoints
    f = s2./(s2 + reg_param(i)^2);
    eta(i) = norm(f.*xi);
    rho(i) = norm((1-f).*beta(1:p));
  end
  if (m > n & beta2 > 0), rho =
sqrt(rho.^2 + beta2); end
  marker = '-'; txt = 'Tikh.';

elseif (strncmp(method,'tsvd',4) |
strncmp(method,'tgsv',4))

  eta = zeros(p,1); rho = eta;
  eta(1) = abs(xi(1))^2;
  for k=2:p, eta(k) = eta(k-1) +
abs(xi(k))^2; end
  eta = sqrt(eta);
  if (m > n)
    if (beta2 > 0), rho(p) = beta2; else
rho(p) = eps^2; end
  else
    rho(p) = eps^2;
  end
  for k=p-1:-1:1, rho(k) = rho(k+1) +
abs(beta(k+1))^2; end
  rho = sqrt(rho);
  reg_param = (1:p)'; marker = 'o';
  if (ps==1)
    U = U(:,1:p); txt = 'TSVD';
  else
    U = U(:,1:p); txt = 'TGSVD';
  end

elseif (strncmp(method,'dsvd',4) |
strncmp(method,'dgsv',4))

  eta = zeros(npoints,1); rho = eta;
reg_param = eta;
  reg_param(npoints) =
max([s(p),s(1)*smin_ratio]);
  ratio =
(s(1)/reg_param(npoints))^(1/(npoint
s-1));
  for i=npoints-1:-1:1, reg_param(i) =
ratio*reg_param(i+1); end
  for i=1:npoints
    f = s./(s + reg_param(i));
```

```
    eta(i) = norm(f.*xi);
    rho(i) = norm((1-f).*beta(1:p));
  end
  if (m > n & beta2 > 0), rho =
sqrt(rho.^2 + beta2); end
  marker = ':';
  if (ps==1), txt = 'DSVD'; else txt =
'DGSVD'; end

elseif (strncmp(method,'mtsv',4))

  if (nargin~=6)
    error('The matrices L and V must
also be specified')
  end
  [p,n] = size(L); rho = zeros(p,1); eta
= zeros(p,1);
  [Q,R] = qr(L*V(:,n:-1:n-p),0);
  for i=1:p
    k = n-p+i;
    Lxk = L*V(:,1:k)*xi(1:k);
    zk =
R(1:n-k,1:n-k)\(Q(:,1:n-k)'*Lxk); zk
= zk(n-k:-1:1);
    eta(i) = norm(Q(:,n-k+1:p)'*Lxk);
    if (i < p)
      rho(i) = norm(beta(k+1:n) +
s(k+1:n).*zk);
    else
      rho(i) = eps;
    end
  end
  if (m > n & beta2 > 0), rho =
sqrt(rho.^2 + beta2); end
  reg_param = (n-p+1:n)'; txt = 'MTSVD';
  U = U(:,reg_param); sm =
sm(reg_param);
  marker = 'x'; ps = 2;  % General form
regularization.

else
  error('Illegal method')
end

% Locate the "corner" of the L-curve,
if required.
if (locate)
  [reg_corner,rho_c,eta_c] =
l_corner(rho,eta,reg_param,U,sm,b,me
thod);
end

end
```

Appendix II: MATLAB code of the model presented in this study

The MATLAB code presented here was written as described and applied in the 3rd manuscript presented in this thesis.

```
function
[Tcomp,Datacomp,BM]=TL_Model_test(Iz
inPer,Irrsurf,pCO2,BMt0)
% input, Calculate irradiance from
function "RTE_TL" Irradiance in microE,
pCO2 in Pa, initial biomass in kg

% the whole spatial domain was discreted
into n=n0+1 layers, 1 to  n0
% layer are the inside layers, and have
initial biomass at t0, the nth
% layer is the surface layer, which is
assumed to have no biomass at t0  or
% directly after a new discretion, all
l to n layer contribute to growth,
% but all the biomass increments are
only inside the nth layer

%% general discretion setups

c=10; %number of variables calculated
using ODEs implicitly
tend=12; %time of simulation in days
LDratio=14/10; %light dark cycle ratio

%% Parameters

XF=220; %biomass concentration in
kg/m^3
BioPoro=0.76; %biofilm porosity, Li et
al, 2015
SubPoro=0.35; %substrate layer
porosity

[
DCO2b,DHCO3b,DCO3b,DNO3b,DHPO4b,DH2P
O4b,DO2b,DNab,DCO2s,DHCO3s ...

,DCO3s,DNO3s,DHPO4s,DH2PO4s,DO2s,DNa
s ]...
    = DiffCoCal_TL( BioPoro, SubPoro);
%calculate diffusion coefficient in
biofilm and substrate
                      % according
to porosity and diffusion
                      %
coefficient in water in m^2/d^-1
DCO2b=DCO2b*1;
SNO3medium=2.94e-3; %NO3 in bulk liquid
in M
SH2PO4medium=1.29e-3; %HPO4 in bulk
liquid in M
SHPO4medium=0.431e-3; %H2PO4 in medium
in M
Sionsmedium=SNO3medium+SH2PO4medium+
2*SHPO4medium; %cations in bulk liquid,
calculated as Na in M
KsCO2=4e-4; %assumed half saturation
constant for CO2 as carbon source in M,
4e-6 M from literature,
KsHCO3=4e-5; %assumed half saturation
constant for HCO3 as carbon source in
M, 4e-6, literature states the value
increase with pH
KsNO3=1e-5; %assumed half saturation
constant for N in M, 5e-4
KsPO4=1.7e-5; %assumed half saturation
constant for P in M, 1.7e-5
KiCO2toHCO3=5e-4; %assumed
inhibition constant for CO2 on growth
using HCO3, 1e-6 PHOBIA
KiO2max=1e-3; %assumed maxim
inhibition constant for O2 in M,
represent photorespiration, high = less
photorespiration
KsO2=1e-4; %assumed half saturation
constant for O2 on dark respiration
Lsub=1e-5; %membrane thickness in meter
```

```
uz=0.23; %convection velocity in m/day
0.23
RHCO3transCO2=1; %efficience of HCO3
assimilation compare to CO2
assimilation
YxsCO2=30; %bimass yield on CO2
consumed in kg_biomass/kmol C, from
digestion measurement,
YxsHCO3=YxsCO2.*RHCO3transCO2;
%bimass yield on HCO3 consumed in
kg_biomass/kmol C, from digestion
measurement,
RHCO3DvsC=1; %ratio of direct hco3
uptake vs extracellular conversion to
CO2
YxsO2= YxsCO2/1.3; %biomass yield of O2
by respiration, assume biomass C:O
ratio is 1:1.5 mole
PCO2O2=1; % production ratio of O2 by
Co2 assimilation, mole to mole
PHCO3O2=1.*RHCO3transCO2; %
production ratio of O2 by HCO3
sassimilation, mole to mole
YxsN=200; %bimass yield on DN consumed
in kg_biomass/kmol N
YxsP=3100; %bimass yield on DP consumed
in kg_biomass/kmol P
KalCO3=10^(-6.35); %equilibrium
constant for CO2+H2O to H+HCO3
Ka2CO3=10^(-10.33); %equilibrium
constant for HCO3 to H+CO3
KaCaOH=10^(7.64); %equilibrium
constant for CO2+OH to HCO3
HenCO2=3.04*10^(-7);%Henry's constant
for CO2 at 25 degree in M/Pa.
HenO2=1.3*10^(-8);%Henry's constant
for O2 at 25 degree, in M/Pa.
Kw=10^(-14); %equilibrium constant of
water
Ka1PO4=10^(-2.15); %equilibrium
constant for H3PO4 to H+H2PO4
Ka2PO4=10^(-7.2); %equilibrium
constant for H2PO4 to H+HPO4
Ka3PO4=10^(-12.1); %equilibrium
constant for HPO4 to H+PO4
kCO2aH2O=10^7.54; %rate constant of
CO2+H2O to H2CO3 in d^-1, Gibbson and
Edsall, 1963, 10^7.54 or from book
below, 10^5.58
kCO2aOH=10^8.86; %rate constant of
CO2+OH to HCO3 in d^-1
kHCO3tCO3=10^4.6; %rate constant of
HCO3 to H+CO3 in d^-1, rate constants
from product and process modelling, a
case study approach, 2011
kH2PO4tHPO4=10^9.74; %rate constant of
H2PO4 to HPO4 in d^-1
pO2=21000; %partial pressure of O2 in
Pa, 21000 in atm
SO2medium=pO2*HenO2*0.01; %medium O2
concentration pO2*HenO2 or 0
SCO2medium=pCO2*HenCO2; %medium CO2
concentration pCO2*HenCO2 or 0
rs=0.05; %surface reflectance
umax=8; % maximal growth, d^-1
BMc=0.6;
% umax=1.5e-4; % maximal growth in
biomass (here as thickness) in m s^-1
Ures=0.134; %respiration rate in day^-1
Lft0=BMt0/XF; %initial biofilm
thickness in m
n0=fix(Lft0/10e-6); %set n0 for initial
dicretion determine
n=n0+1; %set spatial grid, n=n0+1
indicate the nth layer
pHmedium=6.8; %pH in medium
%% preset surface pH and bottom pH, from
measurement if needed
pHSurfaceM=6.8;
pHBottomM=6.8;
```

```
CO2cor=linspace(pHBottomM-pHmedium,p
HSurfaceM-pHmedium,n); % a correction
factor for initial pH guess
%% time span
tL=LDratio ./ ( 1 + LDratio );
%illuminated time in day

%% Initial conditions c*n rows, last cth
elements indicate values in nth layer
ICS=repmat([10^(-pHmedium),
SCO2medium,
KalCO3/10^(-pHmedium)*SCO2medium,
KalCO3*Ka2CO3/(10^(-pHmedium))^2*SCO
2medium,...
        SNO3medium, SHPO4medium,
SH2PO4medium, Sionsmedium, pO2*HenO2,
Lft0/n0],1,n);
%--------->H (guess for initial),
CO2,          HCO3,
CO3,
%----------->DN,          DHPO4,
DH2PO4,     Sions,      DO2,
sLf.
% nth layer biomass has to be se to 0
at t0, to avoid singlarity, set as a very
small value instead of 0
ICS(c*n)=ICS(c*n)/10^10;
ICS(1:c:c*n)=ICS(1:c:c*n).*10.^(-CO2
cor);
% ICS(c*(n-1)+1)=pCO2*HenCO2;
%
ICS(c*(n-1)+2)=KalCO3/10^(-pHmedium)
*pCO2*HenCO2;
%
ICS(c*(n-1)+3)=KalCO3*Ka2CO3/(10^(-p
Hmedium))^2*pCO2*HenCO2;

%% time span
tspan=[0 tend];

%% call ode solver
tcal=0; %set starting point for
dtermine is tend is reached

Datacomp=[]; %set matrix for compiling
pH data,each column is one spatial
            %discretion unit (total n
columns), each row is one time step
(solver defined)
            %pages represent
variables,1 to 9 ---> H, CO2, HCO3, CO3,
Dn,
            %DP, Sions, DO2,Lf (c
pages).

Tcomp=[]; %set matrix for compiling
time data

EventGC=[]; %set matrix for compiling
event time data

ncal=1; %the number of discretions used
during 0 to tend
ReG=0; %growth higher than respiration
%  while tcal<tend, %initial adapting
meshing of the finite elements
while ncal<120&&tcal<tend,

    %set absolute tolernance for each
component
%     ATol=repmat([1e-14,
pCO2*HenCO2/1e2,
KalCO3/10^(-pHmedium)*pCO2*HenCO2/1e
2,
(KalCO3*Ka2CO3/(10^(-pHmedium))^2*pC
O2*HenCO2)/1e2,...
        SNO3medium/1e2,
SPO4medium/1e2,
(SNO3medium+(129/172.1)*SPO4medium+2
*(43.1/172.1)*SPO4medium)/1e2,
pO2*HenO2/1e2, Lft0/n0/1e2],1,n);
```

```
    ATol=10e-14;
    NonNeg=1:c*n;

options=odeset('Vectorized','on','Ab
sTol',ATol,'RelTol',1e-6,'Events',..
.

@EventsLf,'NonNegative',NonNeg); %set
solver option

[T,calS,GridCT,~,~]=ode15s(@ODE_dS,t
span,ICS,options);

    %after dLf reached set
value(dLf=Lf(t=0)/n), reset initial
conditions
    %first accumulate solution

    len=size(Datacomp,1); %calculate
size length of the previous data
compling matrix
    lenT=size(T,1);

    %compile data
    Datacal=permute(reshape(calS',[c n
lenT]),3:-1:1);

Datacomp((len+1):(len+lenT),:,:)=Dat
acal(:,:,:); %compiling data in 3D
matrix

    %compiling time data
    if tcal==0,

Tcomp((len+1):(len+size(T,1)))=T(:);
    else

Tcomp((len+1):(len+size(T,1)))=T(:)+
Tcomp(len);
    end,

%     %compiling event data
%     EventGC(ncal)=GridCT;

    %then test if tend is reached
    tcal=T(length(T));

    %update storage space for solution
    Datacomp=[Datacomp
zeros(size(Datacomp,1),1,c)];

    if
calS(size(calS,1),c*n)<=Lft0/10^10,
%dark, respiration > growth, thickness
decrease
        %set new initial conditions,
consider as new layer added on top and
has
        %the same concentration of
everything as the layer below, except
        %biomass, which is initially 0
        ICS=ICS(1:c*(n-1));
        %set new grid
        n=n+1;
        warning('growth stoped');
        break,
    else
        %set new initial conditions,
consider as new layer added on top and
has
        %the same concentration of
everything as the layer below, except
        %biomass, which is initially 0

ICS=[calS(size(calS,1),:),calS(size(
calS,1),(n-1)*c+1:n*c)];

        %set new grid
        n=n+1;

        %reset nth layer thickness to 0
        ICS(c*n)=ICS(c*n)/10^10;
    end,
    %set new time span and start new
iteration
    tspan=[0 (tend-tcal)];
    ncal=ncal+1;
end,

%% ploting
plotting_End;

    function plotting_End

        for flipi=1:c % flip the x-axis
for better view
```

```
Datacomp(:,:,flipi)=fliplr(Datacomp(
:,:,flipi));
        end,

        figure('Name',['TL-model with
',num2str(Irrsurf),' PAR irradiance
and
',num2str(round((pCO2-39)/1e5*100)),
'% additional CO2']);

subplot(3,3,2),plot(cumsum(Datacomp(
length(Tcomp),1:n-1,10)).*1e6,Dataco
mp(length(Tcomp),2:n,2).*1e3,'o-blue
');
        hold on;
        grid on;

subplot(3,3,2),plot(cumsum(Datacomp(
length(Tcomp),1:n-1,10)).*1e6,Dataco
mp(length(Tcomp),2:n,3).*1e3,'s-blue
');

subplot(3,3,2),plot(cumsum(Datacomp(
length(Tcomp),1:n-1,10)).*1e6,Dataco
mp(length(Tcomp),2:n,4).*1e3,'*-blue
');

subplot(3,3,2),plot(cumsum(Datacomp(
length(Tcomp),1:n-1,10)).*1e6,(Datac
omp(length(Tcomp),2:n,2)...

+Datacomp(length(Tcomp),2:n,3)+Datac
omp(length(Tcomp),2:n,4)).*1e3,'-bla
ck');
        title('DIC in mM vs. depth');

subplot(3,3,4),plot(cumsum(Datacomp(
length(Tcomp),1:n-1,10)).*1e6,Dataco
mp(length(Tcomp),2:n,5).*1e3,'o-blue
');
        hold on;
        grid on;

subplot(3,3,4),plot(cumsum(Datacomp(
length(Tcomp),1:n-1,10)).*1e6,Dataco
mp(length(Tcomp),2:n,6).*1e3,'s-red'
);

subplot(3,3,4),plot(cumsum(Datacomp(
length(Tcomp),1:n-1,10)).*1e6,Dataco
mp(length(Tcomp),2:n,7).*1e3,'o-red'
);

subplot(3,3,4),plot(cumsum(Datacomp(
length(Tcomp),1:n-1,10)).*1e6,(Datac
omp(length(Tcomp),2:n,6)+...

Datacomp(length(Tcomp),2:n,7)).*1e3,
'-red'); %total P

subplot(3,3,4),plot(cumsum(Datacomp(
length(Tcomp),1:n-1,10)).*1e6,Dataco
mp(length(Tcomp),2:n,8).*1e3,'*-gree
n');
        title('NO3, HPO4, H2PO4, total
P, Cations(Na) in mM vs depth');

subplot(3,3,3),plot(cumsum(Datacomp(
length(Tcomp),1:n-1,10)).*1e6,Dataco
mp(length(Tcomp),2:n,9).*1e3,'o-blac
k');
        hold on;
        grid on;
        title('O2 in mM vs depth');

        pHcal=-log10(Datacomp(:,:,1));

subplot(3,3,5),plot(cumsum(Datacomp(
length(Tcomp),1:n-1,10)).*1e6,pHcal(
length(Tcomp),2:n),'o-black');
        hold on;
        grid on;
        title('pH vs depth');

        %Plot Irr(explicit)
        nt=length(Tcomp);
        Lfaccleft=zeros(nt,n);

Lfaccleft(:,1:n)=cumsum(Datacomp(:,:
,10),2);

Irrcalleft(1:nt,1:n)=(Irrsurf.*(1-rs
```

```
)).*polyval(IzinPer,Lfaccleft(1:nt,1
:n));

Lfaccright=zeros(size(Lfaccleft));

Lfaccright(:,1:size(Lfaccright,2)-1)
=Lfaccleft(:,2:size(Lfaccleft,2));

Irrcalright(1:nt,1:n)=(Irrsurf.*(1-r
s)).*polyval(IzinPer,Lfaccright(1:nt
,1:n));

Irrcal=(Irrcalleft+Irrcalright)./2;

subplot(3,3,1),plot(cumsum(Datacomp(
length(Tcomp),1:n-1,10).*1e6,Irrcal
(length(Tcomp),1:n-1),'o-black');
        hold on;
        grid on;
        title('Irradiance in microE vs
depth');

        %plot growth rate(explicit)

GCO2=zeros(nt,n-1);GHCO3=zeros(nt,n-
1);Rd=zeros(nt,n-1);
        GCO2(:,:)=umax.*PCO2O2...

.*Datacomp(:,2:n,9)./(Datacomp(:,2:n
,9)+Datacomp(:,2:n,9).^2./(KiO2cal(D
atacomp(:,2:n,2),Datacomp(:,2:n,9)))
)... O2

.*GroIrr_TL(Irrcal(:,1:n-1))... light

.*min(Datacomp(:,2:n,2)./(KsCO2+Data
comp(:,2:n,2)),...CO2

min(Datacomp(:,2:n,5)./(KsNO3+Dataco
mp(:,2:n,5)),...NO3

(Datacomp(:,2:n,6)+Datacomp(:,2:n,7)
)./(KsPO4+(Datacomp(:,2:n,6)+Datacom
p(:,2:n,7))))); %PO4

GHCO3(:,:)=umax.*PHCO3O2.*RHCO3DvsC.
..

.*Datacomp(:,2:n,9)./(Datacomp(:,2:n
,9)+Datacomp(:,2:n,9).^2./(KiO2cal(D
atacomp(:,2:n,2),Datacomp(:,2:n,9)))
)...O2

.*GroIrr_TL(Irrcal(:,1:n-1))...light

.*min(Datacomp(:,2:n,3)./(KsHCO3+Dat
acomp(:,2:n,3)),...HCO3

min(Datacomp(:,2:n,2)./((Datacomp(:,
2:n,2)+Datacomp(:,2:n,2).^2./KiCO2to
HCO3)),... CO2 inhibition on HCO3

min(Datacomp(:,2:n,5)./(KsNO3+Dataco
mp(:,2:n,5)),... NO3

(Datacomp(:,2:n,6)+Datacomp(:,2:n,7)
)./(KsPO4+(Datacomp(:,2:n,6)+Datacom
p(:,2:n,7)))))); %PO4

Rd(:,:)=-Ures.*Datacomp(:,2:n,9)./(K
sO2+Datacomp(:,2:n,9)); %Respiration
        GrowthR(:,:)=GCO2+GHCO3+Rd;

subplot(3,3,6),plot(cumsum(Datacomp(
length(Tcomp),1:n-1,10).*1e6,Growth
R(length(Tcomp),1:n-1),'o-black');
        hold on;
        grid on;

subplot(3,3,6),plot(cumsum(Datacomp(
length(Tcomp),1:n-1,10).*1e6,GCO2(l
ength(Tcomp),1:n-1),'o-green');

subplot(3,3,6),plot(cumsum(Datacomp(
length(Tcomp),1:n-1,10).*1e6,GHCO3(
length(Tcomp),1:n-1),'s-green');

subplot(3,3,6),plot(cumsum(Datacomp(
length(Tcomp),1:n-1,10).*1e6,Rd(len
gth(Tcomp),1:n-1),'*-red');
        title('Growth in d^-1 vs
depth');
```

```
    %Plot Biomass

Lfcal(1:nt)=sum(Datacomp(:,:,10),2);
    BM=Lfcal.*XF;
    subplot(3,3,[7 8
9]),plot(Tcomp,BM.*1e3);
    hold on;
    grid on;
    title('Biomass in g/m^2 vs.
time');
    EventGCcum=cumsum(EventGC);
    if length(EventGCcum)~=1 &&
isempty(EventGCcum)==0,
    for j=1:length(EventGCcum)-1;
    idxBM=
find(Tcomp>EventGCcum(j),1); %find
and mark the first time step after
rediscretion.
    subplot(3,3,[7 8
9]),plot(EventGCcum(j),BM(idxBM).*1e
3,'or');
    end,
    end,
    if tcal~=tend&&ReG==1,

plot(Tcomp(length(Tcomp)),BM(length(
Tcomp)).*1e3,'*r');
    elseif tcal~=tend&&ReG~=1,

plot(Tcomp(length(Tcomp)),BM(length(
Tcomp)).*1e3,'sr');
    else

plot(Tcomp(length(Tcomp)),BM(length(
Tcomp)).*1e3,'or');
    end,

    end % plot end condition

%% function for ODE systems
%---------------------------------
-----------------------------------
----
    function dS = ODE_dS( t, S )
    %Function handle for
diffusion-convection-reaction PDE
    %ODEs from MOL with upwind scheme,
original PDE is:
    %dDS./dt=Dbio.*d(dDS)./dz.^2 +
uz.*DS(i)./(KsDS+DS(i))./YxsS.*Xf
for
    %DS, and
    dLf(i)./dt=Lf(i).*dzd.*Umax.*DS(i)./
(KsDS+DS(i));
    %upwind scheme: d(dDS)./dz.^2=
DSbio./.*(DS(i-1)-2.*DS(i)+DS(i+1)).
/dz.^2, and

%dDS./dt=uz./Lf.*(DS(i)-DS(i-1))./dz
    %% ODEs:
    dS=zeros(c*n,size(S,2));

    %% ODEs describing pH (column i)
dDCO2./dt (column i+1),ODEs describing
dDHCO3./dt (column i+2), ODEs
describing dDCO3./dt (column i+3)

    %--------------------------bottom
boundary: 1
    %where
    Dbio./*(D(i+c)-D(i-c))./(2.*dz)=Dsub.
/Lsub.*(SDm-D(i))

    i=1;

    %CO2

dS(i+1,:)=DCO2bcal(S,i)./(Lft0./n0).
^2.*((S(i+1+c,:)+2.*(Lft0./n0).*DCO2
s./(Lsub.*DCO2bcal(S,i)).*(SCO2mediu
m-S(i+1,:)))-2.*S(i+1,:)+S(i+1+c,:))
... diffusion

+uz./(Lft0./n0).*(2.*(Lft0./n0).*DCO
2s./(Lsub.*DCO2bcal(S,i)).*(SCO2medi
um-S(i+1,:)))...%convection

-kCO2aH2O.*(S(i+1,:)-(S(i+2,:).*S(i,
:)./KalCO3))-kCO2aOH.*(S(i+1,:).*Kw.
/S(i,:)-S(i+2,:)./KaCaOH) ...
%reaction to HCO3
    -UcalCO2(S,i)./YxsCO2.*XF
...consumption
```

```
+(1-RHCO3DvsC).*UcalHCO3(S,i)./YxsHC
O3.*XF ... from anhydrase
    +RdO2cal(S,i)./YxsO2.*XF;
%prodction

    %HCO3

dS(i+2,:)=DHCO3b./(Lft0./n0).^2.*((S
(i+2+c,:)+2.*(Lft0./n0).*DHCO3s./(Ls
ub.*DHCO3b).*(SCO2medium.*KalCO3./(1
0.^(-pHmedium))-S(i+2,:)))-2.*S(i+2,
:)+S(i+2+c,:)) ... diffusion
    +uz./(Lft0./n0)
.*(2.*(Lft0./n0).*DHCO3s./(Lsub.*DHC
O3b).*(SCO2medium.*KalCO3./(10.^(-pH
medium))-S(i+2,:)))...%convection

+kCO2aH2O.*(S(i+1,:)-(S(i+2,:).*S(i,
:)./KalCO3))... reaction from CO2+H2O

+kCO2aOH.*(S(i+1,:).*Kw./S(i,:)-S(i+
2,:)./KaCaOH)... reaction from CO2+OH

-kHCO3tCO3.*(S(i+2,:)-S(i+3,:).*S(i,
:)./Ka2CO3)... reaction to CO3

-UcalHCO3(S,i)./YxsHCO3.*XF;
%consumption

    %CO3

dS(i+3,:)=DCO3b./(Lft0./n0).^2.*((S(
i+3+c,:)+2.*(Lft0./n0).*DCO3s./(Lsub
.*DCO3b).*(SCO2medium.*KalCO3.*Ka2CO
3./(10.^(-pHmedium)).^2-S(i+3,:)))-2
.*S(i+3,:)+S(i+3+c,:))... diffusion

+uz./(Lft0./n0).*(2.*(Lft0./n0).*DCO
3s./(Lsub.*DCO3b).*(SCO2medium.*KalC
O3.*Ka2CO3./(10.^(-pHmedium)).^2-S(i
+3,:))) ...%convection

+kHCO3tCO3.*(S(i+2,:)-S(i+3,:).*S(i,
:)./Ka2CO3); %reaction from HCO3

    %DN

dS(i+4,:)=DNO3b./(Lft0./n0).^2.*((S(
i+c+4,:)+2.*(Lft0./n0).*DNO3s./(Lsub
.*DNO3b).*(SNO3medium-S(i+4,:)))-2.*
S(i+4,:)+S(i+c+4,:)) ... diffusion

+uz./(Lft0./n0).*(2.*(Lft0./n0).*DNO
3s./(Lsub.*DNO3b).*(SNO3medium-S(i+4
,:))) ...convection

-(UcalCO2(S,i)./YxsN+UcalHCO3(S,i)./
YxsN).*XF...consumption
    +RdO2cal(S,i)./YxsN.*XF;
%prodction

    %DHPO4

dS(i+5,:)=DHPO4b./(Lft0./n0).^2
.*((S(i+c+5,:)+2.*(Lft0./n0).*DHPO4s
./(Lsub.*DHPO4b).*(SHPO4medium-S(i+5
,:)))-2.*S(i+5,:)+S(i+c+5,:))...
diffusion

+uz./(Lft0./n0).*(2.*(Lft0./n0).*DHP
O4s./(Lsub.*DHPO4b).*(SHPO4medium-S(
i+5,:))) ...convection

+kH2PO4tHPO4.*(S(i+6,:)-S(i+5,:).*S(
i,:)./Ka2PO4)... reaction from H2PO4

-(S(i+5,:)./(S(i+5,:)+S(i+6,:))).*(U
calCO2(S,i)./YxsP+UcalHCO3(S,i)./Yxs
P).*XF...consumption

+(S(i+5,:)./(S(i+5,:)+S(i+6,:))).*Rd
O2cal(S,i)./YxsP.*XF; %prodction

    %DH2PO4

dS(i+6,:)=DH2PO4b./(Lft0./n0).^2
.*((S(i+c+6,:)+2.*(Lft0./n0).*DH2PO4
s./(Lsub.*DH2PO4b).*(SH2PO4medium-S(
i+6,:)))-2.*S(i+6,:)+S(i+c+6,:))...
diffusion

+uz./(Lft0./n0).*(2.*(Lft0./n0).*DH2
PO4s./(Lsub.*DH2PO4b).*(SH2PO4medium
-S(i+6,:))) ...convection
```

```
-kH2PO4tHPO4.*(S(i+6,:)-S(i+5,:).*S(
i,:)./Ka2PO4)... reaction to HPO4

-(S(i+6,:)./(S(i+5,:)+S(i+6,:))).*(U
calCO2(S,i)./YxsP+UcalHCO3(S,i)./Yxs
P).*XF...consumption

+(S(i+6,:)./(S(i+5,:)+S(i+6,:))).*Rd
O2cal(S,i)./YxsP.*XF; %prodction

    %Dsions

dS(i+7,:)=DNab./(Lft0./n0).^2.*((S(i
+c+7,:)+2.*(Lft0./n0).*DNas./(Lsub.*
DNab).*(Sionsmedium-S(i+7,:)))-2.*S(
i+7,:)+S(i+c+7,:)) ... diffusion

+uz./(Lft0./n0).*(2.*(Lft0./n0).*DNa
s./(Lsub.*DNab).*(Sionsmedium-S(i+7,
:))); %convection

    %DO2

dS(i+8,:)=DO2b./(Lft0./n0).^2.*((S(i
+8+c,:)+2.*(Lft0./n0).*DO2s./(Lsub.*
DO2b).*(SO2medium-S(i+8,:)))-2.*S(i+
8,:)+S(i+c+8,:)) ... diffusion

+uz./(Lft0./n0).*(2.*(Lft0./n0).*DO2
s./(Lsub.*DO2b).*(SO2medium-S(i+8,:)
))...%convection

+(UcalCO2(S,i)./YxsO2+UcalHCO3(S,i).
/YxsO2.*RHCO3DvsC).*XF ...production
    -RdO2cal(S,i)./YxsO2.*XF;
%consumption

%----------------------non-boundary
2:n-1
    i=(c+1):c:((n-1)*c);

    %CO2

dS(i+1,:)=DCO2bcal(S,i)./(Lft0./n0).
^2
.*(S(i+1-c,:)-2.*S(i+1,:)+S(i+1+c,:)
)...diffusion

+uz./(Lft0./n0).*(S(i+1-c,:)-S(i+1+c
,:));...convection

-kCO2aH2O.*(S(i+1,:)-(S(i+2,:).*S(i,
:)./KalCO3))-kCO2aOH.*(S(i+1,:).*Kw.
/S(i,:)-S(i+2,:)./KaCaOH) ...
%reaction to HCO3
    -UcalCO2(S,i)./YxsCO2.*XF
...consumption

+(1-RHCO3DvsC).*UcalHCO3(S,i)./YxsHC
O3.*XF ... from anhydrase
    +RdO2cal(S,i)./YxsO2.*XF;
%prodction

    %HCO3

dS(i+2,:)=DHCO3b./(Lft0./n0).^2
.*(S(i+2-c,:)-2.*S(i+2,:)+S(i+2+c,:)
)...diffusion

+uz./(Lft0./n0).*(S(i+2-c,:)-S(i+2+c
,:))... convection

+kCO2aH2O.*(S(i+1,:)-(S(i+2,:).*S(i,
:)./KalCO3))... reaction from CO2+H2O

+kCO2aOH.*(S(i+1,:).*Kw./S(i,:)-S(i+
2,:)./KaCaOH)... reaction from CO2+OH

-kHCO3tCO3.*(S(i+2,:)-S(i+3,:).*S(i,
:)./Ka2CO3)... reaction to CO3

-UcalHCO3(S,i)./YxsHCO3.*XF;
%consumption

    %CO3

dS(i+3,:)=DCO3b./(Lft0./n0).^2.*(S(i
+3-c,:)-2.*S(i+3,:)+S(i+3+c,:))
...diffusion

+uz./(Lft0./n0).*(S(i+3-c,:)-S(i+3+c
,:))... convection
```

+kHCO3tCO3.*(S(i+2,:)-S(i+3,:).*S(i,
:)./Ka2CO3); %reaction from HCO3

    %DN

dS(i+4,:)=DNO3b./(Lft0./n0).^2.*(S(i
+4-c,:)-2.*S(i+4,:)+S(i+4+c,:))
...diffusion
            +uz./(Lft0./n0)
.*(S(i+4-c,:)-S(i+4+c,:))...convecti
on

-(UcalCO2(S,i)./YxsN+UcalHCO3(S,i)./
YxsN).*XF...consumption
            +RdO2cal(S,i)./YxsN.*XF;
%prodction

    %DHPO4

dS(i+5,:)=DHPO4b./(Lft0./n0).^2.*(S(
i+5-c,:)-2.*S(i+5,:)+S(i+5+c,:))
...diffusion
            +uz./(Lft0./n0)
.*(S(i+5-c,:)-S(i+5+c,:))...
convection

+kH2PO4tHPO4.*(S(i+6,:)-S(i+5,:).*S(
i,:)./Ka2PO4)... reaction from H2PO4

-(S(i+5,:)./(S(i+5,:)+S(i+6,:))).*(U
calCO2(S,i)./YxsP+UcalHCO3(S,i)./Yxs
P).*XF...consumption

+(S(i+5,:)./(S(i+5,:)+S(i+6,:))).*Rd
O2cal(S,i)./YxsP.*XF; %prodction

    %DH2PO4

dS(i+6,:)=DH2PO4b./(Lft0./n0).^2.*(S
(i+6-c,:)-2.*S(i+6,:)+S(i+6+c,:))
...diffusion
            +uz./(Lft0./n0)
.*(S(i+6-c,:)-S(i+6+c,:))...
convection

-kH2PO4tHPO4.*(S(i+6,:)-S(i+5,:).*S(
i,:)./Ka2PO4)... reaction to HPO4

-(S(i+6,:)./(S(i+5,:)+S(i+6,:))).*(U
calCO2(S,i)./YxsP+UcalHCO3(S,i)./Yxs
P).*XF...consumption

+(S(i+6,:)./(S(i+5,:)+S(i+6,:))).*Rd
O2cal(S,i)./YxsP.*XF; %prodction

    %Dsions

dS(i+7,:)=DNab./(Lft0./n0).^2.*(S(i+
7-c,:)-2.*S(i+7,:)+S(i+7+c,:))
...diffusion

+uz./(Lft0./n0).*(S(i+7-c,:)-S(i+7+c
,:)); %convection

    %DO2

dS(i+8,:)=DO2b./(Lft0./n0).^2.*(S(i+
8-c,:)-2.*S(i+8,:)+S(i+8+c,:))
...diffusion

+uz./(Lft0./n0).*(S(i+8-c,:)-S(i+8+c
,:)) ... convection in

+(UcalCO2(S,i)./YxsO2+UcalHCO3(S,i).
/YxsO2.*RHCO3DvsC).*XF ...production
            -RdO2cal(S,i)./YxsO2.*XF;
%consumption

    %-----------------------top
boundary n

    i=(c*n-(c-1));

    %CO2
        dS(i+1,:)=0;

    %HCO3

dS(i+2,:)=DHCO3b./(Lft0./n0).^2
.*(S(i+2,:)-2.*S(i+2,:)+S(i-c+2,:)).
..diffusion
            +uz./(Lft0./n0)
.*(S(i+2-c,:)-S(i+2,:))...
%convection in

+kCO2aH2O.*(S(i+1,:)-(S(i+2,:).*S(i,
:)./Ka1CO3))... reaction from CO2+H2O

+kCO2aOH.*(S(i+1,:).*Kw./S(i,:)-S(i+
2,:)./KaCaOH)... reaction from CO2+OH

-kHCO3tCO3.*(S(i+2,:)-S(i+3,:).*S(i,
:)./Ka2CO3)... reaction to CO3

-UcalHCO3(S,i)./YxsHCO3.*XF;
%consumption

    %CO3

dS(i+3,:)=DCO3b./(Lft0./n0).^2.*(S(i
+3,:)-2.*S(i+3,:)+S(i-c+3,:))
...diffusion

+uz./(Lft0./n0).*(S(i+3-c,:)-S(i+3,:
)) ...%convection in

+kHCO3tCO3.*(S(i+2,:)-S(i+3,:).*S(i,
:)./Ka2CO3); %reaction from HCO3

    %DN

dS(i+4,:)=DNO3b./(Lft0./n0).^2.*(S(i
+4,:)-2.*S(i+4,:)+S(i-c+4,:))
...diffusion
            +uz./(Lft0./n0)
.*(S(i+4-c,:)-S(i+4,:))...convection
in

-(UcalCO2(S,i)./YxsN+UcalHCO3(S,i)./
YxsN).*XF... consumption
            +RdO2cal(S,i)./YxsN.*XF;
%prodction

    %DHPO4

dS(i+5,:)=DHPO4b./(Lft0./n0).^2
.*(S(i+5,:)-2.*S(i+5,:)+S(i-c+5,:)).
..diffusion

+uz./(Lft0./n0).*(S(i+5-c,:)-S(i+5,:
)) ...convection in

+kH2PO4tHPO4.*(S(i+6,:)-S(i+5,:).*S(
i,:)./Ka2PO4)... reaction from H2PO4

-(S(i+5,:)./(S(i+5,:)+S(i+6,:))).*(U
calCO2(S,i)./YxsP+UcalHCO3(S,i)./Yxs
P).*XF ... consumption

+(S(i+5,:)./(S(i+5,:)+S(i+6,:))).*Rd
O2cal(S,i)./YxsP.*XF; %prodction

    %DH2PO4

dS(i+6,:)=DH2PO4b./(Lft0./n0).^2
.*(S(i+6,:)-2.*S(i+6,:)+S(i-c+6,:)).
..diffusion

+uz./(Lft0./n0).*(S(i+6-c,:)-S(i+6,:
)) ...convection in

-kH2PO4tHPO4.*(S(i+6,:)-S(i+5,:).*S(
i,:)./Ka2PO4)... reaction to HPO4

-(S(i+6,:)./(S(i+5,:)+S(i+6,:))).*(U
calCO2(S,i)./YxsP+UcalHCO3(S,i)./Yxs
P).*XF ... consumption

+(S(i+6,:)./(S(i+5,:)+S(i+6,:))).*Rd
O2cal(S,i)./YxsP.*XF; %prodction

    %Dsions

dS(i+7,:)=DNab./(Lft0./n0).^2.*(S(i+
7,:)-2.*S(i+7,:)+S(i-c+7,:))
...diffusion (out)

+uz./(Lft0./n0).*(S(i+7-c,:)-S(i+7,:
)); %convection in

    %DO2
        dS(i+8,:)=0;

    %----------------------- special
case for pH, with have no boundary
condition, and is discribed as a
algebraic equations

    %dH as state variables, CO3 and HCO3
calculated in their own ODEs, so here
their concentrations are not dependent
on pH

    i=1:c:c*n;

dS(i,:)=(Chcal(S).*(-dS(i+7,:)+dS(i+
4,:)...Cations, NO3,

+((S(i,:)).^2.*Ka1PO4./((S(i,:)).^3+
(S(i,:)).^2.*Ka1PO4+S(i,:).*Ka1PO4.*
Ka2PO4+Ka1PO4.*Ka2PO4.*Ka3PO4).*(dS(
i+5,:)+dS(i+6,:)))... H2PO4

+2.*(S(i,:).*Ka1PO4.*Ka2PO4./((S(i,:
)).^3+S(i,:)).^2.*Ka1PO4+S(i,:).*Ka
1PO4.*Ka2PO4+Ka1PO4.*Ka2PO4.*Ka3PO4)
.*(dS(i+5,:)+dS(i+6,:)))... HPO4

+3.*(Ka1PO4.*Ka2PO4.*Ka3PO4./((S(i,:
)).^3+S(i,:)).^2.*Ka1PO4+S(i,:).*Ka
1PO4.*Ka2PO4+Ka1PO4.*Ka2PO4.*Ka3PO4)
.*(dS(i+5,:)+dS(i+6,:)))... PO4

+(((S(i,:)).*Ka1CO3)./((S(i,:)).^2+
S(i,:)).*Ka1CO3+Ka1CO3.*Ka2CO3).*(dS
(i+1,:)+dS(i+2,:)+dS(i+3,:))) ...
HCO3

+2.*((Ka1CO3.*Ka2CO3)./((S(i,:)).^2+
(S(i,:)).*Ka1CO3+Ka1CO3.*Ka2CO3).*(d
S(i+1,:)+dS(i+2,:)+dS(i+3,:)))) ...
CO3
            ./(1-(Chcal(S).*(-0+0
...Cations, NO3

+(1./(Ka2PO4.*Ka3PO4).*(-(S(i,:)).^4
./(Ka1PO4.*Ka2PO4.*Ka3PO4)+(S(i,:)).
^2./Ka3PO4+2.*(S(i,:))./((S(i,:)).^
3./(Ka1PO4.*Ka2PO4.*Ka3PO4)+(S(i,:))
.^2./(Ka2PO4.*Ka3PO4)+(S(i,:))./Ka3P
O4+1).^2).*(S(i+5,:)+S(i+6,:)) ...
H2PO4

+2.*(1./Ka3PO4.*(-2.*(S(i,:)).^3./(K
a1PO4.*Ka2PO4.*Ka3PO4)+(S(i,:)).^2./
(Ka2PO4.*Ka3PO4)+1)./((S(i,:)).^3./(
Ka1PO4.*Ka2PO4.*Ka3PO4)+(S(i,:)).^2.
/(Ka2PO4.*Ka3PO4)+(S(i,:))./Ka3PO4+1
).^2).*(S(i+5,:)+S(i+6,:)) ... HPO4

+3.*((3.*(S(i,:)).^2./(Ka1PO4.*Ka2PO
4.*Ka3PO4)+2.*(S(i,:))./(Ka2PO4.*Ka3
PO4)+1./Ka3PO4)./((S(i,:)).^3./(Ka1P
O4.*Ka2PO4.*Ka3PO4)+(S(i,:)).^2./(Ka
2PO4.*Ka3PO4)+(S(i,:))./Ka3PO4+1).^2
).*(S(i+5,:)+S(i+6,:)) ... PO4

+(1/Ka2CO3.*(-(S(i,:)).^2./(Ka1CO3.*
Ka2CO3)+1)./((S(i,:)).^2./(Ka1CO3.*K
a2CO3)+(S(i,:))./Ka2CO3+1).^2).*(S(i+
1,:)+S(i+2,:)+S(i+3,:))) ... HCO3

+2.*(-1.*(2.*(S(i,:))./(Ka1CO3.*Ka2C
O3)+1./Ka2CO3)./((S(i,:)).^2./(Ka1CO
3.*Ka2CO3)+(S(i,:))./Ka2CO3+1).^2.*(
S(i+1,:)+S(i+2,:)+S(i+3,:)))))); %CO3

    %----------------------- special
cases for biofilm thickness, Irr in this
case calculated explicitly,
Irr(i,:)=(((Irrsurf.*rs).*exp(-Mex.*
Xf.*sum(Lf(i:n)))))
    i=1:c:c*n-(c-1)); %for 1st to
n0=(n-1)th layer, no thickness
increase.
        dS(i+9,:)=0;

    i=(c*n-(c-1)); %for nth layer (top
most), the cummulative thickness
increase from 1st to nth layers

dS(i+9,:)=(sum(S(c:c:c*n,:).*(UcalCO
2(S,1:c:c*n).*BMc))... CO2 growth

+sum(S(c:c:c*n,:).*(UcalHCO3(S,1:c:c
*n).*BMc.*RHCO3DvsC))... HCO3 growth

-sum(S(c:c:c*n,:).*RdO2cal(S,1:c:c*n
)./BMc)); %decrease from respiration

    %% Ch cal, determine which
function should be used for the

```
calculation direvitive, whether
ph>or<7
        function B=Chcal(Scal)
            Ch=
-Scal(i+6,:)+Scal(i+4,:)...Cations,
NO3

+(Scal(i,:)).^2.*Ka1PO4./((Scal(i,:)
).^3+(Scal(i,:)).^2.*Ka1PO4+Scal(i,:
).*Ka1PO4.*Ka2PO4+Ka1PO4.*Ka2PO4.*Ka
3PO4).*(Scal(i+5,:)+Scal(i+6,:))...
H2PO4

+2.*(Scal(i,:).*Ka1PO4.*Ka2PO4./((Sc
al(i,:)).^3+(Scal(i,:)).^2.*Ka1PO4+S
cal(i,:).*Ka1PO4.*Ka2PO4+Ka1PO4.*Ka2
PO4.*Ka3PO4).*(Scal(i+5,:)+Scal(i+6,
:)))... HPO4

+3.*(Ka1PO4.*Ka2PO4.*Ka3PO4./((Scal(
i,:)).^3+(Scal(i,:)).^2.*Ka1PO4+Scal
(i,:).*Ka1PO4.*Ka2PO4+Ka1PO4.*Ka2PO4
.*Ka3PO4).*(Scal(i+5,:)+Scal(i+6,:))
)... PO4

+(((Scal(i,:)).*Ka1CO3)./((Scal(i,:)
).^2+(Scal(i,:)).*Ka1CO3+Ka1CO3.*Ka2
CO3).*(Scal(i+1,:)+Scal(i+2,:)+Scal(
i+3,:))) ... HCO3

+2.*((Ka1CO3.*Ka2CO3)./((Scal(i,:)).
^2+(Scal(i,:)).*Ka1CO3+Ka1CO3.*Ka2CO
3).*(Scal(i+1,:)+Scal(i+2,:)+Scal(i+
3,:)))); %CO3
            %to maintain stability
            if Ch>=0,

B=0.5.*(Ch./(Ch.^2+4.*Kw).^(1/2)+1);
            else

B=-(Scal(i,:)).^2./(2.*Kw).*(Ch./(Ch
.^2+4.*Kw).^(1/2)-1);
            end,

        end


    %% U, growth rate function for CO2
        function U=UcalCO2(Scal,j)
            U=umax.*PCO2O2...

.*Scal(j+8,:)./((Scal(j+8,:)+Scal(j+
8,:).^2./(KiO2cal(Scal(j+1,:),Scal(j
+8,:)))))... O2

.*UaveIrrLfcal(Scal,j)... light

.*min(Scal(j+1,:)./(KsCO2+Scal(j+1,:
)),... CO2

min(Scal(j+4,:)./(KsNO3+Scal(j+4,:))
,...NO3

(Scal(j+5,:)+Scal(j+6,:))./(KsPO4+(S
cal(j+5,:)+Scal(j+6,:)))))); % PO4
        end

    %% U, growth rate function for
HCO3
        function U=UcalHCO3(Scal,j)
            U=umax.*PHCO3O2 ...

.*Scal(j+8,:)./((Scal(j+8,:)+Scal(j+
8,:).^2./(KiO2cal(Scal(j+1,:),Scal(j
+8,:)))))... o2

.*UaveIrrLfcal(Scal,j)... light

.*min(Scal(j+2,:)./(KsHCO3+Scal(j+2,
:)),... HCO3

min(Scal(j+1,:)./((Scal(j+1,:)+Scal(
j+1,:).^2./KiCO2toHCO3)), ... CO2
inhibition on HCO3

min(Scal(j+4,:)./(KsNO3+Scal(j+4,:))
,... NO3

(Scal(j+5,:)+Scal(j+6,:))./(KsPO4+(S
cal(j+5,:)+Scal(j+6,:)))))); %PO4
        end

    %% Dark respiration
        function Rd=RdO2cal(Scal,j)
```

```
Rd=Ures.*Scal(j+8,:)./(KsO2+Scal(j+
8,:)));
        end

    %% Calculated maximal growth
rate per element when only light is
limiting
        function
Uave=UaveIrrLfcal(Scal,j) % function
for calculating light intensity in the
biofilm
            if t-fix(t)<=tL,
%determine if is light
                Irrcal=Irrsurf;
            else %or dark
                Irrcal=0;
            end,

Lfcumleft=zeros(size(Scal));

Lfcumleft(c*n:-c:c,:)=cumsum(Scal(c*
n:-c:c,:));

IrrLfleft=(Irrcal.*(1-rs)).*polyval(
IzinPer,Lfcumleft(j+9,:));

Lfcumright=zeros(size(Scal));

Lfcumright(c*n-c:-c:c,:)=Lfcumleft(c
*n:-c:c+c,:);

IrrLfright=(Irrcal.*(1-rs)).*polyval
(IzinPer,Lfcumright(j+9,:));

Uave=(GroIrr_TL(IrrLfright)...Right,
closer to suface

+GroIrr_TL(IrrLfleft))... Left,
Further away from surface
                    ./2; %take average
value of left and right as growth in dLf
            end

        end

%% Event function, for determing
whether dLf has reached Lf(t=0)/n
%-----------------------------------
-----------------------------------
----
        function
[value,isterminal,direction]=EventsL
f(t,Scal)
            % the event is now when the nth
layer's thichness reaches the preset
            % Lft0/n0 value, which means the
biomass thickness has increased one
whole
            % grid, and a new discretion is
needed

value=[Scal(c*n,1)-(Lft0./n0),Scal(c
*n,1)-(Lft0./n0)./10^10] ; %Lf(n,t)
reached Lf(t=0)/n0, or the growth is
negative
            isterminal=[1,1];
            direction=[0,-1];
        end

%% Estimate effect of CO2/O2 ration on
photorespiration
        function KiO2=KiO2cal(DCO2,DO2) %
function for estimating the
photorespiration, Monod type
            KRCO2toO2=0.35; %factors
determine the rate of photorespiration
change with CO2/O2 ratio
            KiO2min=3e-4; %assumed minimum
photorespiration factor

KiO2=KiO2max.*(DCO2./DO2)./(KRCO2toO
2+DCO2./DO2)+KiO2min;
        end

%% Estimate the facilitated CO2
transport by EPS & CA ( possiblz also
cell surface) in biofilms
        function
DCO2bfacilitated=DCO2bcal(Scal,j)
            % use a simple log curve to estimate
facilitated CO2 transport,local CO2
            % concentration dependent
                fa=100.2;
```

```
                fb=-1e4;
                fc=1;

DCO2bfacilitated=DCO2b.*(fa.*exp(fb.
*Scal(j+1,:))+fc);
        end

end
% H as state variable


function [ Ipar ] = RTE_TL(XF)
%calculated PAR irradiance inside the
biofilm with
%the RTE method, using DOM methed and
finite volume with upwind scheme, for
%DOM 2 hemisphere each with 24 discrete
directions are used, weighting
%factor are aquired from literature.
This method also take into account the
%case of optically thin and shallow
biofilm, and the reflection by the
%substrate layer membrane is taken into
account.

LF=1000e-6; % assume a very thick
biofilm, i.e. no light penetration.
g=0.98; % assumed asymmery factor
Nnodes=200; %set the number of discrete
elements in depth direction.

load('DOM.mat'); % Load discrete
ordinate
load('OptPro'); % Load biomass optical
properties, mass absorption: Amass;
            % mass scttering: Smass;
and spectral irradiance at biofilm
            % surface (300 total):
SpeIsur; reflectivity of biofilm
surface, rbios;
            % reflectivity of
membrane surface, rmems.

[v,disdir]=size(DOM); %angel and
weighting factors for DOM, 1st row index
(1 to 24)
            %2nd row angle, 3rd angle
in radius,4th row row cos(angle),
            %5th row weighing
factors.
if v~=5,
    error('check discrete ordinate
system setup'),
end,

if g>1||g<-1,
    fprintf('g value out of range,
calculating as no inscattering'),
    g=2;
end,

dz=LF/Nnodes;
dLF=0:dz:LF;

[a,m]=size(SpeGsur); %m:number of
different wavelength,a:2(1st row
wavelength,2nd row intensity)
[n]=length(dLF); %n:bumber of depth
steps(row is the depth of the nodes)
[b,o]=size(Amass); %o:number of
different wavelength,b:2(1st row
wavelength,2nd row mass absorption)
[c,p]=size(Smass); %p:number of
different wavelength,b:2(1st row
wavelength,2nd row mass scattering)

if
m~=o||a~=2||b~=2||c~=2||o~=p||p~=m,
    error('ERROR: wavelegth steps are
not compatible'),
end, %check if the datais compatible

Cabs=zeros(2,m); %absorption
coefficient of the biomass, 1st row
wavelength, 2nd row coefficient
Csca=zeros(2,m); %scattering
coefficient of the biomass, 1st row
wavelength, 2nd row coefficient

for i=1:m, %calculate absorption and
scattering coefficient
    Cabs(1,i)= Amass(1,i);
    Cabs(2,i)= Amass(2,i)*XF;
    Csca(1,i)= Smass(1,i);
    Csca(2,i)= Smass(2,i)*XF;
end,
```

```
ncal=n+1;

%%%%%%%%%%%%%%%%%%%%%%%%%%%%%%%
%%%%%%%%%%%%%%%%%%%%%%%%%%%%%%%
%%%%%%%%%%%%%%%

SpeIsur=zeros(m,disdir);

for i=1:m,
    for j=1:disdir/2,

SpeIsur(i,j)=((1-rbios)*SpeGsur(2,i)
)/2/pi;
    end,
end, %set the diffuse incident
irradiance at different wavelength and
discrete directions, 12 indicate only
for 1/4 sphere

Normalizer=zeros(1,24);
for j=1:24,
    for i=1:24,

Normalizer(1,j)=Normalizer(1,j)+DOM(
5,i)*(HenGrePhase(DOM(3,i),DOM(3,j),
g)+HenGrePhase(DOM(3,i),-DOM(3,j),g)
);
    end,
    if g==2,
        Normalizer(1,j)=0;
    else

Normalizer(1,j)=1/Normalizer(1,j);
    end,
end,

%%%%%%%%%%%%%%%%%%%%%%%%%%%%%%%%%%%
%%%%%%%%%%%%%%%%%%%%%%%%%%%%%%%%%%%
%%%%%%%%%%%%%%
%start iterative procedure
SpeIite=zeros(m,disdir,ncal);

%%%%%%%%%%%%%%%%%%%%%%%%%%%%%%%%%%%
%%%%%%%%%%%%%%%%%%%%%%%%%%%%%%%%%%%
%%%%%%%%%%%%%%
SpeIbot=zeros(1,2); %set stopping
criterion.
ite=0;
Afactor=ones(ncal,m); %set adaptation
factor.
    for k=1:ncal-1;
        Afactor(k,:)=dLF(k)/250e-6;
        Afactor(Afactor>1)=1;
    end

while
SpeIbot(1,1)==SpeIbot(1,2)||abs(SpeI
bot(1,1)-SpeIbot(1,2))/SpeIbot(1,2)>
0.01,
%%%%%%%%%%%%%%%%%%%%%%%%%%%%%%%%%%%
%%%%%%%%%%%%%%%%%%%%%%%%%%%%%%%%%%%
%%%%%%%%%%%%%
%iterative process
ite=ite+1;

    for i=1:m,
        for j=1:disdir,
            if j>disdir/2,

SpeIite(i,j,1)=SpeIite(i,j,2);
            else

SpeIite(i,j,1)=SpeIsur(i,j);
            end,
        end,
    end,%apply new surface boundary
condition

    Bi=zeros(m,disdir);
    ai=zeros(m,disdir);
    bi=zeros(m,disdir,disdir);
    ci=zeros(m,disdir,ncal);
    Ai=zeros(disdir,disdir);
    Ci=zeros(disdir,1);

    for i=1:m,
        for k=2:ncal-1,
            for j=1:disdir ,

Bi(i,j)=Cabs(2,i)*Afactor(k,i)+Csca(
2,i)-Csca(2,i)*DOM(5,j)*(HenGrePhase
(DOM(3,j),-DOM(3,j),g)+HenGrePhase(D
OM(3,j),DOM(3,j),g))*Normalizer(1,j)
;
                if j>disdir/2,
```

```
ai(i,j)=Bi(i,j)*dz-DOM(4,j);

ci(i,j,k)=-DOM(4,j)*SpeIite(i,j,(k+1
));
                else

ai(i,j)=Bi(i,j)*dz+DOM(4,j);

ci(i,j,k)=DOM(4,j)*SpeIite(i,j,(k-1)
);
                end,
                for j1=1:disdir,
                    if j==j1,

bi(i,j,j1)=ai(i,j);
                    else

bi(i,j,j1)=-dz*Csca(2,i)*DOM(5,j1)*(
HenGrePhase(DOM(3,j1),-DOM(3,j),g)+H
enGrePhase(DOM(3,j1),DOM(3,j),g))*No
rmalizer(1,j);
                    end,
                end, %calculate Si, j1
represent incident discretedirection,
j represents outgoing discrete
direction
            end,
            for p=1:disdir,
                for q=1:disdir,
                    Ci(p,1)=ci(i,p,k);
                    Ai(p,q)=bi(i,p,q);
                end,
            end,%establish matrix for
linsolve function

SpeIk=linsolve(Ai,Ci);%solve the
equation system, number of variables
and equation equal number of the
discrete directions
            for j=1:disdir,

SpeIite(i,j,k)=SpeIk(j,1);
            end,%integrate solution
result
        end,
    end, %Calculate local spectral
irradiance

    for i=1:m,
        for j=1:disdir,
            if j>disdir/2

SpeIite(i,j,ncal)=rmems*SpeIite(i,di
sdir-j+1,ncal-1);
            end,
        end,
    end,%transfer new boundary
condition at the substrate biofilm
inteface.

    for i=1:m,
        for k=ncal-1:-1:2,
            for j=1:disdir ,
                if j>disdir/2,

ci(i,j,k)=-DOM(4,j)*SpeIite(i,j,(k+1
));
                else

ci(i,j,k)=DOM(4,j)*SpeIite(i,j,(k-1)
);
                end,
            end,
            for p=1:disdir,
                for q=1:disdir,
                    Ci(p,1)=ci(i,p,k);
                    Ai(p,q)=bi(i,p,q);
                end,
            end,%establish matrix for
linsolve function

SpeIk=linsolve(Ai,Ci);%solve the
equation system, number of variables
and equation equal number of the
discrete directions
            for j=1:disdir,

SpeIite(i,j,k)=SpeIk(j,1);
            end,%integrate soltion
result
        end,
    end, %Calculate local spectral
irradiance
```

```
    SpeGzite=zeros(m,ncal); % Local
spectral intensity
    GpariteB=zeros(1,ncal); % Local
blue PAR irradiance
    GpariteG=zeros(1,ncal); % Local
green PAR irradiance
    GpariteR=zeros(1,ncal); % Local red
PAR irradiance

    for k=1:ncal,
        for i=1:m,
            for j=1:disdir,

SpeGzite(i,k)=SpeGzite(i,k)+2*pi*Spe
Iite(i,j,k)*DOM(5,j);
            end,
            if Cabs(1,i)<=500,

GpariteB(1,k)=GpariteB(1,k)+SpeGzite
(i,k);
            elseif
500<Cabs(1,i)&&Cabs(1,i)<=600,

GpariteG(1,k)=GpariteG(1,k)+SpeGzite
(i,k);
            else

GpariteR(1,k)=GpariteR(1,k)+SpeGzite
(i,k);
            end,
        end
    end, %calculate local spectral
intensity and  PAR irradiance at depth
z, *2 indicate 2 heremisphere for total
and RGB


GpariteT=GpariteB+GpariteG+GpariteR;
% Local total PAR irradiance

    SpeIbot(1,1)=SpeIbot(1,2);
    SpeIbot(1,2)=sum(GpariteT(1,:));

    if g==2,
        break,
    end,

    if ite>300,
        warning('ite > 30, exit loop');
        break,
    end,
%%%%%%%%%%%%%%%%%%%%%%%%%%%%%%%%%%%%
%%%%%%%%%%%%%%%%%%%%%%%%%%%%%%%%%%%%
%%%%%%%%%%%%%%%
%end of iterative process
end,

Ipar=zeros(5,n-1);
Ipar(1,:)=dLF(1:n-1);
for k=2:n;
    Ipar(2,k-1)=GpariteT(1,k); %Total
    Ipar(3,k-1)=GpariteB(1,k); %Blue
    Ipar(4,k-1)=GpariteG(1,k); %Green
    Ipar(5,k-1)=GpariteR(1,k); %Red
end,

if g==0,
    gcha='g=0,isotropic scattering';
elseif (0<g)&&(g<1),
    gcha=['g=',num2str(g),',forward
scattering'];
elseif (-1<g)&&(g<0),
    gcha=['g=',num2str(g),',backward
scattering'];
else
    gcha='No inscattering';
end

figure( 'Name', 'Irradiance
distribution in Twin-layer biofilm' );
%plot
hold on;
plot (Ipar(1,:),
Ipar(2,:)./Ipar(2,2).*100, '-black');
plot (Ipar(1,:),
Ipar(3,:)./Ipar(2,2).*100, '-blue');
plot (Ipar(1,:),
Ipar(4,:)./Ipar(2,2).*100, '-green');
plot (Ipar(1,:),
Ipar(5,:)./Ipar(2,2).*100, '-red');
xlabel('Depth into the biofilm in
meter');
```

```matlab
ylabel('Local irradiance in % of the
total PAR at biofilm surface');
title('Irradiance distribution in
Twin-layer biofilm');
text(Ipar(1,int8(n/2)),Ipar(2,int8(n
/2)),['\leftarrow'
gcha],'HorizontalAlignment','left','
FontSize',12);

end
function [ PhasefunHG ] = HenGrePhase(
Ain,Aout,g )
%HenGreOhase calculate the phase
function apprimation with the
%Henyey-Greenstein method, PhasefunHG
returns the calculated phase function.
%
%   This function calculate the phase
function for strongly forwarding
%   medium, and need to variables for
the approximation, g is the
%   coeffcient, generally between 0.95
to 0.99 for strongly forwarding
%   medium, and the scattering angle,
which can be found in variable DOM.

u0=cos(Ain+Aout);
PhasefunHG=(1-g^2)/(1+g^2-2*g*u0)^(3
/2)/2;
%calculate the HG phase function

end


function [ fIrr ] = GroIrr_TL( Irr )
%Growth when irradiance is the only
factor
%   aI,bI,cI factors, refer to Platt and
Gallegos, 1980

%% factors for irradiance's influence
on growth
ETRmax=49.6; % micromole electron per
m^2 per s, max ETR
alpha=0.24; % initial slope of ETR curve
beta= 0.0068; %factor representing
photo inhibition

%%%%%%%%
PBs=ETRmax;
a=alpha;
b=beta;

fIrr=(1-exp(-a.*Irr./PBs)).*exp(-b.*
Irr./PBs); %Growth rate when
irrandiance is the only factor

end


function [
DbioCO2,DbioHCO3,DbioCO3,DbioNO3,Dbi
oHPO4,DbioH2PO4,DbioO2,DbioNa,DbioH,
...
DsubCO2,DsubHCO3,DsubCO3,DsubN,DsubH
PO4,DsubH2PO4,DsubO2,DsubNa,DsubH
]...
    = DiffCoCal_TL( BioPoro, SubPoro)
%Calculated effective diffusion
coefficient in TL biofilm

%%%%% diffusion coefficients in water
DCO2=1.65e-4; %diffusion coefficient
of CO2 in water in m^2/day^, 1.65e-4
DHCO3=1.02e-4; %diffusion coefficient
of HCO3 in water in m^2/day
DCO3=7.9e-5; %diffusion coefficient of
CO3 in water in m^2/day
DNO3=1.47e-4; %diffusion coefficient
of NO3 in water in m^2/day
DHPO4=8.2e-5; %diffusion coefficient
of HPO4 in water in m^2/day
DH2PO4=6.5e-5; % diffusion coefficient
of H2PO4 in warer in m^2/day
DO2=1.73e-4; %diffusion coefficient of
O2 in water in m^2/day
DNa=1.15e-4; %diffusion coefficient of
Na in water in m^2/day
DH=6.05e-3; %diffusion coefficient of
H in water in m^2/day
%%%%%%

BioRDC=BioPoro/(1+0.5*(1-BioPoro)); %
SubRDC=SubPoro/(1+0.5*(1-SubPoro));%
refer to Weissberg, 1963

DbioCO2=BioRDC*DCO2;
DbioHCO3=BioRDC*DHCO3;
DbioCO3=BioRDC*DCO3;
DbioNO3=BioRDC*DNO3;
DbioHPO4=BioRDC*DHPO4;
DbioH2PO4=BioRDC*DH2PO4;
DbioO2=BioRDC*DO2;
DbioNa=BioRDC*DNa;
DbioH=BioRDC*DH;

DsubCO2=SubRDC*DCO2;
DsubHCO3=SubRDC*DHCO3;
DsubCO3=SubRDC*DCO3;
DsubN=SubRDC*DNO3;
DsubHPO4=SubRDC*DHPO4;
DsubH2PO4=SubRDC*DH2PO4;
DsubO2=SubRDC*DO2;
DsubNa=SubRDC*DNa;
DsubH=BioRDC*DH;

end
```

Appendix III: Author's contribution to the publications included in this thesis

1St manuscript: *A method to determine photosynthetic activity from oxygen microsensor data in biofilms subjected to evaporation* (Published in the journal 'Journal of Microbiological Methods').

> **Authors:** Tong Li, Björn Podola, Dirk de Beer and Michael Melkonian

> **Authorship:** First Author

> **Contribution in experimental work (%):** Sample preparation; Experimental measurement with the microsensors (50%).

> **Contribution in theoretical part (%):** Development of the mathematical concept; Implementation of the mathematical concept; Analysis of data (80%).

> **Contribution in writing (%):** Preparation of the original manuscript including introduction, methods and materials, results and discussion (70%).

2nd manuscript: *Microscale profiling of photosynthesis-related parameters in a highly productive biofilm photobioreactor* (Submitted to the journal 'Biotechnology and Bioengineering', under review).

> **Authors:** Tong Li, Bastian Piltz, Björn Podola, Anthony Dron, Dirk de Beer and Michael Melkonian

> **Authorship:** First Author

> **Contribution in experimental work (%):** Sample preparation; Experimental measurement with the microsensors (90%).

> **Contribution in theoretical part (%):** Data analysis; Discussion of results (80%).

> **Contribution in writing (%):** Preparation of the original manuscript including introduction, methods and materials, results, discussion and supplementary materials (75%).

3rd manuscript: *Investigating dynamic processes in a porous substrate biofilm photobioreactor – A modeling approach* (finished manuscript).

> **Authors:** Tong Li, Björn Podola and Michael Melkonian

> **Authorship:** First Author

> **Contribution in experimental work (%):** Sample preparation; Experimental work carried out in the framework of the study (90%).

> **Contribution in theoretical part (%):** Model development and implementation; Data analysis (90%).

> **Contribution in writing (%):** Preparation of the original manuscript including introduction, methods and materials, results, discussion and supplementary materials (85%).

Erklärung

Ich versichere, dass ich die von mir vorgelegte Dissertation selbständig angefertigt, die benutzten Quellen und Hilfsmittel vollständig angegeben und die Stellen der Arbeit − einschließlich Tabellen, Karten und Abbildungen −, die anderen Werken im Wortlaut oder dem Sinn nach entnommen sind, in jedem Einzelfall als Entlehnung kenntlich gemacht habe; dass diese Dissertation noch keiner anderen Fakultät oder Universität zur Prüfung vorgelegen hat; dass sie − abgesehen von oben (Teil 2 und Appendix III) angegebenen Teilpublikationen − noch nicht veröffentlicht worden ist, sowie, dass ich eine solche Veröffentlichung vor Abschluss des Promotionsverfahrens nicht vornehmen werde. Die Bestimmungen der Promotionsordnung sind mir bekannt. Die von mir vorgelegte Dissertation ist von Prof. Dr. Michael Melkonian betreut worden.

Tong Li

Lebenslauf

Persönliche Informationen:

Name:	**Staatsangehörigkeit:**
Tong Li	China
Geburtsort:	**Geburtsdatum:**
Urumqi, China	20.Nov.1987
Tel.:	**Email:**
+49 (0)221-470 8090	lit2@uni-koeln.de
Anschrift:	

AG Melkonian, Botanisches Institut, Universität zu Köln, Zülpicher Str. 47b, D50674 Köln, Deutschland

Schulbildungen:

09.1993 – 07.1999:   **Urumqi Nr.15 Ground School, China**

09.1999 – 07.2002:   **Urumqi Nr.13 Middle School, China**

09.2002 – 07.2005:   **Urumqi Nr.1 Middle School, China**

Studium:

09.2005 – 07.2009:   **Nanjing Normal University**

Bachelor Studium
Fach: Umwelttechnik

07.2009 - 04.2012:   **Universität zu Cologne**

Master Studium: International master of environmental science (IMES)
Masterarbeit: 'Removal of Zn from wastewater with a continuous treatment system based on microalgae immobilized on Twin-Layer'

07.2012 - heute: **Universität zu Cologne**

Promotion in Prüfungsfach Botanik
Thema der Dissertation: 'Dynamic interactions in an artificial phototrophic biofilm for biotechnological applications'

Forschungsbereiche:

Algenbiotechnologie, Biofilm Modeling, Biofilm Microsensormessungen, Biofilm Imaging

Publikationen:

Continuous removal of zinc from wastewater and mine dump leachate by a microalgal biofilm PSBR. Tong Li, Gengyi Lin, Björn Podola, Michael Melkonian, Journal of Hazardous Materials 297 (2015) 112–118.

A method to determine photosynthetic activity from oxygen microsensor data in biofilms subjected to evaporation. Tong Li, Björn Podola, Dirk de Beer, and Michael Melkonian, Journal of Microbiological Methods 117 (2015) 100-107.

High light and carbon dioxide optimize surface productivity in a Twin-Layer biofilm photobioreactor. Larissa K. P. Schultze, Victoria-Marie Simon, Tong Li, Dorothee Langenbach, Björn Podola, Michael Melkonian, Algal Research 8 (2015) 37–44.

Microscale profiling of photosynthesis-related parameters in a highly productive biofilm photobioreactor. Tong Li, Bastian Piltz, Björn Podola, Anthony Dron, Dirk de Beer, Michael Melkonian. Biotechnology and Bioengineering, manuscript accepted in Oct. 2015.

Investigating dynamic processes in a porous substrate biofilm photobioreactor – A modeling approach. Tong Li, Björn Podola, Michael Melkonian. Manuscript under review.